



UNIVERSITY OF  
BIRMINGHAM

**APPLICATION OF ELECTROSTATICS TO ALIGN SHORT-GLASS  
FIBRE BUNDLES FOR COMPOSITE MANUFACTURING**

by

**ASHWINI PRASAD**

A thesis submitted to  
The University of Birmingham  
For the degree of

**MASTER OF PHILOSOPHY**

School of Metallurgy and Materials  
Sensors and composites Group

**College of Engineering and Physical Science  
The University of Birmingham**  
September 2012



UNIVERSITY OF  
BIRMINGHAM

## **University of Birmingham Research Archive**

### **e-theses repository**

This unpublished thesis/dissertation is copyright of the author and/or third parties. The intellectual property rights of the author or third parties in respect of this work are as defined by The Copyright Designs and Patents Act 1988 or as modified by any successor legislation.

Any use made of information contained in this thesis/dissertation must be in accordance with that legislation and must be properly acknowledged. Further distribution or reproduction in any format is prohibited without the permission of the copyright holder.

## **ABSTRACT**

This research reports on the feasibility of aligning the glass fibre bundles, in the form of short individual filaments, called short-glass fibre bundles for the manufacture of fibre reinforced polymer composites or preforms. Traditionally, preforms are manufactured using ‘chopped fibre bundles’ have been available number of years, here the short-glass fibre bundles arranged randomly, but they cannot be laid over complex moulds without causing significant wrinkles and folds. Aligned short-glass fibre bundles offer superior drape as they can be laid over complex moulds, but they represent a unique challenge to apply electric force and to orientate. Therefore, this research aims to align short-glass fibre bundles for preform manufacture by applying electric forces to them. The influence of electric field on short E-glass fibre bundles is investigated.

## **ACKNOWLEDGEMENTS**

I am grateful to my research supervisor Prof. G F Fernando, who took me on to do this project and gave much support, direction, guidance and opportunity. I would also like to acknowledge my sponsors, EPSRC and TSB for funding this work.

In addition, I would like to acknowledge Dr Raj, Dr S D Pandita, Mr Mark and Dr L Wang for giving all their support, bringing new ideas and for sharing their research experience. I would like to thank Mr F Biddlestone for technical assistance, and appreciation must also go to my colleagues in the Sensors and Composites Group for their help and support during my study.

Finally, I would like to express my deepest gratitude and love for my husband, daughter and son, and to all my family members for their never-ending love, guidance and encouragement. I could not have completed this work without their support.

# CONTENTS

<b>ABSTRACT .....</b>	<b>III</b>
<b>ACKNOWLEDGEMENTS.....</b>	<b>IV</b>
<b>LIST OF FIGURES .....</b>	<b>VIII</b>
<b>LIST OF TABLES .....</b>	<b>XII</b>
<b>CHAPTER 1 .....</b>	<b>1</b>
<b>1.1 Introduction .....</b>	<b>1</b>
<b>1.2 Aims and objectives.....</b>	<b>2</b>
<b>CHAPTER 2 .....</b>	<b>4</b>
<b>2.1 Electrostatic charging of short-glass fibre bundles .....</b>	<b>4</b>
2.1.1 Principle of electrostatic charging.....	4
2.1.2 Static charges and surface charges .....	5
2.1.3 Types of electrostatic charging.....	6
2.1.3.1 Tribo or frictional charging .....	6
2.1.3.2 Contact charging .....	7
2.1.3.3 Corona Charging.....	8
2.1.3.4 Induction Charging .....	10
<b>2.2 Charge distribution on materials .....</b>	<b>11</b>
2.2.1 Dielectric materials and their properties .....	11
2.2.2 Polarization.....	16
2.2.3 Frequency Dependent Polarization .....	19
2.2.4 Dielectric Power Loss .....	20
2.2.5 Polarity of selected materials.....	21
2.2.6 Electrostatic field and electric field lines .....	23
<b>2.3 Techniques to align the fibre bundles.....</b>	<b>26</b>
2.3.1 Fibre alignment using electro-flocking .....	26

2.3.2	Electrostatic force to control the fibre alignment.....	28
2.3.3	Electrostatic fibre alignment circumferentially or vertically.....	34
<b>CHAPTER 3: EXPERIMENTAL METHODS.....</b>		<b>41</b>
<b>3.1</b>	<b>Materials .....</b>	<b>41</b>
<b>3.2</b>	<b>Instrumentation .....</b>	<b>41</b>
<b>3.3</b>	<b>Custom-designed equipment .....</b>	<b>42</b>
<b>3.4</b>	<b>Charge measuring device.....</b>	<b>43</b>
3.4.1	Instrument construction and operation .....	43
3.4.2	Instrument Calibration .....	45
<b>3.5</b>	<b>Fibre deposition and alignment device .....</b>	<b>46</b>
3.5.1	Instrument construction and operation .....	46
<b>3.6</b>	<b>Parallel Plate Capacitor.....</b>	<b>48</b>
3.6.1	Instrument construction and operation .....	48
3.6.2	Calibration .....	50
3.6.2.1	Capacitor plates calibration .....	51
3.6.2.2	Optimization of the camera .....	52
3.6.3	The motion of the fibre bundles in the electric field.....	53
3.6.3.1	Single fibre bundle.....	54
3.6.3.2	Multiple fibre bundles .....	56
3.6.3.3	Dried fibre bundles .....	56
3.6.3.4	Hydrated fibre bundles .....	57
<b>CHAPTER 4: RESULTS AND DISCUSSIONS.....</b>		<b>58</b>
<b>4.1</b>	<b>Charge measuring device.....</b>	<b>58</b>
4.1.1	Calibration of charge measuring device.....	58
4.1.2	Charge measurement on short-glass fibre bundles .....	71
4.1.2.1	Charge measurements at different voltages .....	71
4.1.2.2	Charge measurements at different electrode lengths .....	73
4.1.2.3	Charge Decay of short glass fibre bundles.....	74
4.1.2.4	Effect of surface adsorbed moisture on charging the fibre bundles .....	77

<b>4.2 Fibre bundle alignment .....</b>	<b>79</b>
<b>4.3 Parallel plate capacitor.....</b>	<b>83</b>
4.3.1 Optimization of the camera.....	83
4.3.2 The motion of the fibre bundles in the electric field .....	84
4.3.2.1 Single fibre bundle movement .....	85
4.3.2.3 Multiple fibre bundle motion in the electric field .....	94
4.3.2.4 Influence of electric field on dried fibre bundle.....	101
4.3.2.5 The study of hydrated fibre bundle motion.....	111
4.3.2.6 Graphical representation of the fibre bundle motion in the electric field ....	113
4.3.2.7 Graphical representation of the multiple fibre bundle movement .....	117
 <b>CHAPTER 5: CONCLUSIONS AND FUTURE IMPROVEMENTS .....</b>	 <b>120</b>
<b>5.1 Conclusions .....</b>	<b>120</b>
<b>5.2 Future Improvements .....</b>	<b>121</b>
5.2.1 Fibre alignment rig for pre-pegging.....	122
 <b>APPENDIX.....</b>	 <b>124</b>
 <b>REFERENCES.....</b>	 <b>138</b>

# LIST OF FIGURES

## Chapter 2:

**Figure 2- 1:** Schematic diagram of contact charging of a fibre bundle. (1) Uncharged fibre is brought up to a charged conductor; (2) as fibre approached conductor, charge separation occurs; (3) on contact separated (negative) charges are neutralised; (4) on separation fibre remains positively charged. -8-

**Figure 2-2:** Schematic representation of the charge distribution on the surface of objects of various shapes. -9-

**Figure 2-3:** Illustrating the principle of corona charging from a point. -10-

**Figure 2-4:** Parallel plate capacitor with (a) vacuum between plates, (b) dielectric material between plates and (c) electric field lines between the plates of the parallel plate capacitor is quite uniform except the edges. (d) Idealised case in which the “fringing” at the edges is ignored. -12-

**Figure 2-5:** Schematic diagram of an elementary prism of a polarized material. -17-

**Figure 2-6:** Types of polarization mechanisms in dielectric materials. -19-

**Figure 2-7:** Relaxation and resonance absorption as a function of frequency. -20-

**Figure 2- 8:** Voltage and current vectors with respect to alternating current for (a) a perfect capacitor ( $90^0$  out of phase) and (b) a real capacitor with dielectric (less than  $90^0$  out of phase).

**Figure 2- 9:** Electric field vectors for the two positive charges A and B. -21-

**Figure 2- 10:** Net electric field representation -25-

**Figure 2- 11:** Electric field line representation when two charged objects are in the electric field. -26-

**Figure 2- 12:** Schematic illustration of the EIT process to fabricate CFRP films. -28-

**Figure 2- 13:** Fibre motion in an electric field demonstrated by Kim *et al.* -29-

**Figure 2- 14:** Experimental set-up for the treated short-glass fibre (Kim *et al.*); (a) treated cotton tufts on the lower grounded electrode and (b) after applying  $-5$  kV/cm to the upper electrode: the cotton fibre bundles were aligned and moved upwards in milli-seconds, then oscillated between the electrodes. -30-

**Figure 2- 15:** Electrostatic field line between the two electrodes and direction of the movement of charged cotton fibre bundles in a uniform electric field (Kim *et al.*); -30-



**Figure 2-16:** Schematic illustration of fibre stream delivery and orientation by electrostatic field. -31-

**Figure 2-17:** Fibre alignment rig developed by Kim *et al.* -33-

**Figure 2-18:** Schematic illustration of the fibre orientation between the electrode disc (a) and lay-down process on the adhesive coated grounded electrode (b). -35-

**Figure 2-19:** Fibre distributions at different combinations of electrostatic potential and electrode distances. (a) Electrostatic potential = 10 kV, electrode distances = 20 cm, (b) Electrostatic potential = 10 kV, electrode distances = 10 cm, and (c) Electrostatic potential = 50 kV, electrode distances = 10 cm. -36-

**Figure 2-20:** Experimental set up used by Chirdon *et al.* for aligning the fibre bundles with an influence of electric field. -38-

**Figure 2-21:** Optical micrographs of E-glass reinforced composite aligned by the electric field of 0.75kV/mm with various fibre densities: (a) 1 %, (b) 5 %, (c) 10 % and (d) 25 %.

### Chapter 3:

**Figure 3-1:** Schematic illustration of the charge measurement set up. [A] Solid state electrometer, [B] BNC connector, [C] Faraday pail, [D] Positive electrode, [E] Multiple access ports, [F] Safety enclosure, [G] Positive terminal, [H] Genvolt power supply, and [I] Safety discharge probe. -43-

**Figure 3-2:** Fibre bundle deposition and alignment device: a - vibrating plate, b - solenoid, c - funnel, d - fan arrangement, e - switch to operate the fan, f - power supply to control the vibration plate, g - radial electrode, h - grounded mandrel, i - mandrel winder, j - power supply and k- safety discharge probe. -46-

**Figure 3-3:** Grid arrangement of positive radial electrode, the length ( $l$ ) of the mesh/grid was approximately 15 cm and diameter ( $d$ ) of 10 cm. -47-

**Figure 3-4:** Schematic illustration of the parallel plate set-up. This apparatus used to analyse the influence of electric field on the short-glass fibre bundles. a - positive terminal, b - upper chamber, c - positively charged capacitor plate, d - negatively charged capacitor plate, e - lower chamber, f - negative terminal, g - micrometer, h - safety discharge probe, and i - power supply -49-

**Figure 3-5:** Image analysis to investigate the capacitor plates were parallel to each other

**Figure 3-6:** (a) Schematic illustration of a fibre bundle arrangement on the bottom plate of the capacitor before charging and (b) photograph showing a fibre bundles in contact with the oppositely charged top plate of capacitor. -55-

#### Chapter 4:

**Figure 4.1:** Electrometer scale deflection at  $10^{-08}$  C sensitivity and 10 kV applied voltage with the Faraday pail orifice kept open. - 59-

**Figure 4.2:** Electrometer scale deflection at  $10^{-08}$  C sensitivity and 10 kV applied voltage with the Faraday pail orifice kept closed. -60-

**Figure 4.3:** Electrometer scale deflection at  $10^{-09}$  C sensitivity and 10 kV applied voltage with the Faraday pail orifice kept opened. -61-

**Figure 4.4:** Fluctuations on electrometer scale at  $10^{-09}$  C sensitivity and 10 kV applied voltage with the Faraday pail orifice kept close. -62-

**Figure 4.5:** Charge measurements at different voltages of 15 kV, 12.5 kV and 10 kV applied voltages. -72-

**Figure 4.6:** Charge measurement at different electrode lengths of 160 mm and 80 mm

**Figure 4.7:** Charge decay at 15 kV applied voltage -75-

**Figure 4.8:** Charge decay at 12.5 kV applied voltage -75-

**Figure 4.9:** Charge decay on the fibre bundle at 15 kV applied voltage -76-

**Figure 4.10:** Dried short-glass fibre bundles ( $\sim 0.2$  g) and ‘as-received’ fibre bundle ( $\sim 0.2$  g) from industry. -77-

**Figure 4.11:** SEM images of the cross sectional view of the single short-glass fibre bundle (a) and the enlarged view (b). -79-

**Figure 4.12:** Alignment of the short-glass fibre bundles on the mandrel. -80-

**Figure 4.13:** Degree of rotation of the focus lens with respect to the studs placed on the surface of the electrode. -84-

**Figure 4.14:** Schematic illustration to study the orientation of the fibre bundle in the following tables. -86-

**Figure 4.15:** (a) Schematic illustration of a fibre bundle placement on a grounded capacitor plate and (b) fibre bundle vertically shift vertically towards the top positive plate. -91-

**Figure 4.16:** Schematic illustration of the fibre bundle arrangement on the lower plate

<b>Figure 4.17:</b> Schematic illustration of the fibre bundle arrangement on the lower grounded plate	-98-
<b>Figure 4.18:</b> The initial moment of the fibre bundle after it was charged.	-101-
<b>Figure 4.19:</b> (a) Schematic illustration of the fibre bundle arrangement on the lower plate. All three fibre bundles are kept at the distance of 10 mm apart and (b) photograph showing the motion of the dried fibre bundles in the electric field.	-107-
<b>Figure 4.20:</b> Graphical representation of the ‘as received’ fibre bundle initial movement	
<b>Figure 4.21:</b> Graphical representation of the dried fibre bundle initial movement	-115-
<b>Figure 4.22:</b> Graphical representation of the hydrated fibre bundle initial movement	
<b>Figure 4.23:</b> Graphical representation of the fibre bundle movement between the capacitor plates.	-117-
<b>Figure 4.24:</b> Graphical representation of the multiple fibre bundle movement	-119-

## Chapter 5:

<b>Figure 5.1:</b> Flocking Process, used in textile industry to align the fabric. (a) Flock application by vibration method and (b) flock application by electrostatic method.	-123-
---	-------

## LIST OF TABLES

### Chapter 2:

<b>Table 2.1:</b> Dielectric constants of various common materials.	-15-
<b>Table 2.2:</b> List of contact electrification series that obtained from the several different literatures from the authors Diaz <i>et al.</i> and McCarthy <i>et al.</i>	-22-

### Chapter 4:

<b>Table 4.1:</b> Summary of the instrument calibration at different voltage and sensitivity ranges.	-64-
<b>Table 4.2:</b> Test observations at 15 kV applied voltage.	-65-
<b>Table 4.3:</b> Test observations at 8 kV applied voltage	-67-
<b>Table 4.4:</b> Test observations at 10 kV applied voltage	-68-
<b>Table 4.5:</b> Test observations at 13 kV applied voltage	-69-
<b>Table 4.6:</b> Summary of the electrometer scale reading at 15 kV	-70-
<b>Table 4.7:</b> Results from the electrostatic fibre bundles alignment equipment.	-81-
<b>Table 4.8:</b> Camera adjustment to focus the entire surface of the electrode	-83-
<b>Table 4.9:</b> Orientation of the single short-glass fibre bundles	-88-
<b>Table 4.10:</b> Orientation of the coloured single short-glass fibre bundles	-93-
<b>Table 4.11:</b> Orientation of the three fibre bundles	-96-
<b>Table 4.12:</b> Orientation of the three fibre bundles in the electric field	-99-
<b>Table 4.13:</b> Orientation of the dried fibre	-102-
<b>Table 4.14:</b> Orientation of the dried fibre bundle between the plates	-105-
<b>Table 4.15:</b> Orientation of the dried fibre bundle between the plates	-109-
<b>Table 4.16:</b> Differentiating the fibre bundle behavior in the electric field.	-119-

# CHAPTER 1

## ***1.1 Introduction***

The research was aimed at investigating the application of electrostatic based technique to align the short-glass fibre bundles, for manufacturing pre-forms or composites. These techniques are well-established in industry such as flocking [1] in textile industry, electrostatic precipitator [2], electrostatic filters [3], electro spraying or electrohydrodynamic atomisation [4-6] and crop spraying [7]. But the current research is to extend this technique to composite manufacturing. The composite manufacturing is based on the usage of hybrid materials consisting of reinforcing fibers in a polymer resin, which are formed to a desired shape and engineered to achieve high performance specifications. These are used extensively in areas where the weight of the structure or component is at a premium. For example, satellite communication antennas [8], aerospace components [9, 10] and automobile industry [11]. Although this gives the high performance applications, there is significant interest in developing techniques to manufacture performs where the short-glass fibres are aligned in a specified direction.

Another important aspect of this research is reduction of continuous glass fibre waste via the recycling of short-glass fibre bundles obtained by chopping continuous tows. It is generally appreciated that the mechanical properties of composites are influenced by the fibre volume fraction and the degree of alignment of the reinforcement. In comparison to the preforms made using continuous tows, the short-glass fibre bundle-based composite/preforms offer a relative ease of draping. This research investigated the influence of external electric fields on short E-glass fibre bundles and endeavours to develop

electrostatics-based techniques towards the production of short glass fibre bundle performs. Therefore, it was necessary to study and develop the techniques to charge the short-glass fibre bundles.

## ***1.2 Aims and objectives***

The overall aim of this research was to develop techniques to charge the short-glass fibre bundles via electrostatics and to investigate the degree of alignment in the electric field.

The specific aims of the research were as follows:

- (i) To investigate the optimal length of the electrode required to enable the acquisition of charge on the surface of the short-glass fibre bundles and also to measure the charge retained on the short-glass fibre bundles.
- (ii) To investigate the factors that influence the degree of alignment that can be achieved via electrostatic charging of short-glass fibre bundles.
- (iii) To develop techniques to deposit the charged short-glass fibre bundles on an adhesive substrate.
- (iv) To investigate the influence of an electric field on the short-glass fibre bundles and to capture its motion in the electric field.

This thesis consists of five chapters. The first part of the chapter two provides a theory on charging the materials. The second part provides a literature survey on the various techniques for aligning the short-glass fibre bundles. The third part presents the behaviour of dielectric materials under the influence of electrostatic force.

Chapter three presents a detailed description of the materials, instrumentation and the experimental procedures used in the study. The three main custom-designed equipments used in this study were explained in detail.

Chapter four provides details of the results obtained by the three main custom-designed equipments and their calibrations. The first part in the charge measuring devices provides the eradication of the fluctuations on the electrometer instrument. The second part gives the results obtained from this device. While in case of parallel capacitor, the first part provides the results obtained from the optimization of the camera and the second part gives the moment of the fibre bundles between the capacitor plates.

Finally, in chapter five, the overall conclusions of the research and recommendations of future work are presented.

## CHAPTER 2

The literature review is divided into three parts: (i) electrostatic charging of short-glass fibre bundles; (ii) charge distribution on materials; and (iii) techniques to align the short-glass fibre bundles.

### ***2.1 Electrostatic charging of short-glass fibre bundles***

#### ***2.1.1 Principle of electrostatic charging***

In order to align short-glass fibre bundles of specified dimensions in a desired orientation with respect to the surface of the adhesive coated substrate, the fibre bundles need to be charged and allowed to move towards the substrate via the electrostatic force of attraction. The electrostatic principle was studied in the current investigation in order to charge the fibre bundles and to align them in an electric field. For the purpose of charging the fibre bundles, the electrodes of different designs were studied in order to charge the surface of the fibre bundles through the process called ‘charge transfer’.

The charge transfer on a fibre bundle surface can be achieved by using (i) corona charging, (ii) contact charging or (iii) induction charging. The contact between the two different materials almost always results in the charge transfer. In this investigation the two materials refers to the contact between the fibre bundles and electrode. The force of interaction between the two charged bodies can be described by Coulomb’s Law [12, 13].

$$F = \frac{k(q.Q)}{d^2} \quad \text{Equation 2.1}$$



where  $q$  and  $Q$  are the magnitudes of the respective charges on the two charged bodies,  $d$  is the distance between the two charged bodies and  $k$  a constant. 'k' can be approximated to:

$$k = \frac{1}{4\pi\epsilon_0} \quad \text{Equation 2.2}$$

where  $\epsilon_0$  is the permittivity of free-space [13].

### **2.1.2      *Static charges and surface charges***

The field of Electrostatics mainly deals with the phenomenon of stationary charges i.e. the building up of an electrons on an object [14] that is confined effectively to a surface. These are called static charges, where there is no electrostatic field inside the metal. This is different from the moving electrons in a conductor, which generate an electric current. Mainly, the investigation deals with the static charges which were made to move by surface charging via contact electrification process.

The surface of an object (insulator) can be electrified if it comes in intimate contact with another charged metal. When the surface of an object is found to be electrified, this means there must be an excess of electrons or protons [15]. This object can be either negatively or positively charged. If the material is said to be negatively charged (anions), this means that the excess electrons may be free and mobile. If there are fewer electrons, when compared to the protons, then the object is said to be positively charged. It seems likely that, electrons are passing between the charged metal and the surface of an object, which is said to be contact electrification. But, when the surface has acquired an electric charge, numerous questions arise, such as: (a) whether electrons or ions were transferred [16] (b)

why they moved and (c) whether at some point while charging, transfer must come to an end (i.e. breakdown occurs). An understanding of all these processes provides the appropriate background of the quantum theory of solid states. But, for this project, the classical electrical theory will be sufficient for the experimental investigation.

There are different techniques for transferring the charge between an insulator and a metal.

### ***2.1.3 Types of electrostatic charging***

The process of charging can be divided into:

- (i) Tribo or frictional charging.
- (ii) Contact charging.
- (iii) Corona charging.
- (iv) Induction charging.

#### **2.1.3.1 Tribo or frictional charging**

The tribo or frictional charging results in a transfer of electrons between two objects which are rubbed together [17]. In the context of this investigation, the frictional charging relies on the friction between the fibre bundles and an appropriate dielectric material, which is used for rubbing. However, the considerations of fibre damage due to rubbing alone are sufficient to rule this out, as a practical method for fibre charging.

### 2.1.3.2 Contact charging

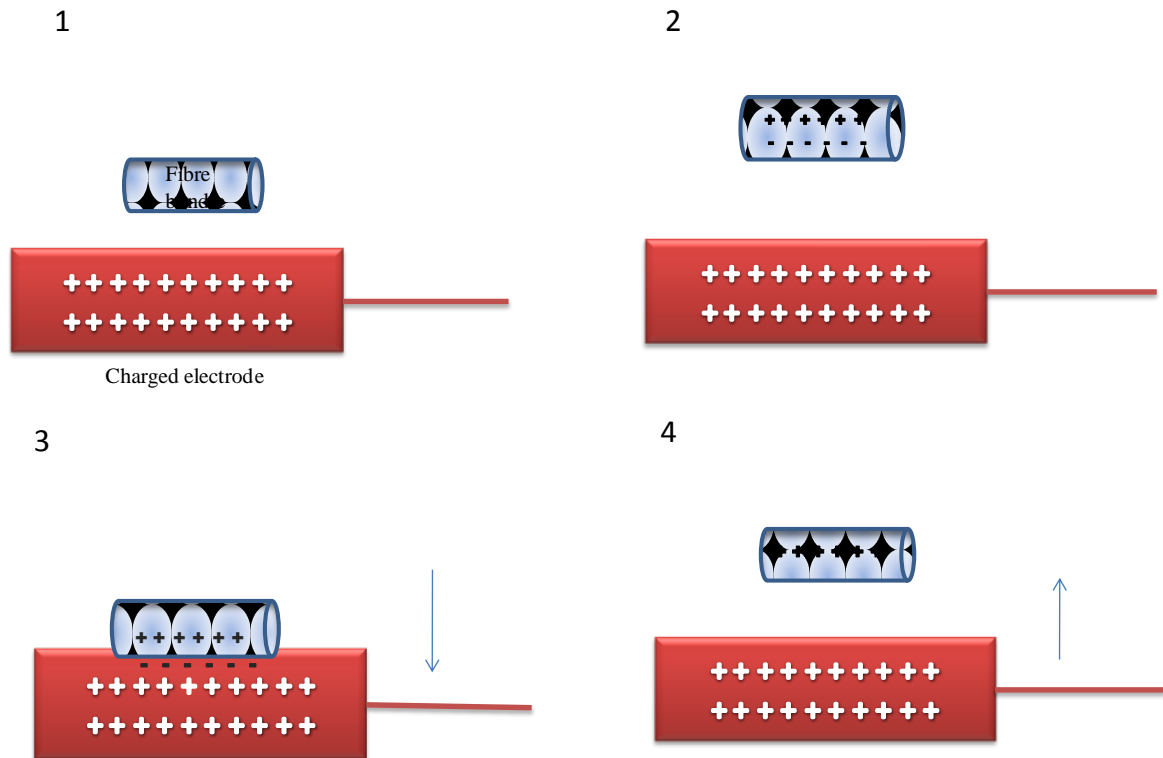
Contact charging involves bringing the fibre bundles into an intimate contact with a charged electrode with a known potential. The charged electrode may be in one of several forms – cylindrical (pin), plate or roller. As shown in the Figure 2-1, the contact between surfaces results in the transfer of charges as electrons to match up energy levels of neighbouring atoms around the point of contact. The flow of charge continues until it is inhibited by the potential difference of the ‘contact potential’ of the surfaces. On separation, the surfaces may retain the transferred charges.

Even highly dielectric (insulating) materials have some ability for the migration of electrons, the rate at which this occurs being related to their relaxation time [18]. This is inversely proportional to the material conductivity, and in its basic form can be given as [19]:

$$\tau = \varepsilon_0 \varepsilon_1 / \sigma \quad \text{Equation 2.3}$$

where  $\tau$  is the relaxation time,  $\varepsilon_0$  and  $\varepsilon_1$  are the absolute and relative permittivity respectively and  $\sigma$  the material conductivity.

The process of contact charging of a fibre bundle is illustrated in Figure 2-1.



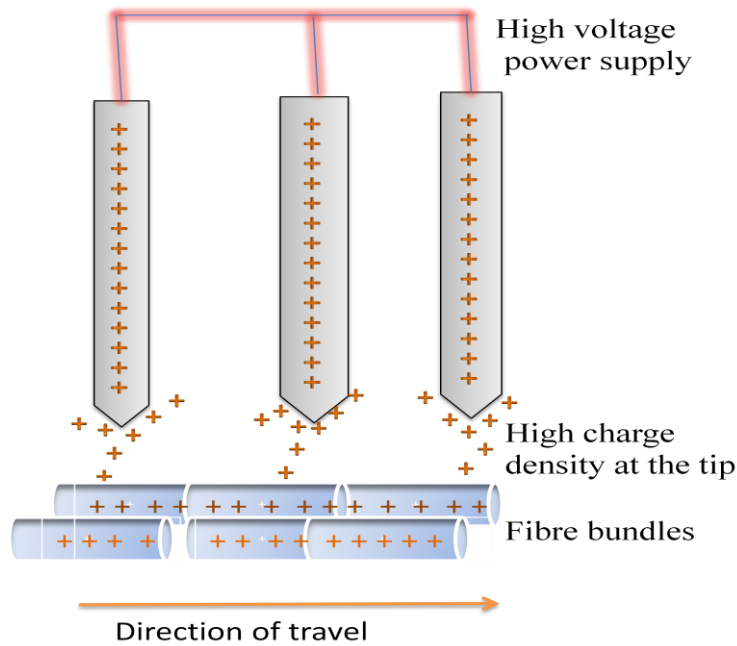
**Figure 2- 22:** Schematic diagram of contact charging of a fibre bundle. (1) Uncharged fibre is brought up to a charged conductor; (2) as fibre approached the conductor, charge separation occurs; (3) on contact, separated (negative) charges are neutralised; (4) on separation, fibre remains positively charged.

The contact charging is the method used in the electro-flocking techniques [20] for charging and aligning the fabric materials.

### 2.1.3.3 Corona Charging

The corona charging method can also be used to charge the polymers (fibre bundles) [21]. The charge distribution on the surface of various shapes of electrodes depends upon their geometry. As shown in Figure 2-2, the sphere (1) has an even distribution, so it is said to have an equipotential surface. Meanwhile, the pear-shaped object (2) shows the charge accumulating preferentially at the small radius end. The pin shaped electrode (3) shows the





**Figure 2-24:** Illustrating the principle of corona charging from a point [12, 13].

#### 2.1.3.4 Induction Charging

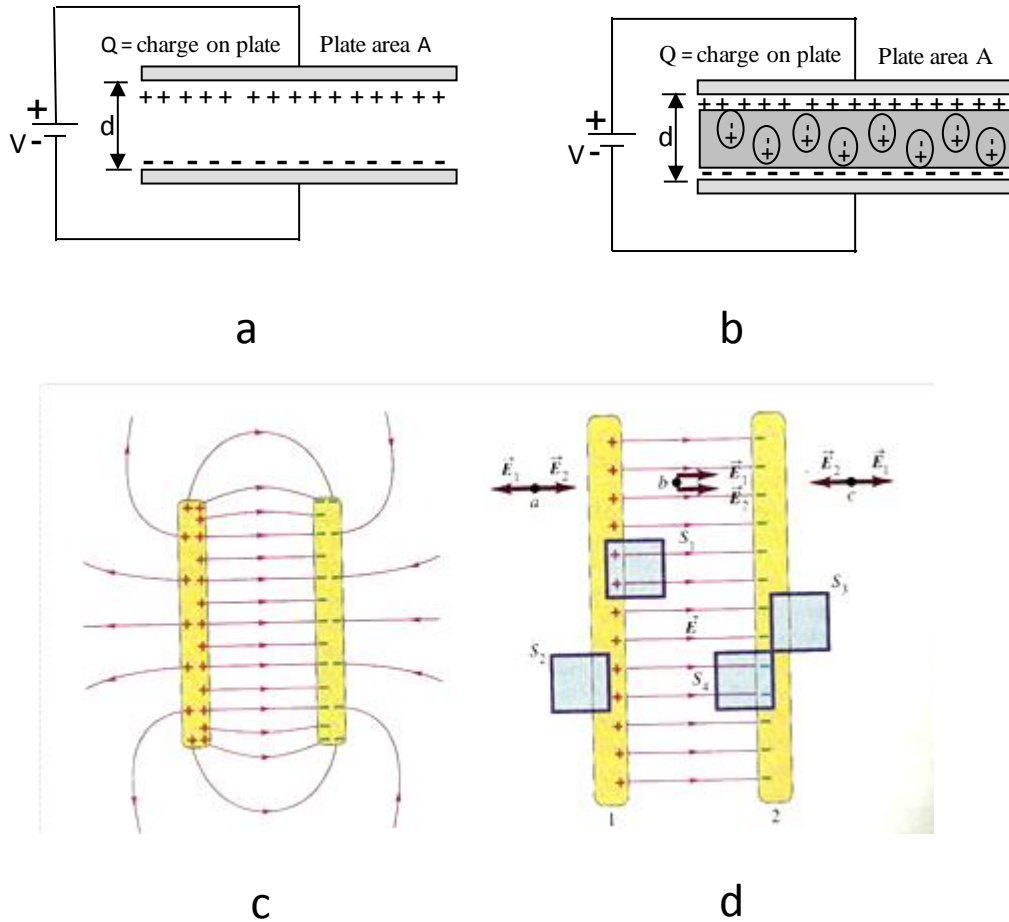
Induction charging is a method used to induce charge on an object without actually touching the electrode. This process is very successfully used in applications such as crop spraying [24], where pre-atomized droplets are charged to make them attractable to their targets. Induction charging is generally considered to be applicable primarily to conductive materials, as the process relies critically on charge separation and migration. Its application to charge the fibre bundles is very poorly understood, but the few published papers [25, 26] suggest that it may prove worthy of pursuit, whereas in case of E-glass fibre bundles, the high resistivity may cause complications. Therefore, the induction charging is sufficient for ruling out this particular investigation of charging short-glass fibre bundles.

## **2.2 Charge distribution on materials**

### **2.2.1 Dielectric materials and their properties**

Dielectric materials are known as insulators and can be defined as the materials with high electrical resistivities [27]. The polar molecules in the dielectric materials are randomly arranged when no electric field is applied. An applied electric field will polarize the material by orientating the dipole moments of polar molecules and other species.

The interaction of a dielectric material with an electric field can be explained in terms of a parallel plate capacitor. Consider a pair of conducting plates with plate area  $A$ , placed parallel to each other and separated by a distance  $d$  (see Figure 2-4).



**Figure 2-4:** The parallel plate capacitor with (a) vacuum between plates, (b) dielectric material between plates and (c) electric field lines between the plates of the parallel plate capacitor is quite uniform except the edges. (d) The idealised case in which the “fringing” at the edges is ignored [12, 13].

The capacitance  $C$  between the plates can be found by knowing the electric field lines ( $E$ , equation 2.8) between the plates. The real capacitor plates are finite in size. Thus, the electric field lines at the edges of the field are not straight lines (see Figure 2-4 C). The field line bulges out at the edges of the plates and field lines are not contained entirely between the plates. This is called ‘edge effects’, with the non-uniform field near edge of the capacitor plates, which are called ‘fringing fields’. In the Figure 2-4, the field lines are drawn by taking the edge effects into consideration. However, an assumption can be made



with reference to an idealized situation (d) where the field lines between the plates are straight lines. Since, when the electric field is applied to parallel plates with a vacuum in between, the electric field  $E$  is given by [13]:

$$E = \frac{\sigma}{\epsilon_0} \quad \text{Equation 2.8}$$

where  $\sigma$  is charge density and  $\epsilon_0$  is permittivity of free space by  $8.854 \times 10^{-12}$  C.

The capacitance  $C$  increases when the space between the plates or conductors is filled with dielectrics. To analyze how this happens, consider the capacitance  $C_0$  when no dielectrics material is inserted between the plates.

When a dielectric material is inserted between the plates, the capacitance increases to [13]:

$$C = K C_0 \quad \text{Equation 2.9}$$

where  $K$  is called the dielectric constant.

The capacitance of the parallel plate can be shown by [13]:

$$C = \frac{Q}{V} \quad \text{Equation 2.10}$$

where  $Q$  is the charge on plate and  $V$  is voltage applied.

$$V = Ed \quad \text{Equation 2.11}$$

$$\sigma = \frac{Q}{A} \quad \text{Equation 2.12}$$

so those for parallel plate capacitor with vacuum:

$$C = \frac{\sigma A}{Ed} = \frac{Q}{V} = \frac{\epsilon_0 A}{d} \quad \text{Equation 2.13}$$

where  $\sigma$  is the charge density,  $A$  is the area of the plates,  $E$  is the electric field,  $d$  is the distance between the plates and  $\epsilon_0$  is permittivity of free space ( $8.854 \times 10^{-12}$  C).

From the above Equation 2.13; it can be seen that capacitance  $C$  depends only on the geometric factors of  $A$  and distance  $d$  between the capacitor plates. Furthermore, the capacitance  $C$  increases linearly with the area ( $A$ ) of the plates for an applied voltage ( $V$ ); that is, a bigger plate can hold more charge. In contrast,  $C$  is inversely proportional to  $d$ ; that is, the smaller the distance  $d$  between the capacitor plates, the applied voltage ( $V$ ) between the capacitor decreases.

However, the expression in Equation 2.13, i.e. the capacitance ( $C$ ) is only valid if the region between the plates is a vacuum and for air [12, 13], because the dielectric constant  $K$  is for vacuum is 1 and for air is 1.00059. If another material such as glass is placed between the parallel capacitor plates, the capacitance ( $C$ ) of the capacitor must have increased by a factor  $K$  (see equation 2.15), where  $K$  is a dielectric constant. The expression below shows the capacitance  $C$  of the dielectric-filled capacitor is,

$$C = \frac{\epsilon A}{d} \quad \text{Equation 2.14}$$

where,

$$\epsilon = K \epsilon_0 \quad \text{Equation 2.15}$$

where,  $\epsilon$  is the permittivity of the dielectric material between the plates and this is always greater than the permittivity of a vacuum  $\epsilon_0$  and  $K$  is the dielectric constant. The table below shows the dielectric constant of the various materials.

Table 2.1: Dielectric constants of various common materials [12, 13].

<i>Material</i>	<i>K</i> <i>(dielectric constant)</i>
Vacuum	1
Air	1.00059
Water	80
Paper	3.5
Glass fibre	4.86
Teflon	2.1

The dielectric constant of the other materials like glass or plastic can be investigated experimentally. First, start with charging the parallel plate capacitor, whose plate is separated by the vacuum gap [12, 13], and measure the voltage difference  $V_0$  between the plates using a voltmeter. Secondly, place a glass fibre-bundle between the parallel plate capacitor and measure the voltage difference, let it be  $V$ . The voltage ratio  $V_0/V$  is  $K$ , the dielectric constant.

Therefore, when an insulating material is placed between the capacitor plates, the capacitance of the device increases by a factor  $K$ . Whereas,  $K$  varies from material to material, few sample values are given in Table 2.1. The air-filled capacitor is

indistinguishable by the vacuum-filled capacitor, because K for air is only 0.06 percent greater than K for a vacuum.

However, when a dielectric material is introduced between the plates under a certain applied voltage, the electric dipole moments orientate. Positive charges move towards the negative end of the electric field and negative charges move towards the positive end of the electric field (Figure 2-4 b). This will reduce the effective electric field between the plates. The effective electric field can be given by [28]:

$$E_{effective} = E - E_{polarization} = \frac{\sigma}{\epsilon_r \epsilon_0} \quad \text{Equation 2.16}$$

where  $\epsilon_r$  is the relative permittivity of material

The capacitance for the dielectric inserted parallel plate capacitor can be given by [12]:

$$C = \frac{\epsilon_r \epsilon_0 A}{d} \quad \text{Equation 2.17}$$

The parallel plate capacitor capacitance increased by factor of  $\epsilon_r$ .

Bergman *et al.* [29] in their paper explained the detailed modeling for obtaining the dielectric constant of a composite material.

### **2.2.2 Polarization**

When an electric field is applied to ideal dielectric materials there is no resultant charge transportation but the electric dipole orient so that the dielectric acquires a dipole moment,

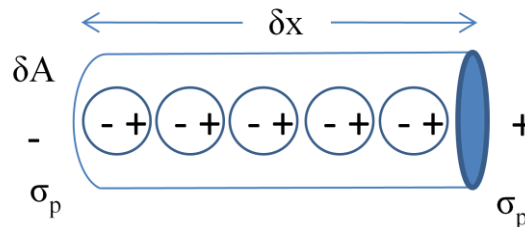
resulting in the dielectrics becoming polarized [30]. The dipole moment  $p$  of the two equal and opposite charges separated by distance  $\delta x$  is given by [12, 13]:

$$p = \delta x \quad \text{Equation 2.18}$$

From this, polarized material can be thought to be made of “elementary dipole prisms” (Figure 2-5), and the end surfaces carry charge densities of  $+\sigma_p$  and  $-\sigma_p$  induced by the electric field. “The dipole moment per unit volume of material is termed as the polarization  $P$  and this can vary from region to region” [12, 13] and is given by:

$$\frac{\delta p}{\delta v} = p = \sigma_p \quad \text{Equation 2.19}$$

where  $\sigma_p = n \times P$ ,  $n$  is unit vector normal to the surface enclosing the polarized material and directed outwards from the material.



**Figure 2-5:** Schematic diagram of an elementary prism of a polarized material (after Moulson and Herbert [27]).

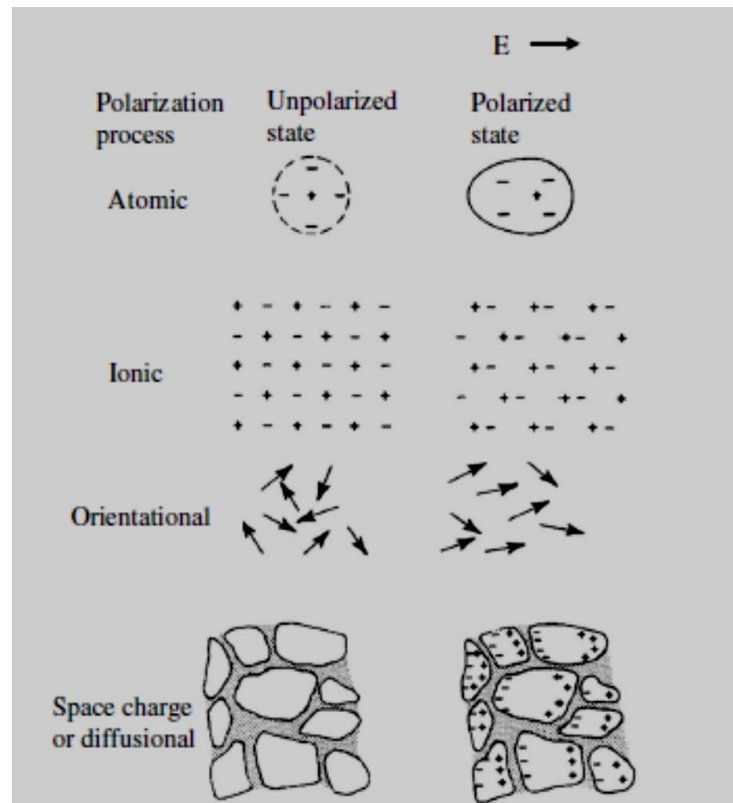
Various factors contribute to the net polarization in dielectric materials. They are summarized below. Schematic representation of the polarization mechanism is shown in Figure 2-6.

- i. Atomic Polarization: This occurs in all materials with respect to the applied electric field  $E$ , and as a result there will be a small displacement of electrons away from the nucleus of atoms [27, 31].

- ii. Ionic Polarization: This is found in ionic materials, resulting from the displacement of cations and anions sub lattices [32].
- iii. Orientational Polarization: This is observed in many organic materials such as polymers. The applied electric field reorients the dipolar molecules in the direction of the field applied [27].
- iv. Space Charge Orientation: Here there will be a small transport of charge carriers until they come in contact with grain boundaries. The mechanism is only important up to 1000 Hz [27].

The resultant average polarizability for a dielectric is the sum of the four polarizabilities - atomic, ionic, orientational and space charge polarization (Equation 2.18).

$$P_{avg} = \alpha_a E_a + \alpha_i E_i + \alpha_o E_o + \alpha_s E_s \quad \text{Equation 2.20}$$

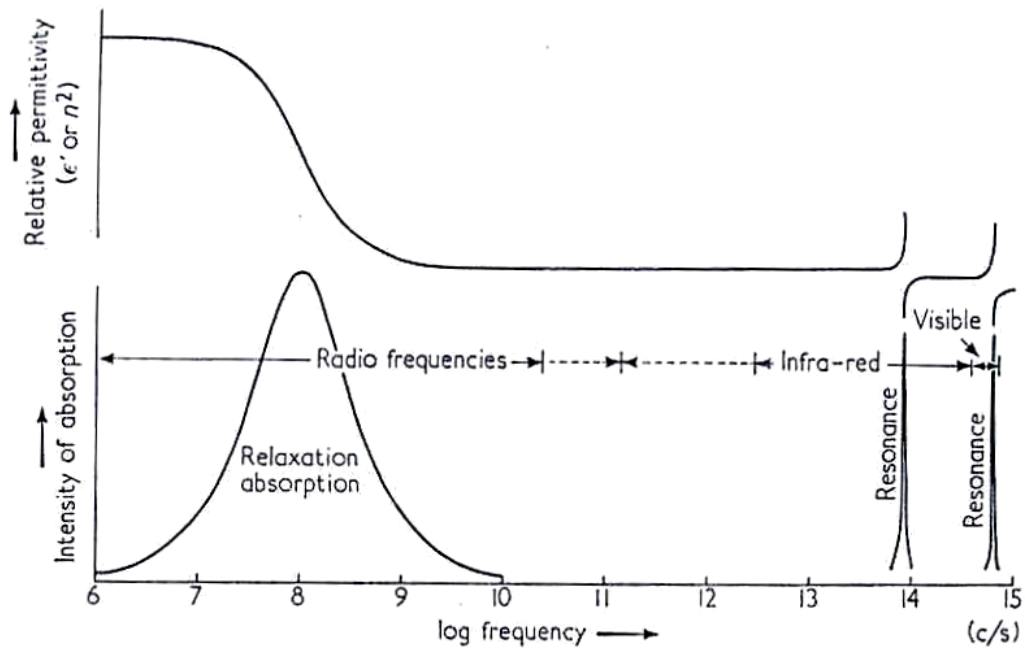


**Figure 2-6:** Types of polarization mechanisms in dielectric materials (Moulson and Herbert [27]).

### 2.2.3 Frequency Dependent Polarization

If a low frequency alternating electric field is applied to a dielectric, the dipoles (Figure 2-7) can rotate with the applied field [33]. If the frequency is increased beyond a critical value, some dipoles will have difficulty in following the field and polarization might not have enough time to gain its value before the field reverses. In this frequency range relative permittivity decreases [33], this is associated with loss or absorption of electric energy which causes heating in the dielectric [33]. The absorption associated with the different types of polarization (Figure 2-6) occurs at different frequencies of the electromagnetic spectrum. Figure 2.20 shows the frequency dependence, absorption and relative permittivity for a model dielectric having all 4 types of polarizations. The atomic and ionic polarizations are observed as large restoring forces with small damping effects,

which lead to the resonance absorptions (Figure 2-7). In contrast, the resistance to orientational motion is the same as the damping effect for space charge polarization, resulting in relaxation type absorption.



**Figure 2-725:** Relaxation and resonance absorption as a function of frequency (Meakins *et al.* [33]).

## 2.2.4 Dielectric Power Loss

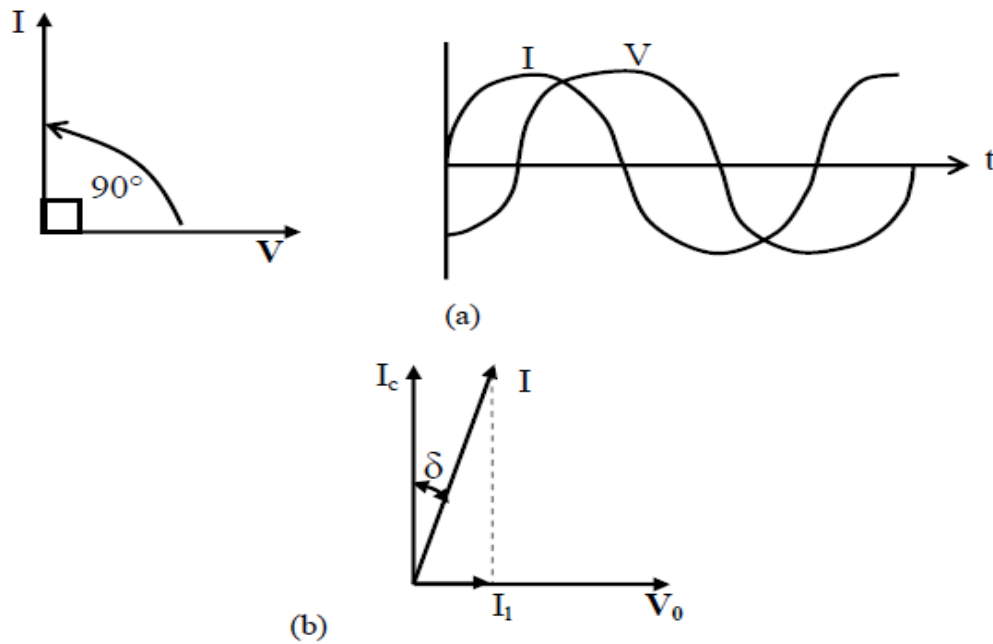
Dielectric losses are important and can limit the applications of the materials. When an electric field applied, electric energy is dissipated during dipole reorientation because the motion is opposed by the frictional forces and some of the energy of the fields is converted into heat in the dielectric material; this effect is known as dielectric loss.

When an alternating current is applied to a perfect capacitor, an AC current will flow and the current (I) leads the voltage (V) by  $90^{\circ}$  (Figure 2-8). If a polar dielectric of relative



permittivity of  $\epsilon'$  and dielectric loss factor  $\epsilon''$  is introduced into a capacitor the displacement current (I) will lead the voltage (V) by less than  $90^\circ$  as shown in Figure 2-8

b. There will be no small current component in phase with the voltage which is called the “charging current”.



**Figure 2-8:** Voltage and current vectors with respect to alternating current for (a) a perfect capacitor ( $90^\circ$  out of phase) and (b) a real capacitor with dielectric (less than  $90^\circ$  out of phase) [12, 13].

### 2.2.5 Polarity of selected materials

As mentioned in the previous sections, two objects/ material surfaces result in charge transfer when brought in intimate contact. The process is also known as contact electrification. Table 2.2 shows the list of the polarity of materials when charged by contact electrification. This list was obtained from various published papers and books by Diaz *et al.* and McCarthy *et al.* [34, 35].

**Table 2.2:** List of contact electrification series that obtained from the several different literatures from the authors Diaz *et al.* [35] and McCarty *et al.* [34].

(+)	Glass
<i>More</i>	Mica
<i>positive</i>	Polyamide (Nylon 6,6)
	Rock salt (NaCl)
	Wool
	Fur
	Silica
	Silk
	Aluminium
	Poly (vinyl alcohol) (PVA)
	Poly (vinyl acetate) (PVAc)
	Paper
	Cotton
	Steel
	Wood
	Amber
	Poly (methyl methacrylate) (PMMA)
	Copper
	Silver
	Gold
	Poly (ethylene terephthalate) (Mylar)
	Epoxy resin
	Natural rubber
	Polyacrylonitrile (PAN)
	Poly (bisphenol A carbonate) (Lexan, PC)
	Poly(vinylidene chloride) (Saran)
	Polystyrene (PS)
	Polyethylene (PE)
<i>More</i>	Polyethylene (PE)
<i>Negative</i>	Poly(vinyl chloride) (PVC)
(-)	Polytetrafluoroethylene (Teflon, PTFE)

To understand the behaviour of the fibre bundles in the electric field, point charge in the electrostatic field and electrostatic field lines are considered.

### 2.2.6 *Electrostatic field and electric field lines*

The electric field (E) is defined as the electric force (F) per unit charge (q) on any given test charge located within the electric field. It is given by [36, 37]:

$$E = \frac{F}{q} \quad \text{Equation 2.21}$$

where E is the electric field in N/C or volts/m, F is the electric force in Newtons and q is the charge in Coulombs. The direction of the field is taken to be the direction of the force it would exert on a positive charge. The electric field is radially outward from a positive charge and radially in-ward to a negative point charge.

The electric field of a point charge can be obtained from Coulomb's law, the Equation 2. 1 can be approximated to the electric field of a point charge E [36].

$$F = \frac{k(q.Q)}{d^2} \quad \text{Equation 2.22}$$

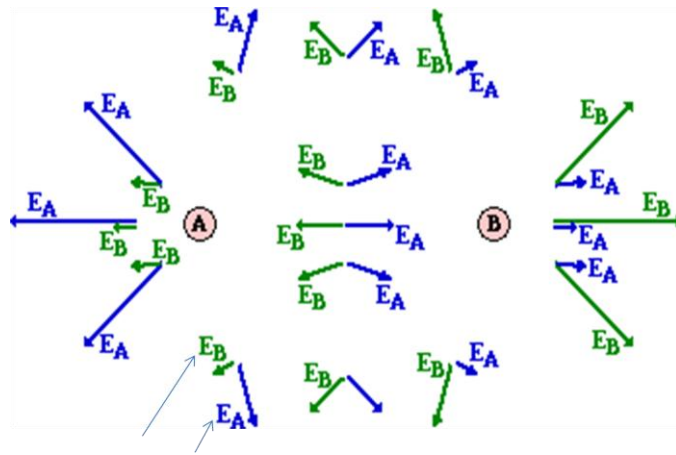
$$E * q = \frac{k(q.Q)}{d^2} \quad \text{Equation 2.23}$$

The electric field of a point charge is given by:

$$E = \frac{k.Q}{d^2} \quad \text{Equation 2.24}$$

where  $E$  is the electric field of a point charge in N/C or volts/m,  $Q$  is the magnitude of the charged body in Coulombs;  $d$  is the distance between the two charged bodies and  $k$  a constant.

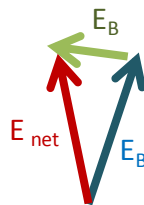
By considering the positive charge as a fibre bundle placed in the electric field, it can be said that the force exerted on the fibre bundle depends upon where the fibre bundle was placed in the electric field. Let's suppose that there are two positive charges / fibre bundles - charge A ( $Q_A$ ) and charge B ( $Q_B$ ) - in a given region of space. Each charge creates its own electric field. At any given location surrounding the charges, the strength of the electric field can be calculated using the expression  $kQ/d^2$  (see Equation 2.1). Since there are two charges, the  $kQ/d^2$  calculation would have to be performed twice at each location - once with  $kQ_A/d_A^2$  and once with  $kQ_B/d_B^2$  ( $d_A$  is the distance from that location to the center of charge A and  $d_B$  is the distance from that location to the center of charge B). The results of these calculations are illustrated in the diagram below with electric field vectors ( $E_A$  and  $E_B$ ) drawn at a variety of locations. The strength of the field is represented by the length of the arrow and the direction of the field is represented by the direction of the arrow.



Electric field vectors

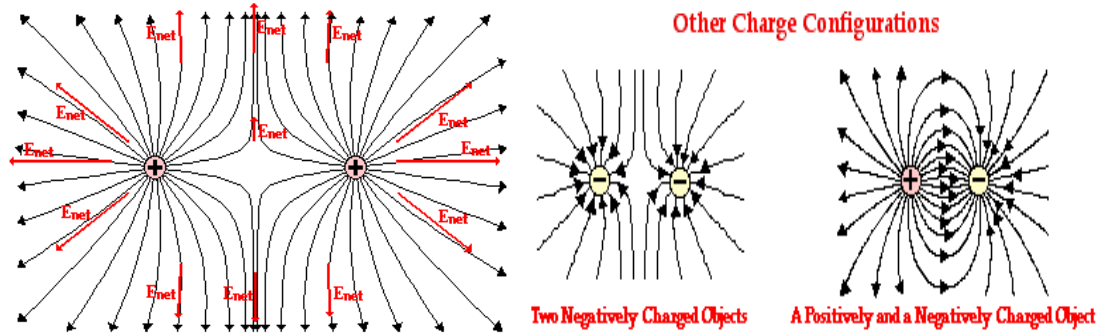
**Figure 2-9:** Electric field vectors for the two positive charges A and B. [13]

The magnitude and direction of the electric field at each location is simply the sum of the electric field vectors ( $E_A$  and  $E_B$ ) for each individual charge. That is, they can be added in head-to-tail fashion in order to determine the resultant or net electric field ( $E_{net}$ ) vector at each location (see Figure 2-10).



**Figure 2- 10:** Net electric field representation.

Figure 2-11 represents the electric field lines when two positively charged bodies are placed in an electric field. Similarly, in other charge configurations the field lines direct radially in towards negative point charges. Whilst in the case of two positively charged bodies, the field lines are radially outward from the positive charge.



**Figure 2- 11:** Electric field line representation when two charged objects are in the electric field [13].

Kim *et al.* [38] proposed the method to understand the electric field lines and to control the fibre alignment using electrostatic force. The critical review of their papers is summarised in the next section.

### **2.3 Techniques to align the fibre bundles**

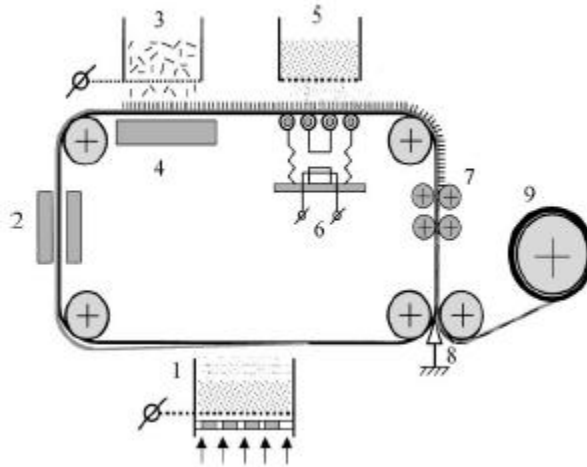
The following section presents an overview of the use of electrostatics based techniques to orientate the short-glass fibre bundles.

#### **2.3.1 Fibre alignment using electro-flocking**

The electro-flocking technique is the process of attracting short-fibres to an adhesive-coated surface. Usually, in a flocking machine [39], the "flock" is given a negative charge whilst the substrate is earthed. Flock material flies vertically onto the substrate, attaching to previously applied adhesive. A number of different substrates can be flocked including; textiles, fabric [1], woven fabric, paper, polyvinyl chloride (PVC), glass [40], sponge, toys

and automotive plastic. The flocking process is used on items ranging from consumer goods to products with high technology military applications [41].

The electro-flocking technique could also be applied to polymer composite technology as it allows the fabrication of a layer of aligned fibre bundles on different substrates. Mironov and Park reported the fabrication of a fibre reinforced polymer composite film by using an electro-flocking technique [39]. In their study, high-modulus carbon fibre (HMCF) with a diameter of 7  $\mu\text{m}$  and the length of 2 mm and low-modulus carbon fibre (LMCF) with a diameter of 6.4  $\mu\text{m}$  and a length of 2-5 mm were used. Three thermoplastic polymer powders: high-density polyethylene (HDPE), polypropylene (PP) and polycarbonate (PC), with a particle size less than 0.32.27 mm were used as matrices. The composite films were fabricated by electron-ion technology (EIT), which was based on the principles of electron-ion charge and mass transfer as well as the interaction of polymer with discrete fibre bundles in a high electric field. A schematic illustration of the EIT process is shown in Figure 2-12. Initially, a thin layer of polymer powder was electrostatically coated onto an intermediate substrate in the spaying chamber (1 in Figure 2-12). Then, it was melted in an oven (2) to form a sub-layer with the thickness of 0.1-0.3 mm. The short-fibre bundles were then deposited onto the molten polymer layer in a highly intensive electric field applied between the hopper (3) and the substrate. The polymer layer was heated with an infrared heater (4). The polymer powder in the chamber (5) was then deposited into the fibre layer using a controlled vibration method. In order to obtain uniform thickness and homogeneity of the materials, the polymer layer was vibrated (6). The film was thermo-formed between the heated rollers (7) and was then separated using a knife (8). Finally, it was wound onto a drum (9). The resulting film had a thickness of 0.1-0.4 mm.



**Figure 2-12:** Schematic illustration of the EIT process to fabricate CFRP films [39].

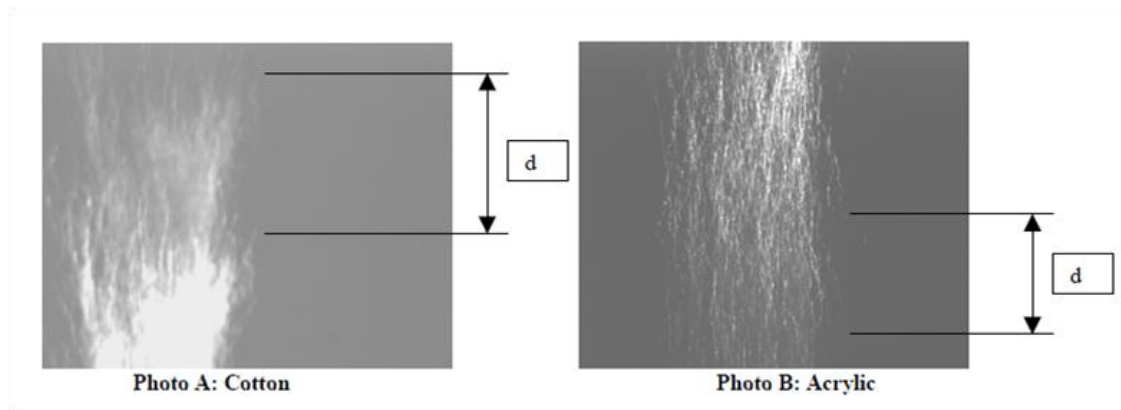
The tensile strength of the composite with a variety of LMCF content was measured. The tensile strength of HDPE/LCMF showed the peak value at about 10 wt%, whereas, the tensile strength of PP/LCMF film decreased with increasing LMCF content. This was said to be due to the different adhesion interaction between polymer and LMCF. The resistivity of HDPE/LCMF films as a function of LMCF content showed a minimum value at 20 wt% of LMCF. The decrease in strength and resistivity could be due to the increase of porosity in the film owing to poor spreading of polymer melt or incomplete wetting.

### 2.3.2 *Electrostatic force to control the fibre alignment*

Kim *et al.* [38, 42] proposed the use of electrostatic force to control fibre orientation and to generate low-weight structured webs. Kim *et al.* [42] studied the difference between the treated (fibre with conductive finish) and untreated fibre bundles. Initially, they examined three untreated fibre bundles. The fibre bundles used for the analysis were cotton, polyester and acrylic, which were placed on the surface of the bottom electrode. All these



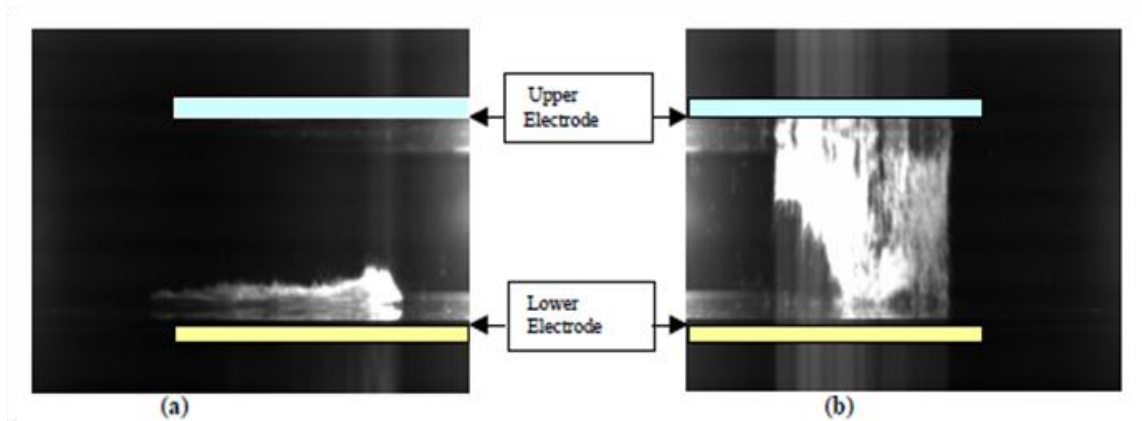
three fibre bundles had different surface conductivity. It was found that the surface conductivity of the acrylic was  $5.0 \times 10^{+09} \Omega$ , cotton was  $2.0 \times 10^{+10} \Omega$  and that of polyester was larger than  $2.0 \times 10^{+12} \Omega$ . It was determined that, the charge transfer by contact charging was comparatively low in the case of polyester when compared to the cotton. Because of the lower charge acquisition on the surface of the polyester fibre bundles, movement of these fibre bundles in the electric field was not observed. In the case of cotton and acrylic fibre, the charge acquisition was found to be large as stated in this paper; therefore, the movement of fibre bundles in the electric field was 1-2 m/sec. From Figure 2.6, it was observed that the movement of the cotton fibre bundles in the electric field was larger than the movement of the acrylic fibre. It was inverteors concluded from this experiment that a conductive coating was required to control the fibre orientation and its movement in the electric field.



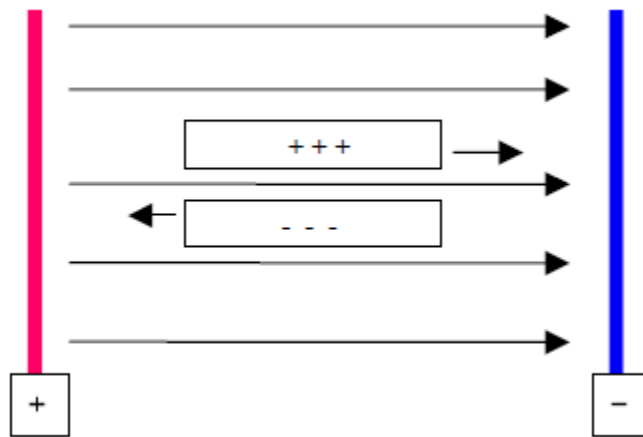
**Figure 2-13:** Fibre motion in an electric field demonstrated by Kim *et al.* [42].

Thereby, after the application of a conductive coating on the fibre bundles and by placing them on uniform electrostatic field, it was found that the fibre bundles with a conductive coating were orientated perpendicular to the potential line and moved along the field line in an electrostatic field (see Figure 2-15). Figures 2-14 (a and b) also shows the treated cotton fibre in contact with the lower electrode and after the voltage was applied

respectively; fibre bundles are orientated and transported to the upper electrode. That is, after applying the voltage of -5 kV/cm to the electrodes the cotton fibre bundles moved in milli-seconds towards the upper electrode.



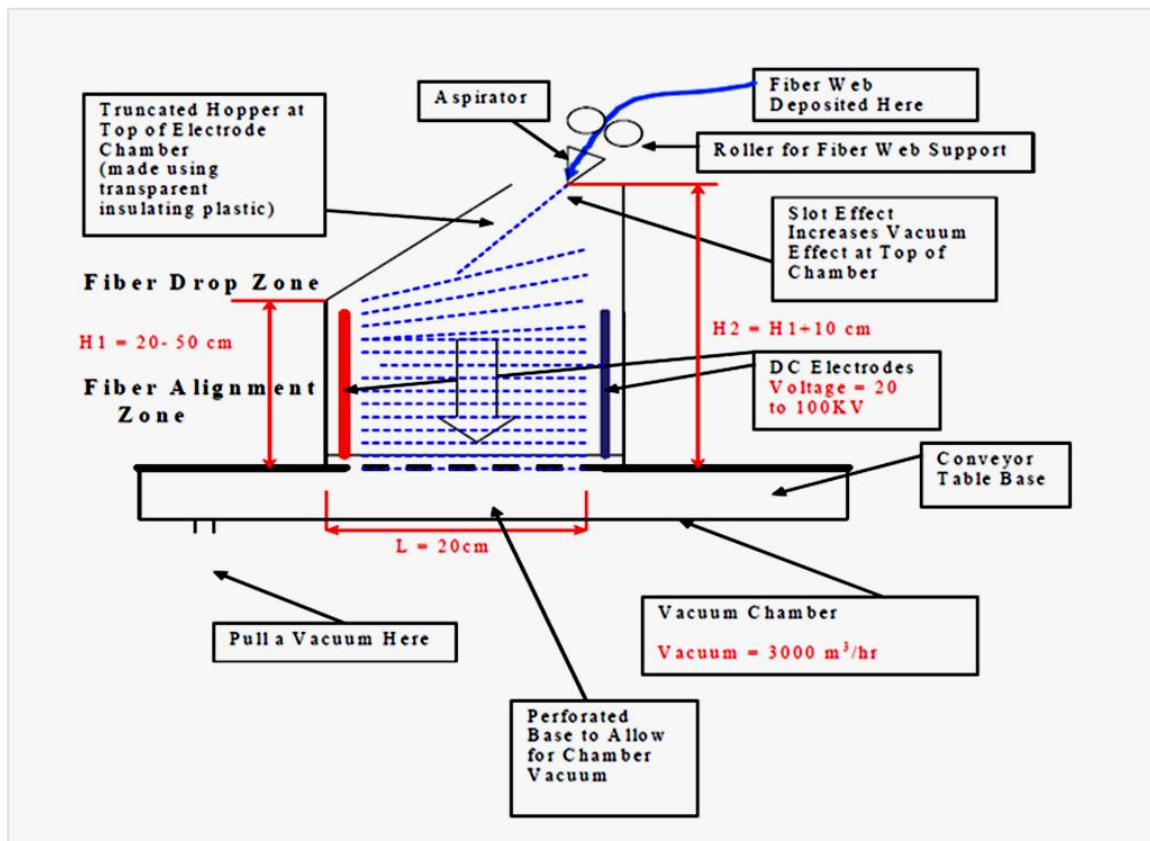
**Figure 2-14:** Experimental set-up for the treated short-glass fibre (Kim *et al.* [42]); (a) treated cotton tufts on the lower grounded electrode and (b) after applying -5 kV/cm to the upper electrode: the cotton fibre bundles were aligned and moved upwards in milli-seconds, then oscillated between the electrodes.



**Figure 2-15:** Electrostatic field line between the two electrodes and direction of the movement of charged cotton fibre bundles in a uniform electric field (Kim *et al.* [42]);

The direction of the movement of the charged fibre with respect to the field line was shown in the Figure 2-15. The significant forces acting on the charged fibre in a uniform

electric field are charge forces and air drag. This makes the fibre bundles in the uniform field move in the particular direction. The equation of the movement for the fibre in the uniform field was derived from the work of Kim *et al.* [42]. By knowing this equation, fibre movement in the uniform electric field can be controlled.



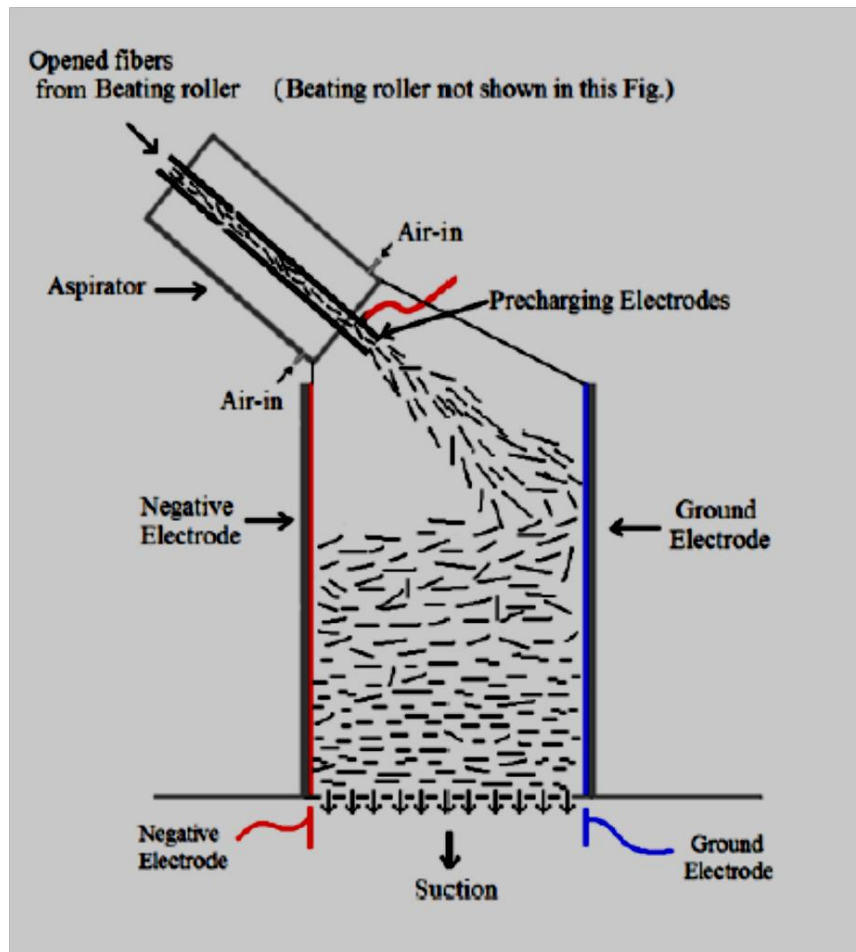
**Figure 2-16:** Schematic illustration of fibre stream delivery and orientation by electrostatic field [42].

Based on their previous studies, Kim *et al.* developed the model to deliver the fibre bundles into the fibre alignment zone and to orientate /align the fibre bundles between the electrodes (see Figure 2-16). Fibre bundles are charged by the inner aspirator nozzle electrode that is connected with the high negative voltage before it enters into the fibre alignment zone. The charged fibre was delivered into the fibre alignment zone (between two electrodes) via the roller and an aspirator. The negatively charged fibre stream enters

the zone at an angle of  $0-5^\circ$  to the horizontal electric field line as shown in the schematic illustration. It was stated in the paper that the orientation of the fibre stream will depend on electrostatic field lines, in the electric field. That is, the fibre stream follows the direction of the electrostatic field lines. The electrode setup and fibre stream delivery aspirator were installed on a table with a vacuum conveyor belt. The aligned fibre web formed on the conveyor belt will roll over via the conveyor table.

They also developed numerical models for predicating the movement of the fibre bundles in electrostatic fields. The models were developed and processed using finite element analysis software package called ANSYS. It was found that the incident angle of the fibre played an important role in its alignment and movement within the electric field. However, it was said that the fibre stream was still aligned to the electrostatic field lines even with a different incident angle under a strong electrostatic force. Fibre orientation distribution was calculated and it was found that major fractions of fibre stream were oriented along the electrical field line direction.

Therefore, the system illustrated in Figure 2-16 controlled the fibre orientation with respect to an electrostatic field line. It is said that several sets of electrodes and feed stations were needed if a different pattern of fibre stream alignment is required.



**Figure 2-17:** Fibre alignment rig developed by Kim *et al.* [43].

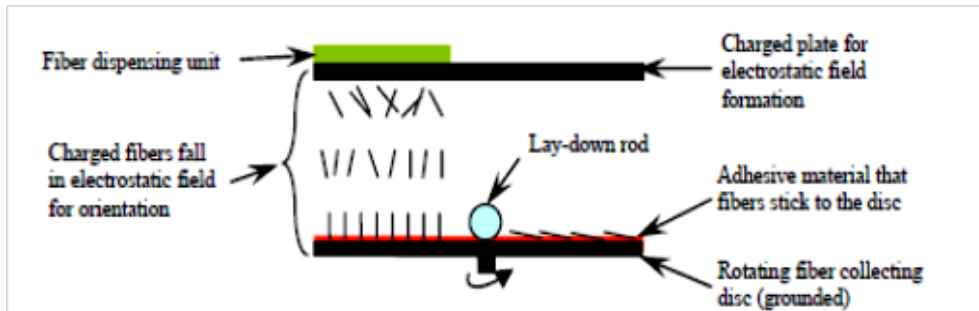
The schematic shown in Figure 2-17 was similar to the Figure 2-16 with slight modification in the aspirator and vacuum table. The above system had the aspirator with pre-charging electrodes, the electrode box having two parallel electrodes, the vacuum table with two bottom electrodes and the fibre feed system. The parallel plate electrodes are made up of polished aluminium surface to enable easy sliding of the fibre bundles and the sharp edges of the parallel plate are grounded to avoid the corona at high voltages. To avoid the charge leakage and for the purpose of insulation, plates were glued to polycarbonate sheet by using an epoxy resin. In between the plates, the flow of charged and polarised fibre bundles from the aspirator was aligned in terms of the electrostatic field lines in an electric field.

For the purpose of pre-charge the fibre bundles; the aspirator was designed to have precharging electrodes (see Figure 2-17) before the fibre bundles entering the main electrostatic field. The gap between the precharging electrodes is adjustable. The air nozzle inside the aspirator was positioned mainly for the purpose of accelerating the fibre bundles towards the electrostatic field. The electrodes inside the aspirator had the polycarbonate sheet for electrical insulation.

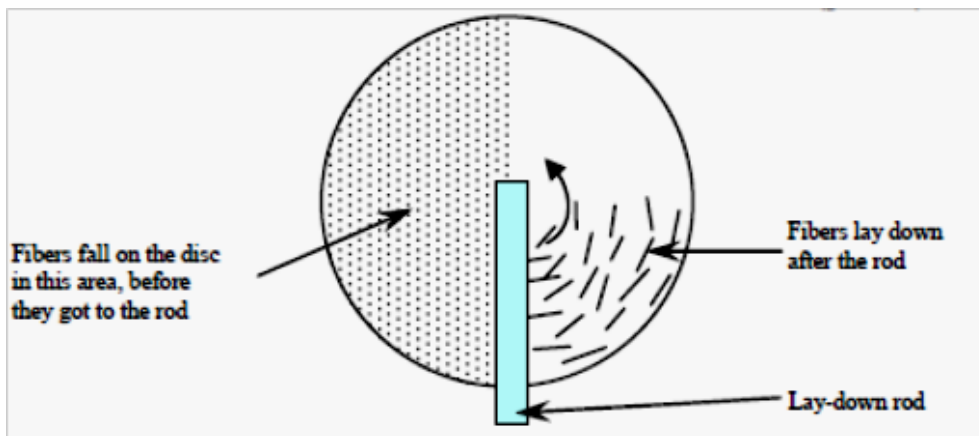
To maintain the field lines' horizontal direction, instead of bulging at the edges of the electrodes, the vacuum table was installed with a vacuum chamber which had suction from the bottom portion of the electrode box. This configuration helps the alignment of the bottom portion of the fibre bundles (see Figure 2-17).

### **2.3.3 *Electrostatic fibre alignment circumferentially or vertically***

Kim *et al.* [44] also proposed another device to align the fibre bundles using electrostatic forces as shown in the Figure 2-18. This model was developed to deliver and align the fibre stream in a circular form on the disc. They found that there are many applications with circular fibre distribution such as carbon fibre reinforced brake discs for aircrafts and automobiles and grinding, cutting and sanding pads for the abrasives industry.



(a)



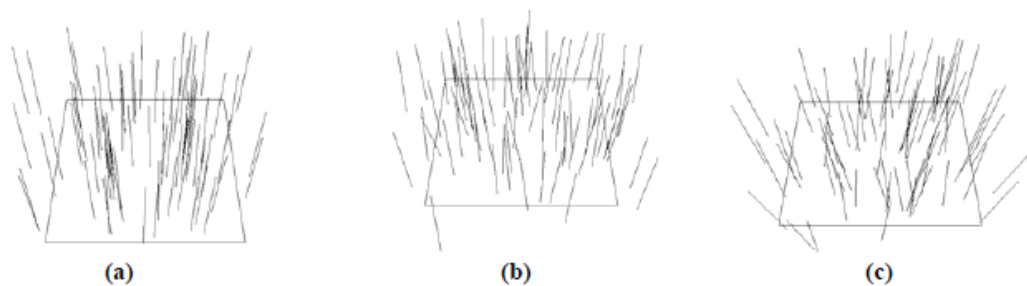
(b)

**Figure 2-18:** Schematic illustration of the fibre orientation between the electrode disc (a) and the lay-down process on the adhesive coated grounded electrode (b) [44].

In this case, two circular electrodes were employed (see Figure 2-18a); the upper electrode (made of aluminium and 400 mm in diameter) had the dispensing unit for the fibre delivery where the fibre became charged as it passed through the dispensing metal screen. Whilst the lower grounded electrode (made up of brass and 400 mm in diameter) was able to be rotated and also fixed with the lay-down rod. This was detachable so that it could have different diameters, if required. It was stated that because the lay-down rod was fixed to the lower electrode the fibre web could have a circular fibre orientation. The turning lower electrode attracted and aligned the fibre bundles dispensed from the flocking dispenser. Both electrodes were designed so that uniform field lines could be formed between the electrodes in the electric field. Because of the uniform field lines the grounded

turning lower electrode accelerated the charged fibre bundles and aligned them in a direction perpendicular to the disc. The surface of the disc was coated with a layer of adhesive so that the fibre bundles would adhere to them once they hit the surface. It was stated that the fibre aligns in the circumferential direction because the rod was installed in the radial direction. The desired circumferential fibre alignment could be obtained by controlling the speed of the disc. The electrostatic field could be controlled by adjusting the distance between them and by the applied voltage.

Kim *et al.*, during their series of experiments, they altered various parameters such as disc rotational speed, the diameter of the lay-down rod. In addition, they also investigated that the influence of the electric field, which was mainly by changing distance between the electrodes, and applied voltage to obtain the desired circumferential fibre alignment. Experimental results are shown in the Figure 2-19, for different combinations of electrostatic potential and electrode distances.



**Figure 2-19:** Fibre distributions at different combinations of electrostatic potential and electrode distances. (a) Electrostatic potential = 10 kV, electrode distances = 20 cm, (b) Electrostatic potential = 10 kV, electrode distances = 10 cm, and (c) Electrostatic potential = 50 kV, electrode distances = 10 cm.

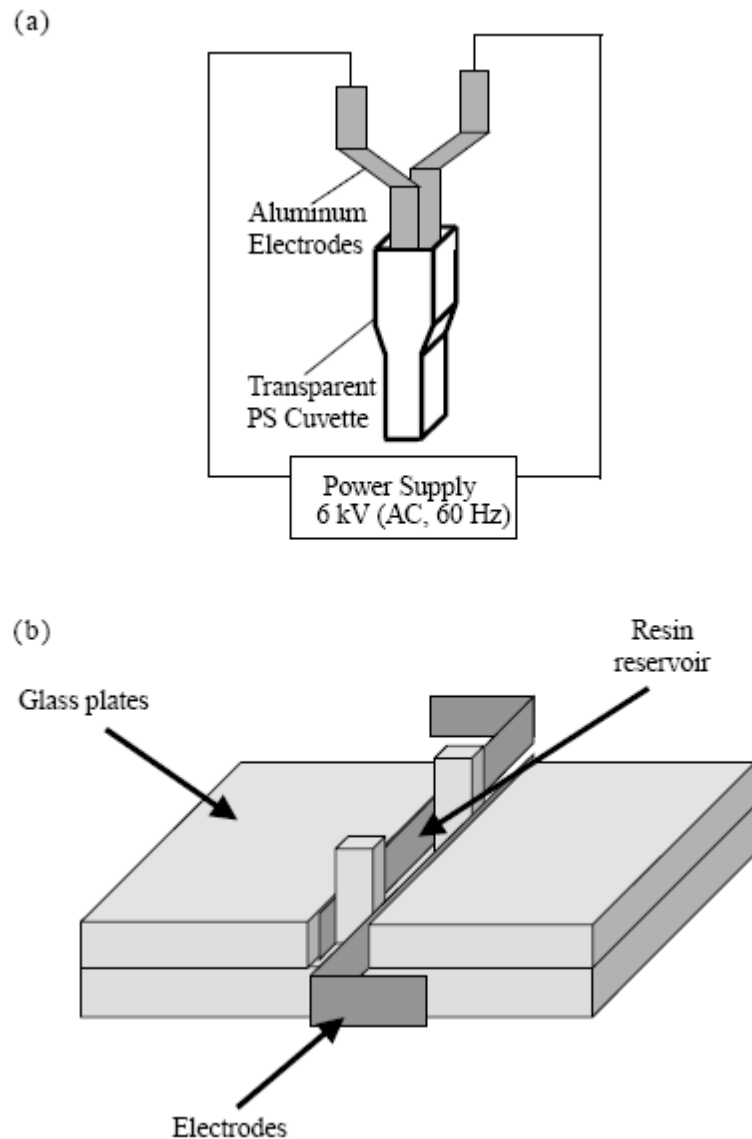
Figure 2-19 represents the fibre bundle alignment on substrate at different combinations of electrostatic potential and at electrode distances which were obtained from the rig shown in the Figure 2-18. It can be seen that at higher potential (50 kV) fibre bundles would



move faster because of higher field strength and less time for fibre bundles to align vertical to the collecting surface. Whereas, at 10 kV applied voltage, fibre bundles are perpendicular to the disc surface and also a larger quantity of fibre bundles were observed on the collecting surface. Apart from these two parameters, the fibre alignment was said to depend on to a number of parameters such as; the length of the fibre bundle, the geometry of the electrodes, the application of fibre bundles to the electrode surface, the arrangement of the electrodes, and the edge effects of the electrodes. All these parameters must be identified from the series of experimentation.

Chirdon *et al.* [45] explained the production of rectangular composite specimens that were aligned with short E-glass fibre bundles (120 micron length, 15 micron diameter) to contents of 1, 5, 10, and 25% (vol%). The fibre bundles were oriented perpendicular to the surface using an alternating electric field of 0.75 kV/ mm. Chirdon *et al.* produced a short-glass fibre bundles reinforced composite by using electrostatic force.

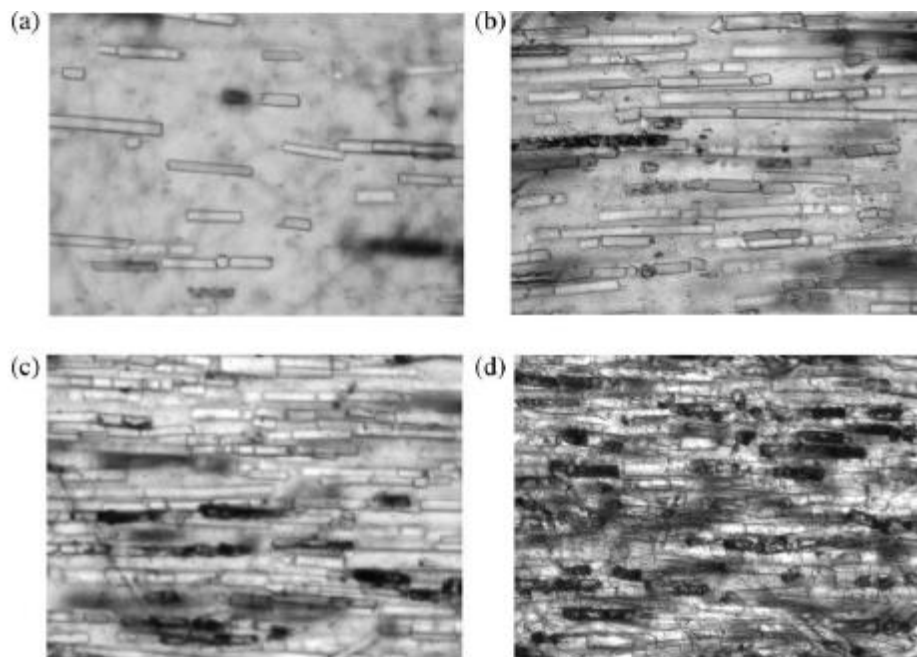
They paid attention to the effect of the orientation of the fibre bundles on diffused reflectance and Fraunhofer diffraction (that is the exact form of the reflection captured depending on the structure of the material). The fibre bundles used were un-sized E-glass fibre with a length of 2.260  $\mu\text{m}$  and diameter of 2.26  $\mu\text{m}$ . Figures 2-20 (a) and (b) shows the experimental set-up for producing perpendicular- and parallel-aligned composites. In Figure 2-20 (a), the disposable cell was assembled from a polystyrene transparent cuvette with rectangular chamber having dimensions of 4x10 x20 mm. The aluminium electrodes were used. The aluminium electrode strips with dimensions of 4 mm wide and 1 mm thick were glued to the inside of the cell. The distance between the electrodes was 8 mm. The reusable cell used for the parallel alignment is shown in Figure 2-20 (b).



**Figure 2-20:** Experimental set up used by Chirdon *et al.* [45] for aligning the fibre bundles with an influence of electric field.

The experimental procedure followed in this paper [30] to produce the composite material was as follows: (i) The resin was mixed with the short-glass fibre bundles and then warmed in an oven at 100 °C for 1 minute to reduce the viscosity. (ii) The prepared sample was then poured into the cell for fibre alignment and placed in a vacuum chamber for approximately 5 minutes until the entrapped air was removed. (iii) The electrodes were

charged by the applied voltage of 6 kV. (iii) After 1 minute, the composite was cured by using an Optilux 500 blue-light lamp without disconnecting the applied voltage. (iv) After curing, the high voltage was turned off and the contents of the cell were again cured for an additional 5 minutes on each side by using an Optilux 500 blue-light lamp. (v) By breaking the cell the composites were removed and post-cured in an oven at 100 °C for 1 hour. The composite was polished using a diamond blade. Sections of the composites were examined using an optical microscope. Micrographs of the composites with various densities of fibre bundles are shown in Figure 2-21.



**Figure 2-21:** Optical micrographs of E-glass reinforced composite aligned by the electric field of 0.75kV/mm with various fibre densities: (a) 1 %, (b) 5 %, (c) 10 % and (d) 25 %. [45].

This literature review has discussed various electrostatics-based techniques used for aligning fabric materials with the rationale of producing predetermined geometries in order to engineer the properties of the fabrics. Fabric materials include materials such as nylon, cotton and acrylic. Aligning fabric materials via electrostatic forces is mainly based on pre-charging the fabric material followed by alignment as determined by an externally applied electric field. The pre-charged fabric materials were driven towards the external electric field in a controlled fashion by using gravity-, pneumatic- or vibration-based techniques. The resultant of the electrostatic forces in conjunction with the forces driving the fabric projectiles determines the direction of alignment on an adhesive coated substrate which serves to form the basic prepreg material. The other techniques were based on subjecting the resins premixed with fabric materials to external electric fields to induce alignment within the resin. The instrumentation of electrodes, field strengths and other aspects of engineering the alignment techniques were mainly governed by the dielectric properties of the component materials and the intended application.

This thesis is aimed at investigating the feasibility and optimisation of electrostatic forces in order to induce alignment of short E-glass fibre bundles. The efficiency of electrodes of different geometries in charging E-glass fibre bundle in order to align in desired orientation with respect to adhesive substrates was studied. Another important aspect of this research is investigating the influence of adsorbed moisture on charging and alignment of E-glass fibre bundles. These aspects of research are thought to form a basis for developing the techniques further towards large scale production of aligned short-glass fibre bundle prepegs. It is envisaged that such techniques could be useful for addressing the issues involved in the waste disposal or recycling of E-glass fibre.

## **CHAPTER 3**

### **EXPERIMENTAL METHODS**

This chapter gives details of the materials employed and explains the equipment used in the various experiment.

#### **3.1 *Materials***

The fibre bundles used in these investigations were as-received short E-glass fibre bundles supplied by PPG industries. Fibre bundles of lengths of 3 mm and 4.5 mm were used. The width of these bundles was ~1.3 mm.

#### **3.2 *Instrumentation***

The following instruments that were utilised for the investigation are as follows:

- i. The power supply (Model: 73030) employed was supplied by Genvolt, UK. It was equipped with LCD digital voltage readout with an adjustable voltage from 0 kV to 30 kV and capable of a maximum output current of 1.0 mA.
- ii. An electrometer was used to measure the charge on the surface of the material, as a coulombmeter. The model employed was 610C/610CR, manufactured by Keithley Instruments Inc., UK. It has sensitivity in the range of  $10^{-07}$  C to  $10^{-10}$  C.
- iii. A suction-based device (Dymax 30, Charles Austin Pumps Ltd., UK) was used for handling the short-glass fibre bundle.

- iv. A micrometer (Model: 263M) was supplied by L.S. Starrett. Co. Ltd., UK. It was used for measuring the distance between the capacitor plates.
- v. A feeler-gauge (Jetch 23 blade filler gauge, Axminster tool centre, UK) was used for gap measurement between the capacitor plates. It was equipped with an an ideal and precise tool for measuring gaps between 0.02 mm up to 1.00 mm.
- vi. The Camera (PixeLINK PL-A662 Color Firewire Camera, Pixelink, Canada.) was employed to capture the short glass-fibre bundles movements between the capacitor plates in the electric field. The resolution of the camera was 1.3 megapixels (1280 X 1024 pixels). It also includes pixelink capture SE, a software package designed to support fast, efficient and consistent image capture.

### ***3.3 Custom-designed equipment***

The custom-design apparatus used in this work were as follows:

- i. a charge measuring device;
- ii. fibre deposition and alignment device; and
- iii. a parallel plate capacitor.

The details of these equipment are given in the following sections.

### 3.4 Charge measuring device

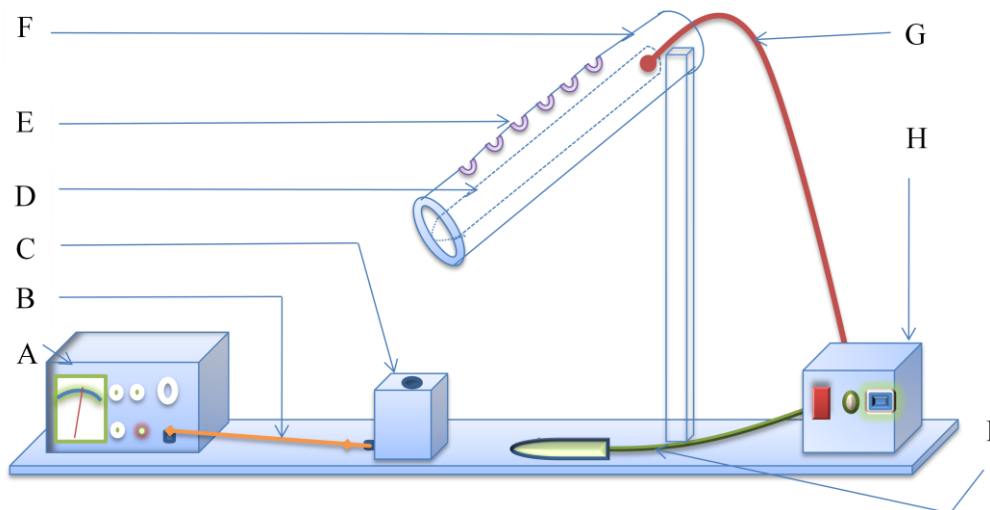
The charge measuring device was assembled to investigate the optimal length of the electrode required for the charge acquisition on the surface of the short-glass fibre bundles.

This instrument was also used to measure the following parameters:

- (i) charge decay on the short-glass fibre bundles; and
- (ii) charge on the as-received fibre bundles and that of the dried fibre bundles.

The following section presents the details of the construction of the charge measuring instrument, its operation and calibration.

#### 3.4.1 Instrument construction and operation



**Figure 3-1:** Schematic illustration of the charge measurement set up. [A] Solid state electrometer, [B] BNC connector, [C] Faraday pail, [D] Positive electrode, [E] Multiple access ports, [F] Safety enclosure, [G] Positive terminal, [H] Genvolt power supply, and [I] Safety discharge probe.

Figure 3.1 represents a schematic illustration of the set-up used to investigate the surface charge of the short-glass fibre bundles. The short-glass fibre bundles used were 3 mm in length and the voltage employed to charge the electrode ranged from 10 kV to 15 kV. The voltage of the power supply could be varied from 0 kV to 30 kV. The positive terminal (G) from the power supply was connected to one end of the electrode (D), which is 30 cm long. This was enclosed with in a cylindrical safety enclosure (F) made of PMMA (poly methyl methacrylate) material which provided electrical insulation to the equipment. Multiple access ports (E) were made in the form of circular holes on the surface of the cylinder at two centimeter intervals to drop the fibre bundles on to the electrode. The fibre bundles inserted from access ports were made to slide down along the length of the electrode. These bundles acquired a charge whilst sliding down the charged electrode; and they were then allowed to fall into the Faraday pail (C). The charge gained by the fibre bundles was measured by the electrometer (A), which had a sensitivity range of  $10^{-07}$  C to  $10^{-10}$  C. The electrometer was connected to the Faraday pail by means of a BNC connector (B). A safety discharge probe was used for discharging the electrodes at the end of each experiment. The probe was inserted into the power supply grounding point whenever the instrument was in use for a safe and quick means of discharging the electrode.

While the charge measurements were being taken, it was noted that the electrometer reading was unstable. It was speculated that the fluctuation in the electrometer scale was due to the electric field caused by the electrode [C]. To overcome this problem, some modifications were carried out to the charge measuring device. These were as follows. (i) The six tests were conducted with the aim of eradicating the fluctuations by isolating the Faraday pail from the electric field. The isolation was carried out by enclosing the Faraday pail using wooden slabs wrapped with aluminum foil. The wrapped aluminum foil was



grounded. A circular opening was made to the wooden slab to allow the charged fibre bundles to drop into the pail. (ii) Further ten tests were conducted by replacing the electrode. The reconstruction of a new electrode was carried out by using tapered edges. It was envisaged that this would minimise the drift.

### **3.4.2 Instrument Calibration**

To calibrate the charge measurement equipment and to minimise the fluctuations observed on the electrometer, the following modifications made to the device:

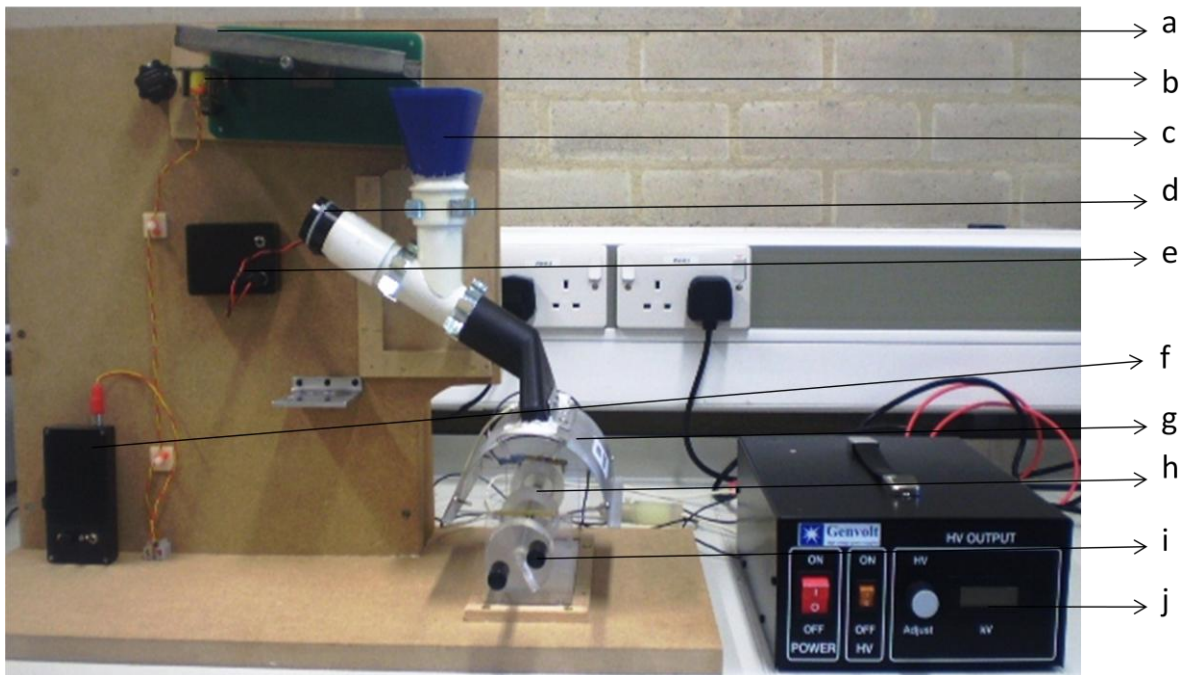
- (i) shielding the Faraday pail by enclosing all the sides by wooden slabs;
- (ii) by shielding the wooden slabs by aluminum foil and grounding it; and
- (iii) by using the new electrode design.

The six tests were conducted by shielding the Faraday pail. The procedures followed in these tests were as follows. (i) The Faraday pail was shielded with wooden slabs on all sides. (ii) The voltage applied to charge the short-glass fibre bundles was from 10 kV to 15 kV. (iii) The electrometer sensitivity range used for the tests were from  $10^{-08}$  C to  $10^{-09}$  C. (iv) The fluctuation on the electrometer scale started immediately after applying the voltage. The amount of fluctuation noticed on the electrometer scale was recorded at certain sensitivity and applied voltage. The time taken for the electrometer scale to fluctuate was noted at 10 second intervals for a given time period i.e., until the full scale deflection was observed. After the tests were completed, the voltage was reduced to 0 kV and the electrode was discharged using a safety discharge probe. Further tests were carried out by reconstructing the new electrode.

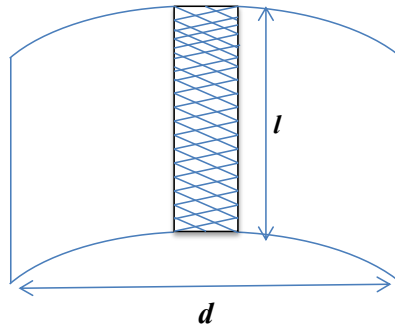
### 3.5 Fibre deposition and alignment device

In order to analyse the efficacy of electrostatic fibre bundle charging, deposition and attraction, the set-up shown in Figure 3-2 was assembled. This set-up was designed in collaboration with the Charles Labs and was investigated on-site at the University of Birmingham.

#### 3.5.1 Instrument construction and operation



**Figure 3-2:** Fibre bundle deposition and alignment device: a - vibrating plate, b - solenoid, c - funnel, d - fan arrangement, e - switch to operate the fan, f - power supply to control the vibration plate, g – radial electrode, h - grounded mandrel, i - mandrel winder, j - power supply and k- safety discharge probe.



**Figure 3-3:** Grid arrangement of positive radial electrode, the length ( $l$ ) of the mesh/grid was approximately 15 cm and diameter ( $d$ ) of 10 cm.

With reference to Figure 3-2, the key components were as follows: the vibration plate (a) which accepts the short-glass fibre bundles. Vibration of plate (a) was driven by a solenoid (b). The frequency of the vibration of the plate was varied by the power supply (f) which was connected to the solenoid. The fibre bundles from the vibrating plate descended into the funnel (c) which acted as the fibre bundle receptor. The fan arrangement (d) blew the fibre bundles into the radial electrode (g). The radial electrode was provided with a grid arrangement shown in Figure 3-3; when passing through the grid, the fibre bundles acquired a positive charge as the radial electrode was connected to the positive probe of the Genvolt power supply (j). The fibre bundles, after acquiring the positive charge, were attracted towards the grounded mandrel (h). The mandrel could be rotated by means of the manual mandrel rotator (i), which was provided with a PMMA insulated handle. A safety discharge probe was used for discharging the electrodes at the end of the experiment. This probe was inserted into the power supply grounding point whenever the instrument was in use for a safe and quick means of discharging the electrode.

For operator safety, the device was enclosed in PMMA material after the fibre bundles had been placed on the vibrating plate.

### **3.6 Parallel Plate Capacitor**

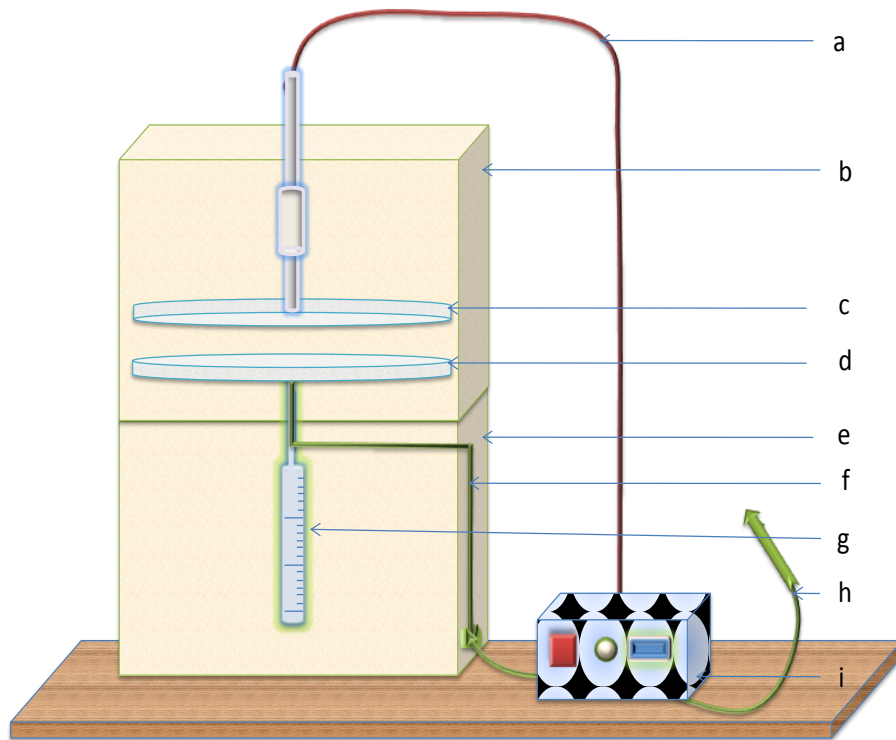
The parallel plate capacitor rig was assembled to investigate the influence of an electric field on the short-glass fibre bundles. This rig also allowed the acquisition of photographs to record the fibre bundles in the electric field; this was achieved using camera set-up. The parallel plate capacitor construction and its operation are explained.

#### **3.6.1 Instrument construction and operation**

The instrument comprises two chambers:

- (i) the upper chamber consists of the parallel plate capacitor arrangement, as shown in Figure 3-4; and
- (ii) the lower chamber consists of a micrometer to measure and vary the distance between the capacitor plates .

Both the chambers were provided with sliding doors. The sliding door to the upper chamber provided access for placement of the fibre bundles on the lower capacitor plate. The sliding door on the lower chamber was used to vary the micrometer in order to adjust and measure the distance between the capacitor plates.



**Figure 3-4:** Schematic illustration of the parallel plate set-up. This apparatus used to analyse the influence of electric field on the short-glass fibre bundles. a - positive terminal, b - upper chamber, c - positively charged capacitor plate, d - negatively charged capacitor plate, e - lower chamber, f – negative terminal, g - micrometer, h – safety discharge probe, and i - power supply

As shown in Figure 3-4, the upper chamber contains the parallel plate capacitor set-up. The diameter of the circular parallel capacitor plates are 60 mm. The capacitor plate (c) was connected to the positive terminal (a) of the high voltage power supply. The capacitor plate (d) could be moved vertically by means of a micrometer screw (g); the distance between the capacitor plates was measured by using the micrometer to an accuracy of 10  $\mu\text{m}$ . The lower capacitor plate (d) was connected to the ground terminal of the high voltage supply. A safety discharge probe was used for discharging the capacitor plates at the end of each experiment. This probe was inserted into the power supply grounding point for a safe and quick means of discharging the capacitor plates. Both the chambers are made from polymethylmethacrylate (PMMA) which provides satisfactory electrical insulation to

the equipment. The chambers' sliding doors allow access when no charging potential applied, but provide operator safety when closed.

The short-glass fibre bundles of 3 mm length provided by PPG industries were used for the experiment. The single fibre bundle was placed on the grounded lower electrode after the electrode was cleaned using lint free tissue and isopropyl alcohol. Vacuum suction was used to handle the fibre bundles, which minimise possible breakage. The weight of the sample was measured just before the experiment. After the sample had been placed on the lower electrode, the chamber was closed. In the lower chamber, the micrometer was used to adjust the distance between the electrodes. After the distance had been adjusted, the lower chamber was closed. For safety precautions, both the chambers were checked twice to ensure they were fully closed before the high voltage supply was applied. It was also ensured that the both the lower capacitor plate (d) and safety discharge probe were connected to the grounded terminal of the power supply. After the equipment set-up, the camera set-up was carried out to capture all the possible motion of the fibre bundles in the electric field. The voltage was then increased gradually for the investigation of the fibre bundles movement in the electric field.

### **3.6.2 Calibration**

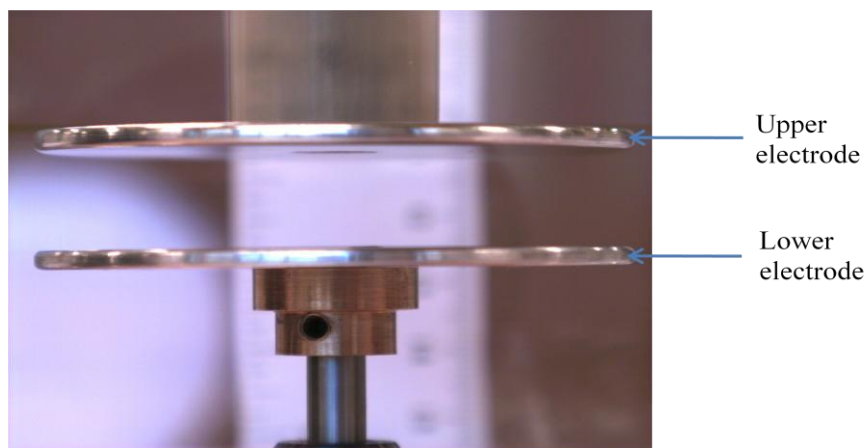
Before the performing the experimental programme, the following calibrations were undertaken:

- (i) the capacitor plates calibration was carried out to ensure that they were parallel to each other; and

- (ii) the camera set-up was evaluated to ensure that the entire surface of both the capacitor plates were in focus. This was necessary to capture the images of the motion of fibre bundles between the plates under the influence of an applied electric field.

### 3.6.2.1 Capacitor plates calibration

The procedures used were as follows: (a) Both the upper and lower capacitor plates were cleaned with lint free tissue and isopropyl alcohol. (b) The distance between the two electrodes was adjusted to 0.04 mm using the micrometer. (c) A feeler gauge was used to check that the distances between the plates were approximately 0.04 mm. (e) The 0.04 mm feeler blade was inserted between the plates and it was found that only half of the diameter of the plates was at 0.04 mm. By increasing the distance between the plates from 0.04 mm to 0.05 mm, it was found that the other half of the diameter of the plates was lower by 0.01 mm. By repeating this process several times, using a feeler-gauge, it was found that the error was  $\pm 0.01$  mm. However, for larger distances ( $>1$  cm) between the two plates, an image analysis was carried out using a camera.



**Figure 3-5:** Image analysis to investigate the capacitor plates were parallel to each other.

### 3.6.2.2 Optimization of the camera

Adjustments to the camera were made to analyse the movement of the fibre bundles in the electric field between two capacitor plates and also to capture accurately the motion of the fibre bundles in the electric field. To allow it to focus on specific areas of the plates, the following steps were taken:

(a) A cardboard template of the lower capacitor plate was taken, (b) five sample studs were attached firmly at 10-centimetre intervals across the diameter of the template, (c) the cardboard template with the five studs, was placed on the lower capacitor plate. This arrangement allows adjustments to the camera so as to capture the entire surface of the electrode plate. In addition, the degree of movement of the focus lens ('focal length of the camera lens') of the camera on each stud can be calculated. By this calculation it is easy to focus accurately when the fibre bundles are in the electric field. The distance between each stud was calculated with respect to the first stud. The degree of rotation made on the focus lens was calculated.

The procedure followed to measure the degree of rotation on the focus lens is as follows. The distance between adjacent studs was 10 mm; the rotation made on the focus lens of the camera was calculated for each stud. The circumference of the focus lens was 196 mm. A ruler of same length was printed to this length (196 mm) and pasted on the focus lens of the camera. The diameter of the electrode was 60 mm. In order to focus the entire surface of the electrode, the studs were arranged so that, from the circumference of the electrode plate to the first stud (S1) was 10 mm. Again from stud S1 to stud S2 the distance was 10 mm and so on. All the studs from S1 to S5 were arranged diametrically along a straight



line, so that all of them are in the field of view of the camera. Therefore, the optimisation of the camera can capture the motion of the fibre bundles between the capacitor plates. In other words, focusing of the camera was calibrated against the spatial location of the studs along the capacitor plate diameter. This optimization will enable the clear view of the fibre bundles moving in between the capacitor plates when the plates are charged (see Table 4.8 in results and discussion chapter).

In order to accurately record the motion of the fibre bundles between the electrodes, pixelink capture SE, a camera software package was calibrated to enable data acquisition in real-time. Repeated test runs on the camera software found that 366 seconds of the software time was equal to 600 seconds of the real time. From the repeated test runs, the equation below was obtained.

$$\text{Software time} = 0.61 \times (\text{Real-time}) \qquad \text{Equation 3.1}$$

### **3.6.3     *The motion of the fibre bundles in the electric field***

The following investigations were conducted to study the movement of short-glass fibre bundles.

- (i)     A single fibre bundle placed on the lower electrode and its movement in the electric field was investigated.
- (ii)    The three fibre bundles were placed on the lower plate and their movement in the electric field was analyzed.
- (iii)   A single fibre bundle was dried at a certain temperature for studying their movement in the electric field.

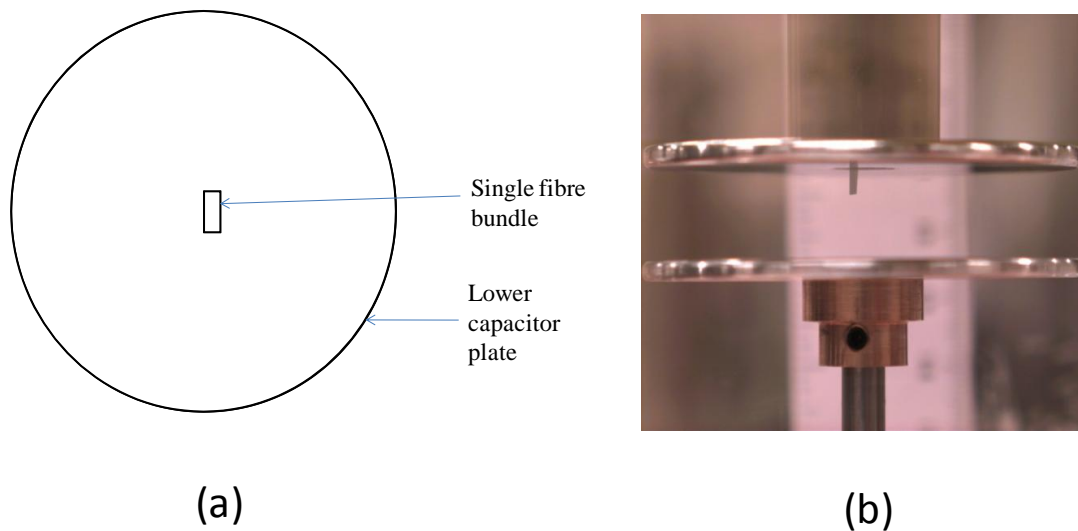
- (iv) A fibre bundle was hydrated, and their results were compared with the results of dried and 'as received' fibre bundles.
- (v) Finally, the motion of the fibre bundles subjected to hydration was studied. Then the same batch of fibre bundles were dried and their movement was studied subsequently and compared with the as received fibre bundles.

### **3.6.3.1 Single fibre bundle**

Two experiments were conducted to study the movement of a single fibre bundle in the electric field. That is, in one of the experiments, a corner of the fibre bundle was marked with a colour, while, in the other experiment, the fibre bundle movement was analyzed without any marking. The marking on the fibre bundle was to find out which particular corner of the fibre will lift and come in contact with the electrodes, when the voltage was applied. The experimental procedure followed is explained below.

The single fibre bundle of 3 mm length was placed at the centre of the lower capacitor plate as shown in Figure 3-6. Before placing the fibre bundle on the grounded plate, the preliminary set-up of equipment was made. The capacitor plates were cleaned by a lint free tissue, using isopropanol. The power supply connections were checked for safety reasons. The distance between the plates was adjusted by using a micrometer.

The camera adjustments were made to cover the entire circumference of the capacitor plates, so that the motion of the fibre bundles all across the plates could be captured.



**Figure 3-6:** (a) Schematic illustration of a fibre bundle arrangement on the bottom plate of the capacitor before charging and (b) photograph showing a fibre bundles in contact with the oppositely charged top plate of capacitor.

The procedure adopted throughout all the experiments were as follows. (i) The camera was set to 366 seconds (600 seconds - real time) at frequency 16 MHz, obtained 1 frame per second. (ii) The type of fibre bundles used was 3 mm short-glass fibre bundles. (iii) The mass, length and width of the fibre bundles will be recorded for all the experiments (iv) Ten trails were conducted. (v) Temperature and humidity were recorded for each trial, and (vi) A single fibre bundles was placed at the centre of the grounded electrode plate. The distance between the plates was 10 mm at each run.

The methodology adopted to perform the experiment was, after the placement of the fibre bundles on the plate, the voltage was gradually increased to charge the fibre bundles. But, once the initial moment the fibre bundles are noticed, the voltage incremental was stopped and recorded, and simultaneously, the stop watch was started. The fibre bundles movement was observed for 300 seconds, keeping the voltage constant. The motion of the fibre bundles in the electric field was recorded by the camera. After 5 minutes of observation, the voltage was gradually decreased to zero. While decreasing the voltage to 0

kV, fibre bundles movement was observed and recorded. Further experiments were carried out by the placement of the three fibre bundles and studying their behaviour in the electric field.

### **3.6.3.2 Multiple fibre bundles**

In this study three fibre bundles are placed on the bottom plate. The mass of each fibre bundles were measured and recorded. The multiple fibre bundles movement was studied in the electric field. This was mainly to observe the fibre bundle impetus and its orientation.

Further experiments were carried out by drying and hydrating the fibre bundles. The procedure followed was explained in the following section.

### **3.6.3.3 Dried fibre bundles**

In this experiment, a single fibre bundle was dried. The objective of this experiment was to study the motion of the dried fibre bundle in the electric field, and also, to compare with the 'as received' fibre bundles from the industries. The fibre bundles were dried for a period of 48 hours and at 80 °C. Silica gel was placed inside the apparatus to absorb the moisture content and to keep the instrument dry. The set of experimental results were reported in Tables 4.16, 4.17 and 4.18.

Further the fibre bundles were hydrated and their alignment was observed between the external electric field.

#### **3.3.6.4 Hydrated fibre bundles**

The fibre bundles were conditioned for 24 hours in an enclosed chamber containing supersaturated solution of sodium chloride. This solution was prepared by using the sodium chloride and distilled water in the ratio of 70 gram and 200 ml respectively. The aim of the experiment was to measure the charge on the “moist” fibre bundle and compare the results with dried and ‘as received’ fibre bundles from the industry. Silica gel, wrapped with breather fabric was placed in the chamber to remove atmospheric moisture from the equipment.

## **CHAPTER 4**

### **RESULTS AND DISCUSSIONS**

#### ***4.1 Charge measuring device***

With reference to the previous chapter, the charge measuring device (see Figure 3.1) was calibrated and charge acquisition on the surface of the short-glass fibre bundles (length of 3 mm and width of ~ 1.3 mm) was measured. Then, the optimal electrode length required to charge the fibre bundles was obtained.

##### ***4.1.1 Calibration of charge measuring device***

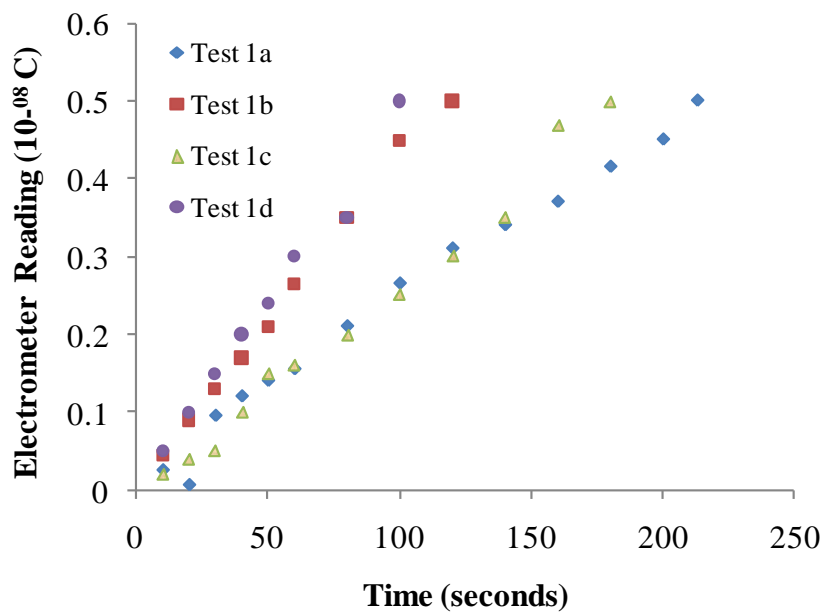
The tests that were conducted to calibrate the charge measuring device are explained in this section. They are as follows. (i) The first four tests were conducted to minimise the fluctuation on the electrometer by shielding the Faraday pail. (ii) Two other tests were conducted by grounding the shield of the Faraday pail. (iii) A further four tests were conducted by using the new electrode design.

###### ***i. Influence of open orifice on electrometer deflection at the sensitivity of $10^{-08}$ C***

To minimize the fluctuation of the electrometer reading, the Faraday pail was shielded with wooden slabs on all sides and on the top and a small circular orifice was made at the centre of the top slab to allow access for the short-glass fibre bundles to drop into the pail. The pail was shielded because, it was envisaged that it would be affected by the electric field lines.

The temporal evolution of the electrometer deflection was observed at a specified sensitivity of  $10^{-08}$  C and at the applied voltage of 10 kV to the electrode. The deflection on the electrometer scale was recorded until it reached its full scale. After the completion of the test, the voltage was reduced to 0 kV and the electrode was discharged using a safety discharge probe.

The experiment was repeated four times and the fluctuations obtained on the electrometer scale are shown in Figure 4.1. It can be seen from the graph that as the time increases the fluctuation on the electrometer scale also increases gradually, and it reaches full scale deflection after certain time.



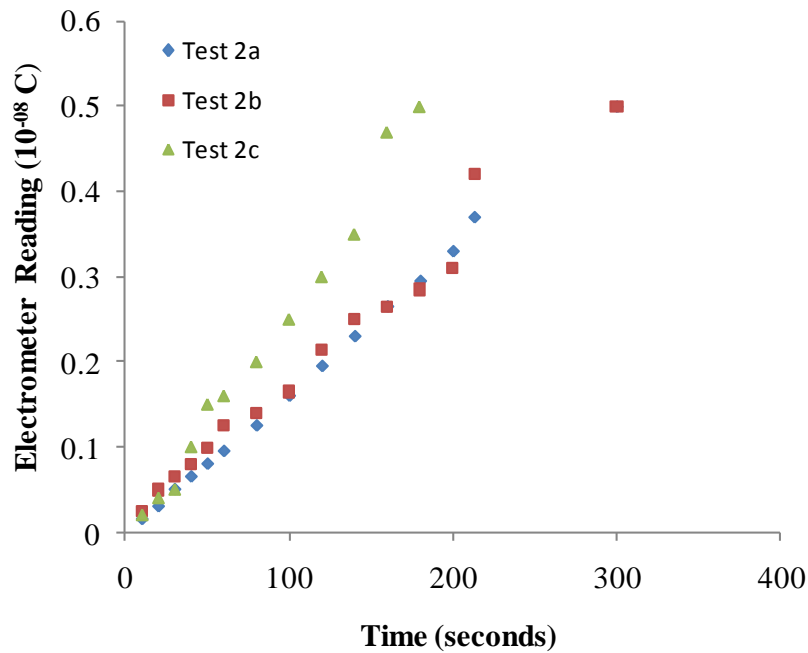
**Figure 4.1:** Electrometer scale deflection at  $10^{-08}$  C sensitivity and 10 kV applied voltage with the Faraday pail orifice kept open.

It was observed that the fluctuation started immediately after applying the voltage of 10 kV. The fluctuation on the electrometer scale increased until the full scale deflection was observed. For example, in Test 1b at 125 seconds the electrometer scale reached the full

scale deflection of  $0.5 \times 10^{-08}$  C. But it was observed that the different tests took the different times to reach the full scale deflection.

*ii. Influence of closed orifice on electrometer deflection at the sensitivity of  $10^{-08}$  C*

The experimental procedure followed in Test 2 was similar to Test 1 with slight modifications. In this test 1, the orifice of the pail was not protected from the electric field lines, while in this test the orifice was enclosed with wooden slab. At  $10^{-08}$  C sensitivity and at 10 kV applied voltage, the fluctuation observed on the electrometer scale was recorded at 10 second intervals. Figure 4.2 shows the electrometer scale fluctuation with respect to time.



**Figure 4.2:** Electrometer scale deflection at  $10^{-08}$  C sensitivity and 10 kV applied voltage with the Faraday pail orifice kept closed.

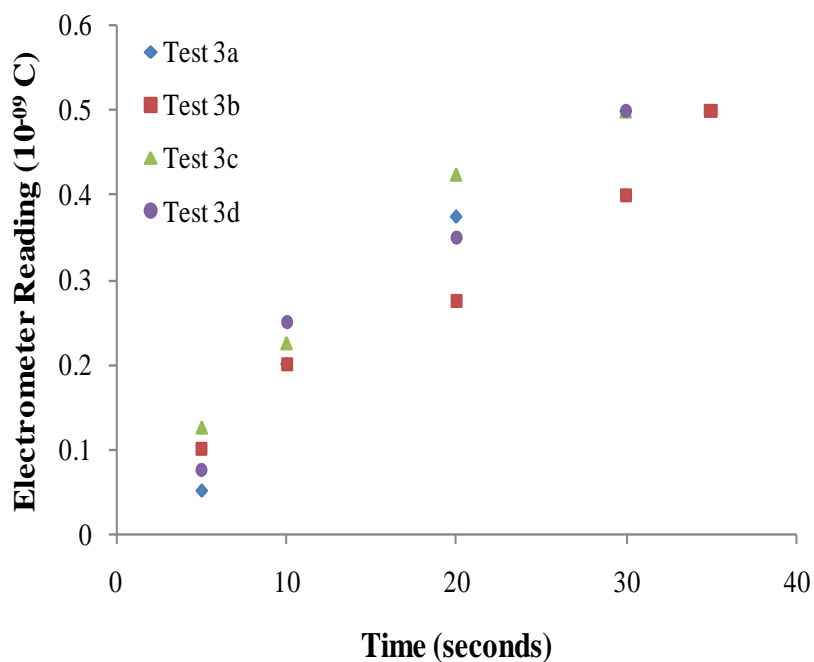
When compared to Figure 4.1 and Figure 4.2, in Figure 4.2 the time taken to reach the full scale deflection on the electrometer scale was relatively high. Further calibration was also carried out at 10 kV but the sensitivity on the electrometer was increased to  $10^{-09}$  C. In Test



3, the top orifice was kept open and while in Test 4, the top orifice was enclosed by the wooden slab.

*iii. Influence of the open orifice on electrometer deflection at the sensitivity of  $10^{-09}$  C*

The procedure followed was similar to the tests 1 and 2 but the sensitivity on the electrometer was set to  $10^{-09}$  C.



**Figure 4.3:** Electrometer scale deflection at  $10^{-09}$  C sensitivity and 10 kV applied voltage with the Faraday pail orifice kept opened.

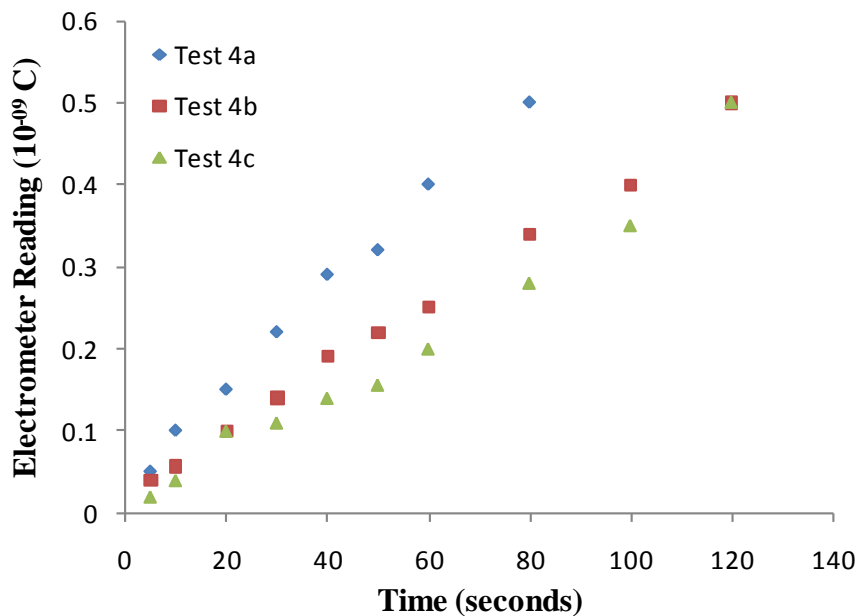
The fluctuations obtained on the electrometer scale are shown in Figure 4.3. It was observed from the graph that as the time increases, the fluctuation on the electrometer scale also increases gradually, and reaches full scale after a certain time. In this test, it took relatively less time to reach the full scale deflection. While in Tests 1 and 2, the electrometer took a significantly long time to reach full scale deflection at  $0.5 \times 10^{-08}$  C.

From the data obtained it can be said at higher sensitivity of  $10^{-09}$  C, the time taken to reach the full scale deflection was significantly less.

*iv. Influence of closed orifice on electrometer deflection at the sensitivity of  $10^{-09}$  C*

The experimental procedure followed in this test was similar to the previous with modifications, i.e. the orifice of the pail was closed with the wooden slab.

The Figure 4.4 shows the fluctuations on the electrometer scale with respect to time.



**Figure 4.4:** Fluctuations on electrometer scale at  $10^{-09}$  C sensitivity and 10 kV applied voltage with the Faraday pail orifice kept close.

When compared with Figure 4.2 and Figure 4.4, in Figure 4.4 the amount of time taken to reach the full scale deflection on electrometer scale was significantly smaller. At this stage, from these set of tests it can be concluded that the impact of electric field lines can be reduced by closing the orifice.

It was thought that by wrapping the wooden slabs with aluminium foil and by grounding it, the deflection on the electrometer could be reduced.

Two further tests were conducted by wrapping the aluminium foil and grounding the shield, which are explained in detail in the following section.

v. ***Influence of grounding the pail on electrometer deflection***

The deflection on the electrometer scale was observed for the set of voltage ranges from 10 kV to 16 kV and at  $10^{-08}$  C and  $10^{-09}$  C sensitivity. After applying voltage to the electrode, the deflection of the electrometer scale was observed for 10 minutes and is summarized in the Table 4.1.

**Table 4.1:** Summary of the instrument calibration at different voltage and sensitivity ranges.

<i>Voltage applied</i>	<i>Sensitivity set to <math>10^{-08}</math> C on electrometer (10 minutes observation)</i>	<i>Sensitivity set to <math>10^{-09}</math> C on electrometer (10 minutes observation)</i>
10 kV	Fluctuation was not observed on the electrometer.	Fluctuation was not observed on the electrometer.
12 kV	Fluctuation was not observed on the electrometer.	Fluctuation was not observed on the electrometer.
13 kV	Fluctuation was not observed on the electrometer.	Fluctuation was observed after five minutes on the electrometer scale.
14 kV	Fluctuation was not observed on the electrometer.	Fluctuation was observed after five minutes on the electrometer scale.
15 kV	Fluctuation was not observed on the electrometer.	Fluctuation was observed after five minutes on the electrometer scale.
16 kV	Fluctuation was not observed on the electrometer.	Fluctuation was observed after one minute.

It was concluded from the data that by wrapping the wooden slabs using an aluminium sheet and by grounding it, the fluctuation at a sensitivity of  $10^{-08}$  C was eliminated. But, at a sensitivity of  $10^{-09}$  C and at applied voltages of 15 kV and 16 kV, the fluctuation was observed after 5 and one minute respectively.

The next test was carried out to distinguish the effect of deflection on the electrometer scale when the pail was open and kept closed.

**vi. *The effect of the orifice on the electrometer deflection***

At the sensitivities of  $10^{-08}$  C and  $10^{-09}$  C and at the applied voltage of 15 kV, the observations made are summarised in Table 4.2.

**Table 4.2:** Test observations at 15 kV applied voltage.

<i>Shielding of the Faraday pail</i>	<i>Sensitivity set to <math>10^{-08}</math> C on electrometer</i>	<i>Sensitivity set to <math>10^{-09}</math> C on electrometer</i>
Faraday pail was shielded and grounded but the orifice was kept open.	Fluctuation on the electrometer was observed after 30 seconds.	Fluctuation on the electrometer reading was observed after 3 seconds.
The orifice was kept closed.	Fluctuations were not observed on the electrometer reading.	Fluctuations on the electrometer reading were observed only after 5 minutes.

From the Table 4.2, it can be observed that, when the orifice of the pail was open, fluctuations on the electrometer reading were seen. But when the pail orifice was kept closed, the fluctuations on the electrometer reading were minimised. However, the orifice

must be kept open, to investigate the charge on short-glass fibre bundles and to enable the fibre bundles to be dropped into the pail.

At this stage, it was speculated that the excess drift created by the electric field lines was due to the tapered edges [13] of the electrode, which were causing an impact on the surrounding instruments. Electrons are emitted from the sharp tip creating the larger electric field strength. For example; positive corona discharge (see Figure 2-2 and Figure 2-3) was formed [46]. Therefore, the electrode was reconstructed by smoothing the tapered edges.

*vii. Effect on the electrometer deflection after the replacement of the new electrode and at an applied voltage of 8kV*

The modified electrode was replaced in the charge measuring device. The Faraday pail was shielded and grounded to the instrument grounding point. In this test the pail orifice was unveiled. The laboratory temperature and humidity were recorded during experimentation were 24.6 °C and 53% respectively. The voltage was set to 8 kV. The Table 4.3 shows the results obtained by replacing the reconstructed electrode.

**Table 4.3:** Test observations at 8 kV applied voltage.

<i>Sensitivity of electrometer was set to <math>10^{-8}</math> C</i>		<i>Sensitivity of electrometer was set to <math>10^{-9}</math> C</i>	
<i>Electrometer Reading (C)</i>	<i>Time (seconds)</i>	<i>Electrometer Reading (C)</i>	<i>Time (seconds)</i>
0	10	0	10
0	20	0	20
0	30	0	30
0	40	0	40
0	50	0.01	50
0	60		

It was observed from the test results that the deflection on the electrometer reading was minimised, because the corona discharge [13] at the electrode sharp edges was reduced by the replacing with an electrode, having smoothened edges. Further tests were conducted for the higher voltages.

**vii. *Effect on the electrometer deflection after the Replacement of the new electrode and at an applied voltage of 10kV***

In this test the applied voltage was changed to 10 kV and the laboratory temperature and humidity recorded were 24.6 °C and 53% respectively. The test observations are given in Table 4.4.

**Table 4.4:** Test observations at 10 kV applied voltage

<i>Sensitivity of electrometer was set to <math>10^{-8}</math> C</i>		<i>Sensitivity of electrometer was set to <math>10^{-9}</math> C</i>		<i>Sensitivity of electrometer was set to <math>10^{-10}</math> C</i>	
<i>Electrometer Reading (C)</i>	<i>Time (seconds)</i>	<i>Electrometer Reading (C)</i>	<i>Time (seconds)</i>	<i>Electrometer Reading (C)</i>	<i>Time (seconds)</i>
0	10	0	10	0	10
0	20	0	20	0	20
0	30	0	30	0.1	30
0	40	0	40	0.3	40
0	50	0	50	0.4	50
0	60	0.01	60		

It was observed that deflection on the electrometer was minimized at applied voltage of 10 kV. Further calibration was carried out for the applied voltages of 13 kV and 15 kV.

*ix. Effect on the electrometer deflection after the replacement of the new electrode and at an applied voltage of 13 kV*

The laboratory temperature and humidity recorded during experiment were 24.6 °C and 53% respectively. The test observations are reported in Table 4.5.



**Table 4.5:** Test observations at 13 kV applied voltage

<i>Sensitivity of electrometer was set to <math>10^{-8}</math> C</i>		<i>Sensitivity of electrometer was set to <math>10^{-9}</math> C</i>		<i>Sensitivity of electrometer was set to <math>10^{-10}</math> C</i>	
<i>Electrometer Reading (C)</i>	<i>Time (seconds)</i>	<i>Electrometer Reading (C)</i>	<i>Time (seconds)</i>	<i>Electrometer Reading (C)</i>	<i>Time (seconds)</i>
0	10	0	10	0	10
0	20	0	20	0	20
0	30	0	30	0.13	30
0	40	0	40	0.2	40
0	50	0	50	0.3	50
0	60	0.01	60		

At a sensitivity of  $10^{-08}$  C,  $10^{-09}$  C and  $10^{-10}$  C and at applied voltage of 13 kV, the deflection on the electrometer scale was minimised. At the higher sensitivity of  $10^{-10}$  C, the deflection on the electrometer scale was observed after 20 seconds. However, the time taken to measure the charge on the surface on the fibre bundles was not more than 10 seconds.

*x. Effect on the electrometer deflection after the replacement of the new electrode and at an applied voltage of 15 kV*

In this experiment, a tapered edge of the electrode was smoothed to avoid or to completely eliminate the drift [47] that was previously caused due to the sharp edges. Therefore, corona discharge occurring at the tapered edges of an electrode was minimized.

The applied voltage was increased to 15 kV. The laboratory temperature and humidity recorded during experiment were 24.6<sup>0</sup> C and 53% respectively.

**Table 4.6:** Summary of the electrometer scale reading at 15 kV

<i>Sensitivity of electrometer was set to 10<sup>-9</sup> C</i>		<i>Sensitivity of electrometer was set to 10<sup>-9</sup> C</i>		<i>Sensitivity of electrometer was set to 10<sup>-10</sup> C</i>	
<i>Electrometer Reading (C)</i>	<i>Time (seconds)</i>	<i>Electrometer Reading (C)</i>	<i>Time (seconds)</i>	<i>Electrometer Reading (C)</i>	<i>Time (seconds)</i>
0	10	0	10	0	10
0	20	0	20	0	20
0	30	0	30	0.1	30
0	40	0	40	0.2	40
0	50	0	50	0.3	50
0	60	0.01	60	0.4	60

From the above tests it can be concluded that, after replacing the electrode to the charge measuring device, deflection on the electrometer reading was minimised.

The maximum time required to measure the charge on the short-glass fibre bundles was not more than 10 seconds. However, these tests accomplished the elimination of fluctuation on the electrometer scale. Thereby, the errors on the charge measurement of the short-glass fibre bundles can be reduced.

## **4.1.2 Charge measurement on short-glass fibre bundles**

The following parameters of the short-glass fibre bundles were investigated using the charge measuring device.

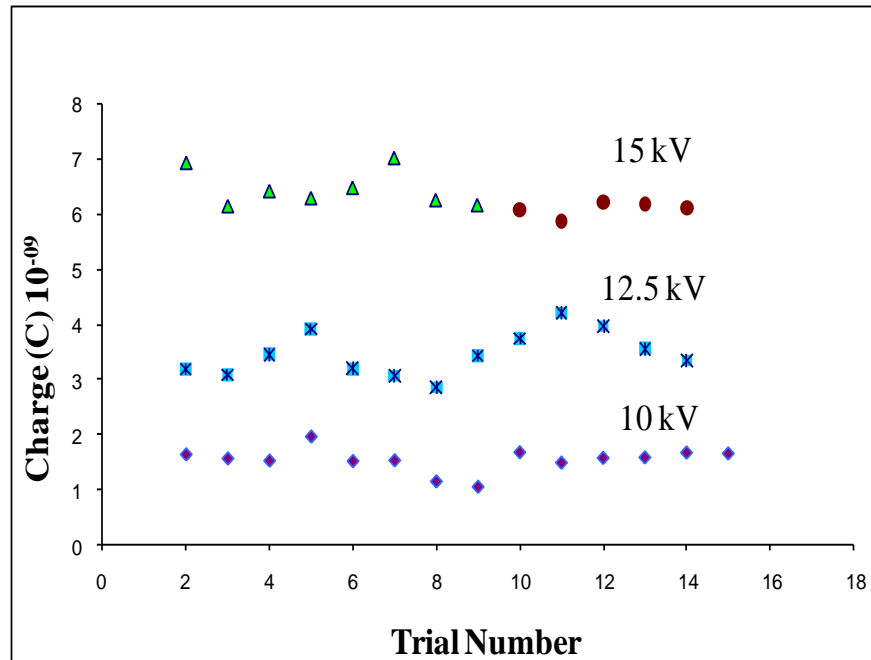
- (i) Charge measurements at different voltages.
- (ii) Charge measurements at different electrode lengths.
- (iii) Charge decay.
- (iv) Effect of moisture on charging of the short-glass fibre bundles.

The parameters mentioned above form the basis for aligning the short-glass fibre bundles in an external electric field. The 3 mm length short-glass fibre bundles were supplied by the PPG industries. The experimental results obtained using the charge measurement equipment are explained in the following section.

### **4.1.2.1 Charge measurements at different voltages**

Charge measurement on the short-glass fibre bundles was carried out at different voltages. The voltage applied was 10 kV, 12.5 kV and 15 kV. The room temperature recorded was 21 °C at 10 kV, 24.6 °C at 12.5 kV and 22.9 °C at 15 kV. The humidity was 43 % at 10 kV, 41% at 12.5 kV and 42% at 15 kV. For each voltage applied, 15 trials were carried out and for each trial the charge acquisition on the batch of the short-glass fibre bundles was recorded. The fibre bundles introduced via the access ports were made to slide down along the length of the electrode. These bundles acquired charge, whilst sliding down the charged electrode

and they were then allowed to fall into the pail. The electrometer measures the charge gained by the fibre bundles.



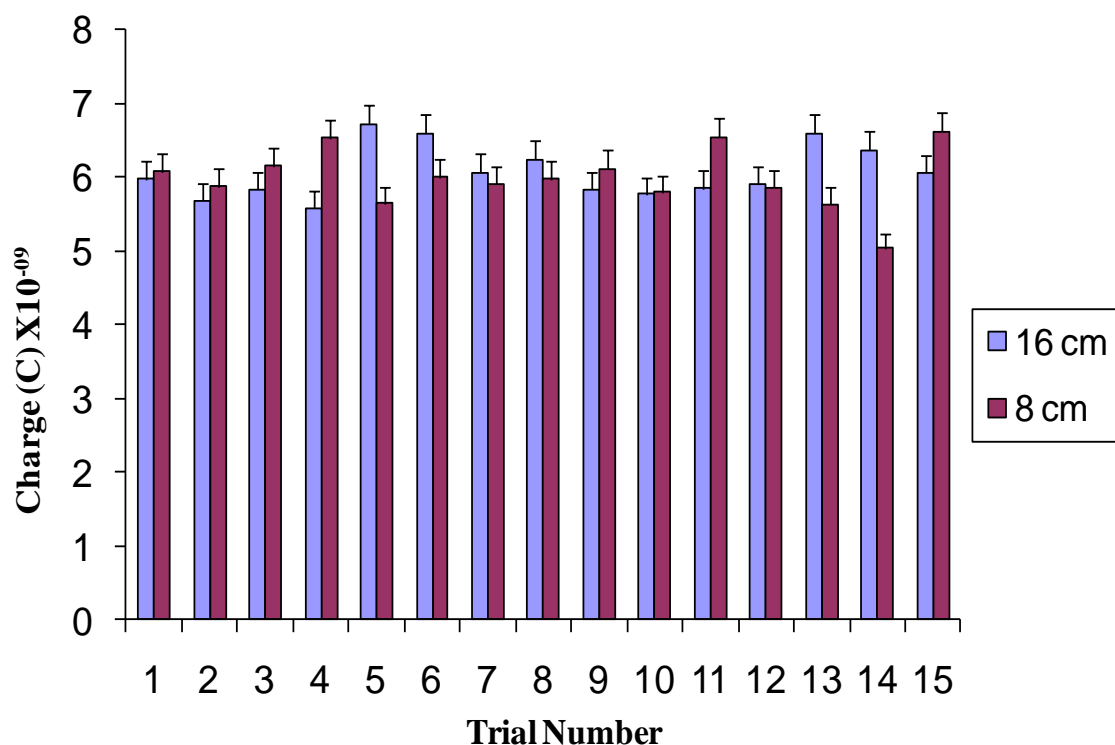
**Figure 4.5:** Charge measurements at different voltages of 15 kV, 12.5 kV and 10 kV applied voltages.

Figure 4.5 represents the charge measurements at the applied voltages of 10 kV, 12.5 kV and 15 kV. For the applied voltage of 10 kV, the charge acquisition on the surface of the fibre bundles was found to be between  $1 \times 10^{-09}$  C to  $2 \times 10^{-09}$  C, for the applied voltage of 12.5 kV, and the charge acquisition on the surface of the fibre bundles was found to be between  $2.9 \times 10^{-09}$  to  $4.1 \times 10^{-09}$  C and for the high voltage of 15 kV, the charge on the surface of the fibre bundles was found to be  $6 \times 10^{-09}$  to  $7 \times 10^{-09}$  C. From this investigation, it was observed that, as the voltage increases, the charge acquisition on the short-glass fibre bundles also increases. From Figure 4.5, it can be seen that at the applied voltage of 15 kV the charge acquisition on the fibre bundles are maximum. Therefore, an applied voltage of 15 kV was

considered for the following investigations. After concluding that 15 kV was the optimal voltage, the next step was to find the optimal electrode length.

#### 4.1.2.2 Charge measurements at different electrode lengths

To find the optimal electrode length required for charging the short-glass fibre bundles, the batch of fibre bundles was introduced at different lengths of the electrode access ports such as, at 160 mm, 80 mm and 40 mm. The fibre bundles were made to slide over these lengths and fall in to the Faraday pail. The applied voltage was set to 15 kV and the Faraday pail was shielded as previously explained in the Section 4.1, keeping orifice of the pail open. The charge acquired by the fibre bundles was recorded after sliding down over a specified length of the charged electrode.



**Figure 4.6:** Charge measurement at different electrode lengths of 160 mm and 80 mm.

Figure 4.6 represents the charge measurements on the short-glass fibre bundles at 15 kV applied voltage for the electrode lengths of 160 mm and 80 mm. The charge on the 160 mm and 80 mm was found to be in between  $5.5 \times 10^{-09}$  C to  $7 \times 10^{-09}$  C. The average charge acquisition on the surface of the fibre bundles for both electrode lengths (160 mm and 80 mm) was  $6.25 \times 10^{-09}$  C. But for the electrode length of 40 mm, the fibre bundles were observed to bounce and deflect towards the safety enclosure unit of the electrode. At a contact length of 40 mm, the charge measurement was found to be critical since the fibre bundles were not falling into the pail. When comparing the 80 mm with the 160 mm electrode lengths, it was observed that during trial numbers 1, 2, 3, 4, 9, 10, 11, 12 and 15 the charge acquired on the surface of the fibre bundles at 80 mm was found to be higher. Therefore, from this experiment the electrode length was fixed at 80 mm for subsequent experiments.

#### **4.1.2.3 Charge Decay of short glass fibre bundles**

These experiments were conducted to determine the charge decay-time of short-glass fibre bundles, in other words, how quickly any charge induced on the material dissipates or decays through the material as a function of time [48]. The procedure adopted to measure the charge decay on the surface of the fibre bundles was as follows. (i) The batch of fibre bundles was made to slide on the charged electrode at the applied voltage range of 15 kV and 12.5 kV and they were then allowed to fall into the pail. The charge acquisition on the surface of the fibre bundles was recorded. (ii) The charge on the fibre bundles were recorded until the deflection of the electrometer scale reaches to zero coulombs, which represents the charge decay on the fibre bundles. (iii) The room temperature and humidity was recorded.

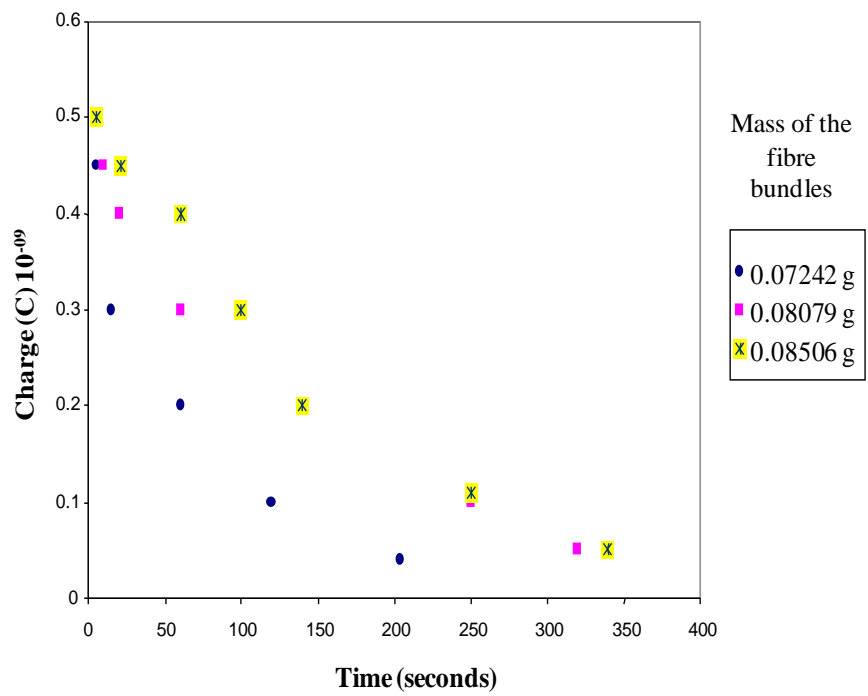


Figure 4.7: Charge decay at an applied voltage of 15 kV.

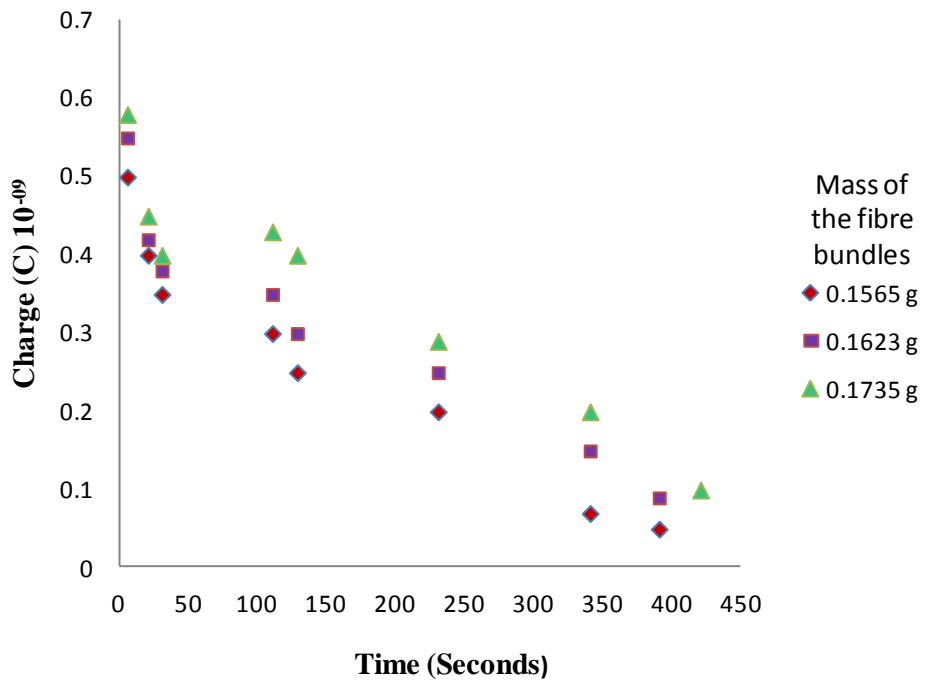
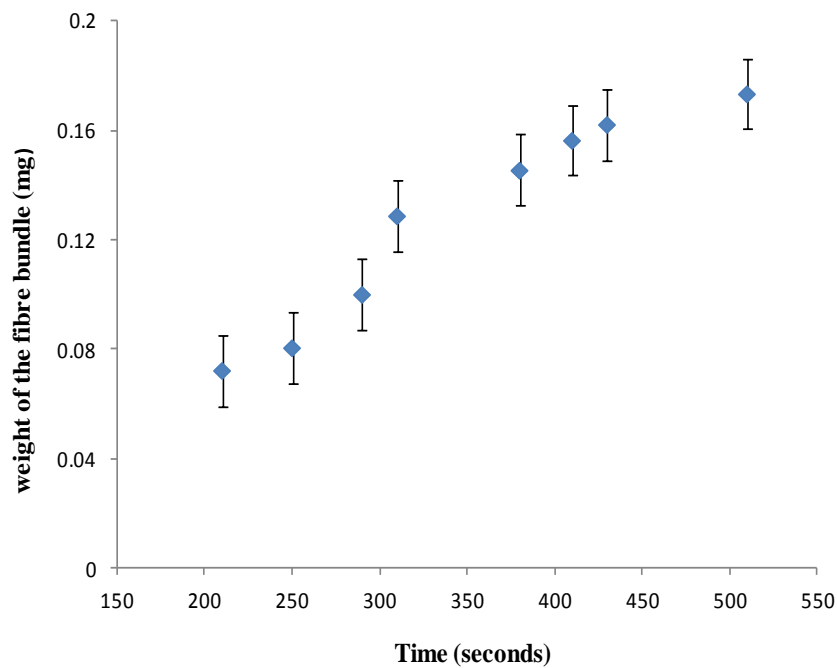


Figure 4.8: Charge decay at an applied voltage of 12.5 kV.

The graphs 4.7 and 4.8 show the experimental results for the charge decay. It was apparent from the graphs that charge on the fibre bundles gradually discharges as the time elapses. The room temperature and humidity were found to be 22.9 °C and 42% respectively. From this experimentation it can be concluded that the time taken for the charge to decay increases as the mass of the fibre bundle increases.



**Figure 4.9:** Charge decay on the fibre bundle at an applied voltage of 15 kV.

Figure 4.9 represents the weight of the fibre bundles and the time taken for the charge on the fibre bundles to decay. From the graph it is evident that as the weight of the fibre bundle increases, then the time taken for the charge to decay on the fibre bundles also increases.

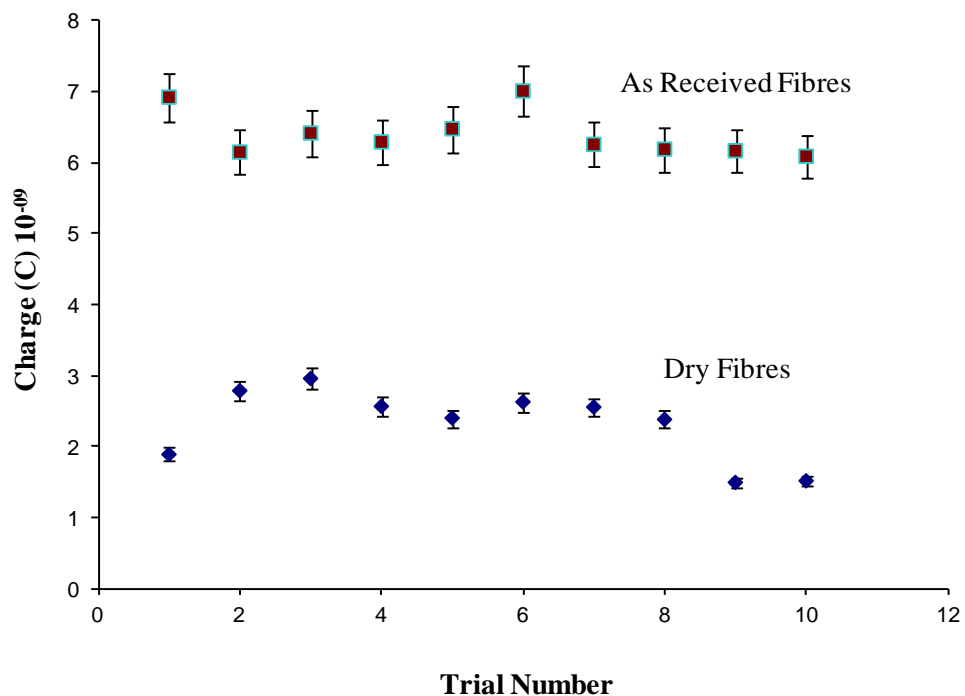
Further experimentation was carried out to investigate the effect of surface adsorbed moisture on charging the short-glass fibre bundles.



#### 4.1.2.4 Effect of surface adsorbed moisture on charging the fibre bundles

The reason for this investigation was to study the amount of charge acquisition on the dried fibre bundles. Therefore, the fibre bundles were dried for a certain amount of time and temperature, i.e. they are dried at 80 °C for 48 hours to remove the moisture content. The applied voltage to the electrode was set to 15 kV. The room temperature and humidity recorded at the time of the experiments were 23.9 °C and 40% respectively.

The Figure 4.10 distinguishes the charge on the ‘as received’ fibre bundles and dried fibre bundles. In both dried and ‘as-received’ fibre bundles, the same batch of fibre bundles were utilised for charge measurements.



**Figure 4.10:** Effect of surface adsorbed moisture on charging the fibre bundles such as dried short-glass fibre bundles (~ 0.2 g) and ‘as-received’ fibre bundles (~ 0.2 g) from industry.

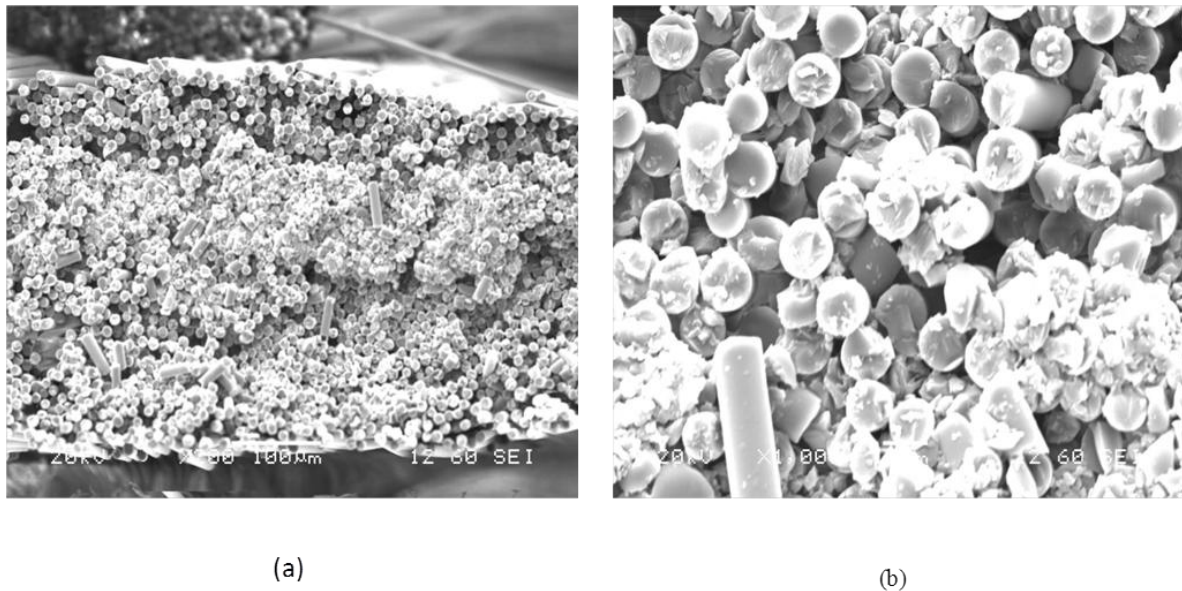
This investigation clarifies that the charge density on the surface of the dried fibre bundles was approximately three times more when compared to the 'as received' fibre bundles. It may be predicted by using the dried fibre bundles, and the degree of alignment of the fibre bundles may be comparatively higher than the 'as received' fibre bundles. This is demonstrated by using the parallel plate capacitor experiments in section 4.3.

In order to obtain higher degree of alignment of the short-glass fibre bundles (3 mm, PPG fibre bundles) for composite manufacturing or pre-pegging, the investigation of the charge acquisition on the surface of the short-glass fibre bundles is important. This was accomplished by the charge measurement experiments. The experimental results obtained from this device were summarized. (i) The amount of voltage required to charge the short-glass fibre bundles was found to be 15 kV. But Kim *et al.* [43] for charging fabric materials used the voltage of 8 kV, (ii) The optimal electrode length required was 80 mm. (iii) The time taken for the charge decay on the surface of the fibre bundles was found to be approximately 350 seconds. (iv) The dried fibre bundles acquire three times more charge, when compared to the 'as received' fibre bundles on an average. The forces of the external electric field acting on the fibre bundles can be enhanced by drying the fibre bundles.

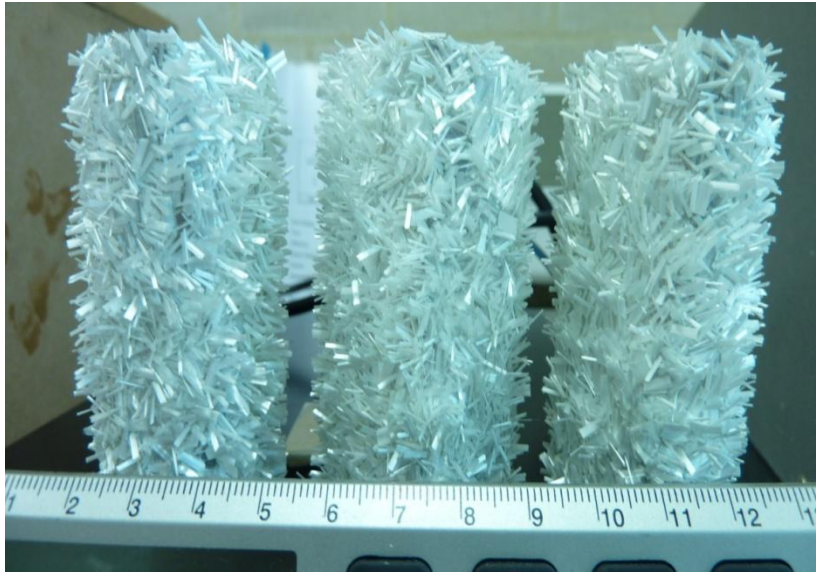
## 4.2 Fibre bundle alignment

The fibre alignment rig was used for aligning the short-glass fibre bundle on the mandrel (see Figure 3.6). The short-glass fibre bundles get charged positively, when they come under the influence of the electrostatic forces of the alignment equipment. The charge from the surface of the fibre bundles moves towards the end of the fibre bundles. The reason for the movement of the charges towards the end of the fibre bundles might be due to the sharp cut-edges of the fibre bundles [12, 13].

The Figure 4.11 (a) represents the SEM images of the cross sectional view of the short-glass fibre bundles (3 mm length) and (b) represents the magnified view of the portion of the cross sectional view shown in (a).



**Figure 4.11:** SEM images of the cross sectional view of the single short-glass fibre bundle (a) and the enlarged view (b).



**Figure 4.12:** Alignment of the short-glass fibre bundles on the mandrel.

As explained in the Section 3.5.1, the short-glass fibre bundles acquire positive charge under the influence of the electrostatic force at the radial electrode (see Figure 3-2) and they get attracted towards the grounded mandrel. The Figure 4.12 represents the alignment of short-glass fibre bundles on the mandrel. It can be seen that the positively charged fibre bundles are propelled to the grounded mandrel and then the fibre bundles continue to adhere to the mandrel since it has adhesive substrate. The reason for the adhesive substrate was the fibre bundles must remain adhered to the mandrel even when the electrostatic force was withdrawn from the equipment. Figure 4.12 show the short-glass fibre bundles have vertical alignment on the adhesive substrate of the mandrel. The degree of fibre bundle alignment recorded for different voltage range is shown in the Table 4.7. The percentage of fibre bundles (given in Table 4.7) retained on the grid, flooded on the floor and adhered to the mandrel was quantified by weighing the mass of the fibre bundles initially fed to the equipment. The degree of fibre alignment on the mandrel was approximated by the counting the number of short-glass fibre bundles that have aligned vertically on the mandrel.

**Table 4.7:** Results from the electrostatic fibre bundles alignment equipment.

<i>Sl. No.</i>	<i>Potential (kV)</i>	<i>Mass of the fibre bundles (gram)</i>	<i>Percentage of fibre bundles on the mandrel</i>	<i>Percentage fibre bundles retained on grid</i>	<i>Percentage fibre bundles on floor or wasted</i>	<i>Percentage of fibre bundles vertical on the mandrel</i>	<i>Fan</i>
1	12	0.67228	25	60.5	11	68.1	ON
2	12	0.59873	27.8	71	14	69	OFF
3	14	0.70928	22.5	57.22	10.28	70	ON
4	14	0.55927	28.1	58.7	13.2	78	OFF
6	18	0.69876	27.2	64.2	12	72.4	ON
5	18	0.65659	26	63.39	10	69.2	OFF
<i>Average</i>		0.649152	26.1	62.50167	11.74667	71.11667	

From the Table 4.7 it can be seen that, the high degree (71%) of fibre bundles orientation can be achieved, when the short-glass fibre bundles are charged positively and then propelled to the grounded mandrel. The mesh or grid that was used to contact charge the fibre bundles tended to misdirect the fibre bundles away from the mandrel. By repeated experimentation, it was determined that the significant volume that is approximately 62.5% of short-glass fibre bundles was being retained on the grid or mesh. In addition, only 26% of short-glass fibre bundles were propelled to the grounded mandrel. In order to achieve an acceptable volume fraction of short-glass fibre bundles on the mandrel, it was necessary to flood the delivery system, but this resulted in a significant volume (approximately 12%) being deposited outside the mandrel, that is, on the floor. The desired lens-effect was not realised because the air stream that propelled the fibre bundles was not adjustable and it proved to be too high. For these reasons, the equipment is required to be modified. The suggestion for how the equipment could be modified is given in the Chapter 5.

### ***4.3 Parallel plate capacitor***

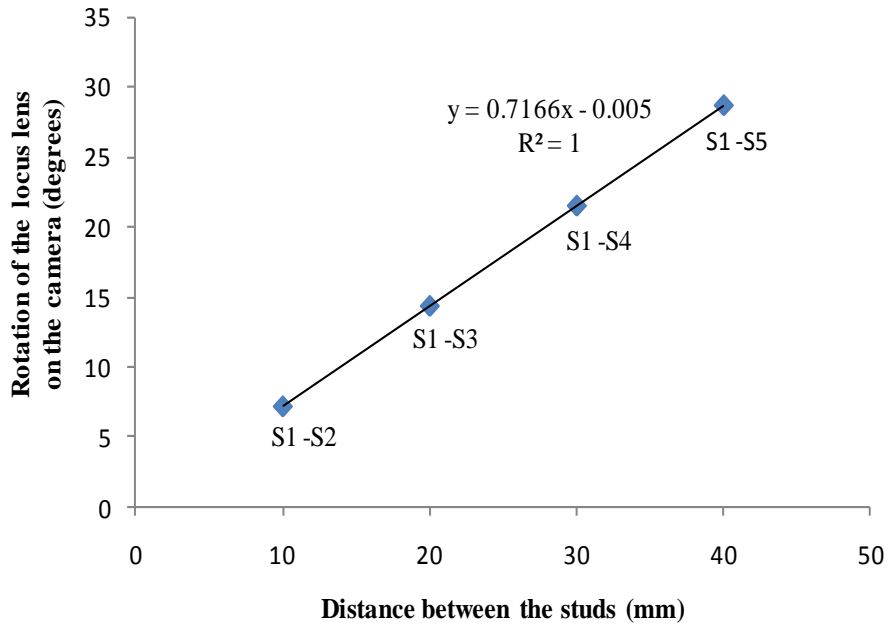
With reference to Section 3.6, the parallel plate capacitor device results are summarized. The result of optimization of the camera is discussed in the following section.

#### ***4.3.1 Optimization of the camera***

The camera was optimised to focus on the entire surface of the capacitor as shown in the Table 4.8. As explained in Section 3.6.2.2, the degree of rotation of the focus lens with respect to the sample studs placed on the surface of the electrode was calculated.

**Table 4.8:** Camera adjustment to focus the entire surface of the electrode

<b><i>Studs</i></b>	<b><i>Distance between the studs (mm)</i></b>	<b><i>Rotation of the focus lens with respect to first stud L (mm)</i></b>	<b><i>Degree of rotation of the focus lens (degrees)</i></b>
S1 to S2	10	3.9	7.16
S1 to S3	20	7.8	14.33
S1 to S4	30	11.7	21.495
S1 to S5	40	15.6	28.66



**Figure 4.13:** Degree of rotation of the focus lens with respect to the studs placed on the surface of the electrode.

The rotation of the locus lens made on the camera was approximately of 0.72/mm.

### **4.3.2 The motion of the fibre bundles in the electric field**

With reference to Section 3.6, the following experiments were conducted to study the direction of the elevation of the fibre bundles when it was charged. As stated by Kim et al, ‘charge forces’ and air drag are the significant forces acting on the charged fibre bundles in an electric field. The time taken by the ‘charge force’ (electrostatic force) to pull the fibre bundles into various orientations was studied experimentally using the parallel plate capacitor.

To visualise the above reason, a quick experiment was performed by placing a 0.2 g of short-glass fibre bundles between the parallel capacitor plates. From this experiment, the following observations were speculated. (i) 10% of the fibre bundles were levitating in



between the plates; (ii) Approximately 80% of them were stuck to the upper plate; and (iii) 10% stood vertically on the lower plate. Given the rationale for random moment of fibre bundles in an electric field, as stated by Kim *et al.* and also based on the theory of corona charging (as described in Section 2.1.3), there may be significant forces (air drag, electrostatic force, gravity) pulling the fibre bundles in various directions, and thus causing levitation. In order to control levitation of the fibre bundles between the plates an enclosed chamber is required, where air drag on the fibre bundles can be prevented. Therefore to control levitation, the parallel plates were enclosed by PPMA material as explained in the experimental Section 3.6. The reason for the fibre to stick to the upper plate might be due to the geometry of the fibre bundle or weight of the individual single fibre bundle. The fibre bundle might have very sharp edges, which accumulate charge (see Figure 2-2) in this region. Thereby, sharp edges have higher charge density [49, 50] that makes the fibre bundles move faster towards the oppositely charged plate.

Considering all these aspects, the detailed study was conducted on the single short-glass fibre bundle in order to investigate its moment in an electric field.

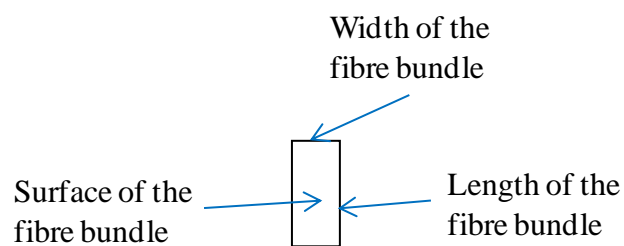
#### **4.3.2.1 Single fibre bundle movement**

A single short-glass fibre bundle was placed at the centre of the lower capacitor plate as explained in the experimental section. The following experiment was conducted to study the influence of electric field on the fibre bundle motion.

(i) *Influence of electric field on the fibre bundle motion*


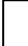
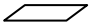
The mass of the fibre bundles of 0.73 mg, the length of the fibre bundles of 3.06 mm and the width of 1.75 mm were placed on the grounded plate. Ten trials were conducted and all the ten trials were performed using the same fibre bundles.

Every movement of the fibre bundles between the plates in an electric field was recorded, as summarised in Table 4.9. The symbolic representation of the fibre bundles and its orientation (horizontal, vertical and flat fibre) is shown below; this leads to the easy explanation to understand Table 4.9.



**Figure 4.14:** Schematic illustration to study the orientation of the fibre bundle in the following tables.

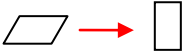

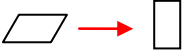

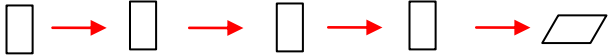
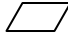

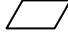


The following represents the symbolic representation of the fibre bundle alignment to read the tables:



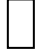

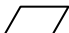
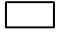
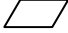
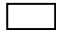

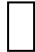




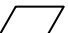


-  = Horizontal alignment of the fibre bundles (length of the fibre bundles in contact with the plate)
-  = Vertical alignment of the fibre bundles (width of the fibre bundles in contact with the plate)
-  = Flat fibre bundles (surface of the fibre bundles in contact with the plate)

If a fibre bundles elevated towards the top electrode, it was represented by 'T' (top electrode), and similarly, if a fibre bundles came into contact with the bottom electrode, it was represented by 'B' (bottom electrode).

Table 4.9 presents a schematic illustration of the orientation of the fibre bundles in an electric field. The first column states the number of runs, i.e. the repetition of experiments. The second column indicates the voltage required for the initial lift of the fibre bundle in an electric field. The forth column presents fibre bundle orientation between the plates. For example, in the first run, Table 4.9 explains that while increasing the voltage from 0 to 15 kV (maximum), at a voltage of 15 kV the first orientation of the fibre bundle was observed, and that was flat. In the first run of the fourth column, at 15 kV applied voltage, the fibre bundle shifts to the top plate (T) and its orientation is 'flat', that is the surface of the fibre bundle in contact with the plate for 23 seconds. After 23 seconds, the fibre bundles shifted vertically, i.e. the width of the fibre bundle in contact with the top plate (T) for 277 seconds. These are the two orientations observed in the first row of the Table 4.9. At each run, fibre bundle orientation (5 minutes observations) was recorded. The last column of the first row represents that, while reducing the voltage to zero, again the orientation of the fibre bundle was observed. For example, while reducing voltage, at 7.2 kV applied voltage, the fibre bundle shifted to the bottom plate (B) and its orientation was vertical. With the further gradual reduction of voltage, at 0 kV, the fibre bundle lies flat. That is, the surface of the fibre bundles is in contact with the bottom electrode. The fibre bundle may start losing its energy initially as observed in Table 4.9, and the fibre bundle shifts towards the bottom plates. Eventually, when voltage was reduced, the fibre bundle may deteriorate its charge and become flat on the bottom plate. At the end of each run, the electrodes will be discharged by a safety discharge probe.

**Table 4.9:** Orientation of the single short-glass fibre bundles

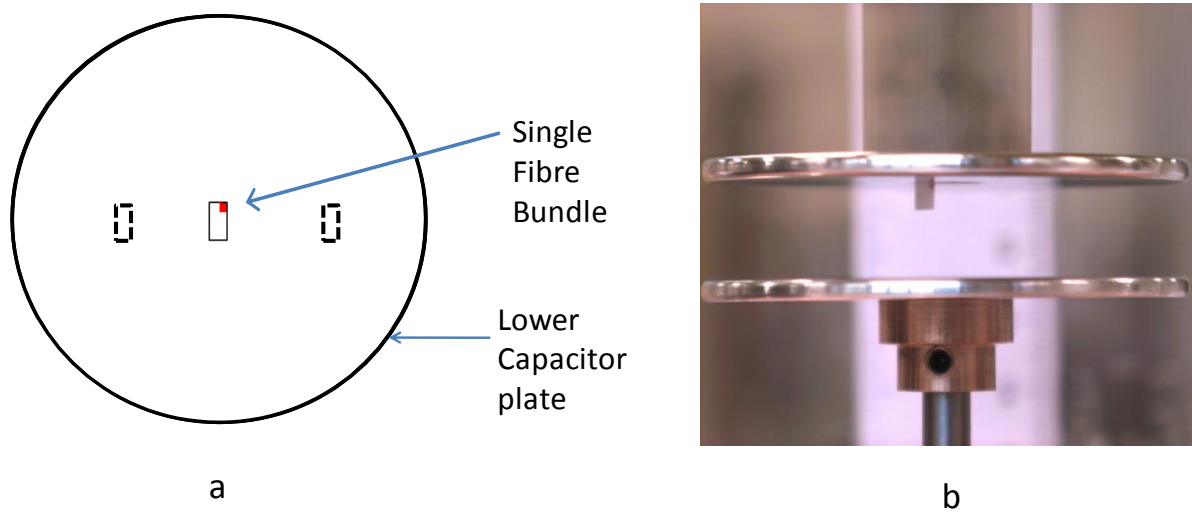
<i>Number of runs</i>	<i>Voltage (kV)</i>	<i>Temperature/ Relative Humidity</i>	<i>Fibre bundle orientation between the plates (While increasing the voltage from 0 kV to 15 kV)</i>	<i>Fibre bundle orientation while reducing the voltage from 15 kV to 0 kV</i>
Run 1	15	24 °C / 22%	 (T- 23 sec) (T-277 sec)	 (B-7.2kV) (B-2.9kV)
Run 2	15	24 °C / 22%	 (T-28 sec) (B-246 sec)	 (B-9.9 kV) (B-0 kV)
Run 3	6.5	24 °C / 22%	 (T-89 sec) (B-16 sec) (T-51 sec) (B-15 sec) (T-100 sec)	 (B-0 kV)
Run 4	10.7	24 °C / 22%	 (T-300 sec)	 (B-7.4 kV)
Run 5	9.2	24.5 °C /22%	 (T-20 sec) (B-223 sec) (T-64 sec)	 (B-8.1 kV) (B-0 kV)

<i>Number of runs</i>	<i>Voltage (kV)</i>	<i>Temperature/ Relative Humidity</i>	<i>Fibre bundle orientation between the plates (While increasing the voltage from 0 kV to 15 kV)</i>	<i>Fibre bundle orientation while reducing the voltage from 15 kV to 0 kV</i>
Run 6	9.7	24.5 °C / 22%	 (T-300 sec)	 (B-0 kV)
Run 7	13.4	25.1 °C / 24%	 (T-300 sec)	 →  (B-7.1 kV) (B-2.7 kV)
Run 8	9.4	4.9 °C / 24%	 →  →  (T-146 sec) (B-72 sec) (T-103 sec)	 (B-5 kV)
Run 9	12.5	24.9 °C / 24%	 (T-300 sec)	 →  →  (B-8.3 kV) (T-2.7 kV) (B-0 kV)
Run 10	9.9	24.9 °C / 24%	 →  →  (T-121 sec) (B-73 sec) (T-103 sec)	 (B-6.4 kV)

From Table 4.9, it was repeatedly observed that the fibre bundle got attracted towards the top positive plate during the initial movement. It means that the fibre bundle after charging gets attracted to the positively charged top electrode. In 6 trials, the fibre bundle got stuck vertically on the top plate. However, at this stage it can be considered the reason for the fibre bundle moving vertically towards the top plate. Because of the surface charging (also called direct charging by Kim *et al.* [23]) on the fibre bundle, the fibre bundle is charged and polarised. Mainly, the cut edges of the fibre bundles are pin pointed and it is assumed that the charge travels towards these cut edges (Refer to chapter 2, geometry of the object and different types of polarization). Thereby, the charge density at the end of the fibre bundles increases gradually. Therefore, the end of the fibre bundles will be attracted to the top positive plate. The voltage required for charging the fibre bundles was between 9 kV to 15 kV.

**(ii) *Influence of electric field on the corner coloured fibre bundle motion***


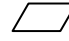



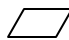
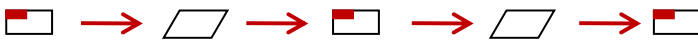
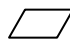

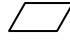
The corner of the fibre bundles was marked in red colour as shown in the Figure 4.15 and placed at the centre of the capacitor plate. The reason for colouring the corner of the fibre bundle was: (i) to investigate out of the four corners, the frequency of particular corner (vertex) of the fibre bundles could be lifted for its initial movement, (the moment the fibre bundles immediately after the charge acquisition) that is, the very first movement of the fibre bundle in an electric field, (ii) to observe the time taken by the fibre bundle to get adhered in each position, and (iii) the optimal voltage required for the fibre bundle to get charged and make its first move. The Figure 4.15 (b) shows that the fibre bundle (0.78 mg), after charging, shifted towards the top positive electrode vertically, that is the width of the fibre bundle was in contact with the plate.










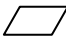
**Figure 4.15:** (a) Schematic illustration of a fibre bundle placement on a grounded capacitor plate and (b) fibre bundle vertically shift vertically towards the top positive plate.

Table 4.3 presents schematic illustrations of the orientation of the fibre bundle in an electric field.

**Table 4.10:** Orientation of the coloured single short-glass fibre bundles

<i>Number of runs</i>	<i>Voltage (kV)</i>	<i>Temperature/ Relative Humidity</i>	<i>Fibre bundle orientation between the plates (While increasing the voltage from 0 kV to 15 kV)</i>	<i>Fibre bundle orientation while reducing the voltage from 15 kV to 0 kV</i>
Run 1	15	23.6 °C / 22%	 (B-261 sec)	 (B-0 kV)
Run 2	10	24 °C / 22%	 (B-160 sec) (T-46 sec) (B-58 sec) (B-55 sec)	 (T-9.9 kV) (B-0 kV)
Run 3	10.5	24 °C / 22%	 (T-5 sec) (B-300 sec)	 (B-5 kV)
Run 4	13.5	24.1 °C / 22%	 (T-64 sec) (B-23 sec) (B-25 sec) (T-23 sec) (B-176 sec)	 (B-0 kV)
Run 5	9.2	24.5 °C / 22%	 (B-10 sec) (T-61 sec) (T-274 sec)	 (B-4.3 kV)



<i>Number of runs</i>	<i>Voltage (kV)</i>	<i>Temperature/ Relative Humidity</i>	<i>Fibre bundle orientation between the plates (While increasing the voltage from 0 kV to 15 kV)</i>	<i>Fibre bundle orientation while reducing the voltage from 15 kV to 0 kV</i>
Run 7	13.5	24.6 °C / 20%	 (T-300 sec)	 (B-5.5 kV) (B-0 kV)
Run 8	13.5	24.9 °C / 20%	 (T-300 sec)	 (B-6.5kV) (B-0 kV)
Run 9	10.4	24.9 °C / 21%	 (T-300 sec)	 (B-5.9 kV) (B-0 kV)
Run 10	13.5	24.5 °C / 21%	 (T-80 sec)	 (B-6.4 kV)

From Table 4.3, it was observed that, 80% of the fibre bundle moved towards the top plate and stood vertical. Further study was carried out by changing the position of placement (i.e. at the centre, on the right side of the plate and on the left side of the plate) of the fibre bundle on the lower electrode. The same fibre bundle having mass of 0.78 mg was used for the study for all the three positions indicated by dotted line as shown in Figure 4.15a. The initial moment of the fibre bundle in all the three positions is explained by the graphical representation in the next section.

#### **4.3.2.3 Multiple fibre bundle motion in the electric field**

In this study two experiments were conducted, and they were as follows. (i) To study the motion of all the three fibre bundles simultaneously in the electric field. (ii) The same batch of three fibre bundles were coloured at the corner and their motion in the electric field was observed.

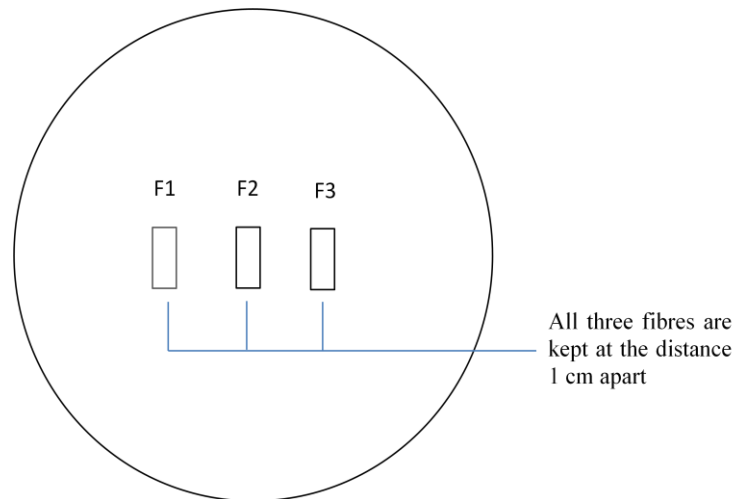
##### ***(i) Study of the multiple fibre bundle motion in the electric field***

The schematic illustration shown in Figure 4.16 represents the fibre bundle arrangement on the lower capacitor plate, where F1, F2 and F3 are the three fibre bundles placed at the distance of 10 mm apart. The fibre bundle F2 was placed exactly at the centre of the plate. The mass (M), length (L) and width (W) of the fibre bundles used for the experimentation were as follows:

F1: M= 0.73 mg, L=2.97 mm, W= 1.54 mm

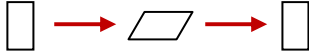

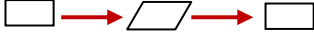
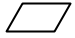

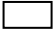




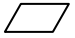
F2: M= 0.73 mg, L=3.06 mm, W= 1.76 mm



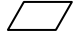

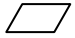


F3: M= 0.73 mg, L=3.01 mm, W= 1.76 mm



**Figure 4.16:** Schematic illustration of the fibre bundle arrangement on the lower plate

**Table 4.11:** Orientation of the three fibre bundles

Number of runs	Voltage (kV)	Temperature/ Relative Humidity	Fibre bundle orientation between the plates (While increasing the voltage from 0 kV to 15 kV)			Reducing the voltage from 15 kV to 0 kV
			F1	F2	F3	
Run 1	11	24.5 <sup>0</sup> C/22%	 (T-32 sec)(B-13 sec)(T-259 sec)	Movement Observed after 4 minutes   (T-60 sec)	 (T-32sec)(B-13sec)(T-259sec)	 (B-7 kV)
Run 2	13	23.6 <sup>0</sup> C/22%	 (T-300 sec)	No Movement observed	 (B-300 sec)	 (T-7.2kV)
Run 3	11.2	23.5 <sup>0</sup> C / 22%	 (T-300 sec)	 (T-300sec)	 (T-79 sec) (B-210 sec)	 (B-6 kV)

<i>Number of runs</i>	<i>Voltage (kV)</i>	<i>Temperature/ Relative Humidity</i>	<i>Fibre bundle orientation between the plates (While increasing the voltage from 0 kV to 15 kV)</i>			<i>Reducing the voltage from 15 kV to 0 kV</i>
			<i>F1</i>	<i>F2</i>	<i>F3</i>	
Run 4	13.2	23.9 <sup>0</sup> C/ 22%	 (T-43 sec) (B-257 sec)	No movement observed	 (T-300 sec)	 (B-7.4 kV)
Run 5	12.6	23.6 <sup>0</sup> C / 22%	 (T-300sec)	 (T-157 sec)	 (T-300 sec)	 (B-7.8 kV)

From the experiments, the initial lifts/ motions of the fibre bundles were observed, the fibre bundles moved immediately towards the top plate and stood vertical. The voltage required to observe the motion of the fibre bundles was between 11 kV to 13 kV.

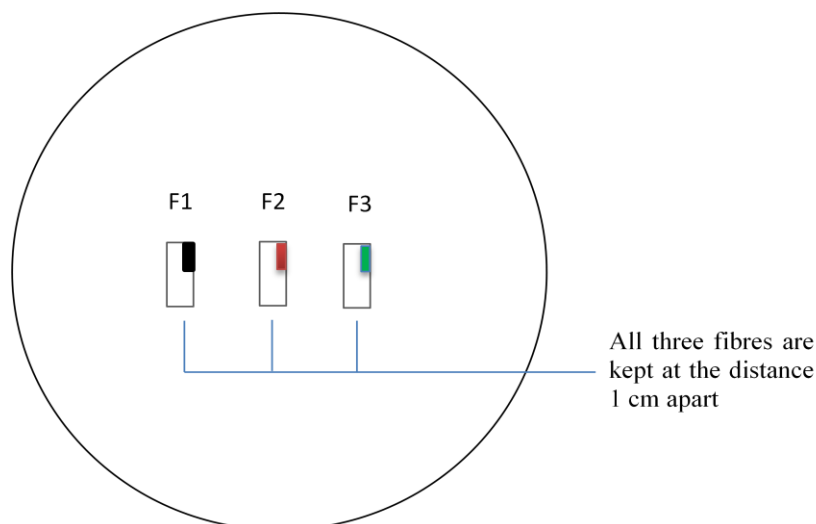
(ii) *Study of the multiple fibre bundle motion in the electric field, where the corner of the fibre bundles were marked.*

Figure 4.17 represents the arrangement of fibre bundles on the lower grounded plate. F1, F2 and F3 are the fibre bundles which were coloured at the corner in order to distinguish the fibre bundles in between the capacitor plates. F1, F2 and F3 show the fibre bundles placed at a distance of 10 mm apart. The fibre bundle F2 was placed exactly at the centre of the grounded plate. All the fibre bundles are marked at the corner with different colours. The reason for the marking on the fibre bundles with different colours is to identify and analyse the motion of the particular fibre bundle. The mass (M), length (L) and width (W) of the fibre bundles are noted.

F1: M= 0.73 mg, L=2.97 mm, W= 1.54 mm



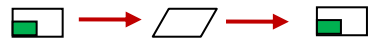
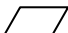




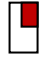

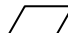
F2: M= 0.73 mg, L=3.06 mm, W= 1.76 mm


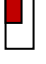






F3: M= 0.73 mg, L=3.01 mm, W= 1.76 mm



**Figure 4.17:** Schematic illustration of the fibre bundle arrangement on the lower grounded plate

**Table 4.12:** Orientation of the three fibre bundles in the electric field

Number of runs	Voltage (kV)	Temperature/Relative Humidity	Fibre bundle orientation between the plates (While increasing the voltage from 0 kV to 15 kV)			Fibre bundle orientation (reducing voltage from 15 kV to 0 kV)
			F1	F2	F3	
Run 1	12	25.4 °C/30%	 (T-32 sec)(B-264 sec) (T-5sec)	 (T-300 sec)	 (T-15sec) (B-13sec)(T-259sec)	 (B-5.2 kV)
Run 2	12.5	25.5 °C/30%	 (T-300 sec)	 (B-300 sec)	 (B-300 sec)	 (T- 5.8 kV)
Run 3	12.4	25.9 °C/29%	No movement observed	 (T-300sec)	 (T-146 sec) (B-103 sec)	 (B-6 kV)

<i>Number of runs</i>	<i>Voltage (kV)</i>	<i>Temperature/ Relative Humidity</i>	<i>Fibre bundle orientation between the plates (While increasing the voltage from 0 kV to 15 kV)</i>			<i>Fibre bundle orientation (reducing voltage from 15 kV to 0 kV)</i>
			<i>F1</i>	<i>F2</i>	<i>F3</i>	
Run 4	13.4	25.9 °C/ 28%	 (B-300 sec)	 (T-300sec)	 (T-300 sec)	 (B-7.4 kV)
Run 5	12.6	25.9 °C/ 28%	 (T-300 sec)	 (T-157sec)	 (T-300 sec)	 (B-7.8 kV)



It was observed that most of the fibre bundles came in contact with the top plate in the first instance. The voltage required was approximately between 11 kV to 13 kV for the movement of the fibre bundle between the plates. Later, experiments were conducted to discover whether dried and hydrated fibre bundles might give different results in their orientation between the plates.

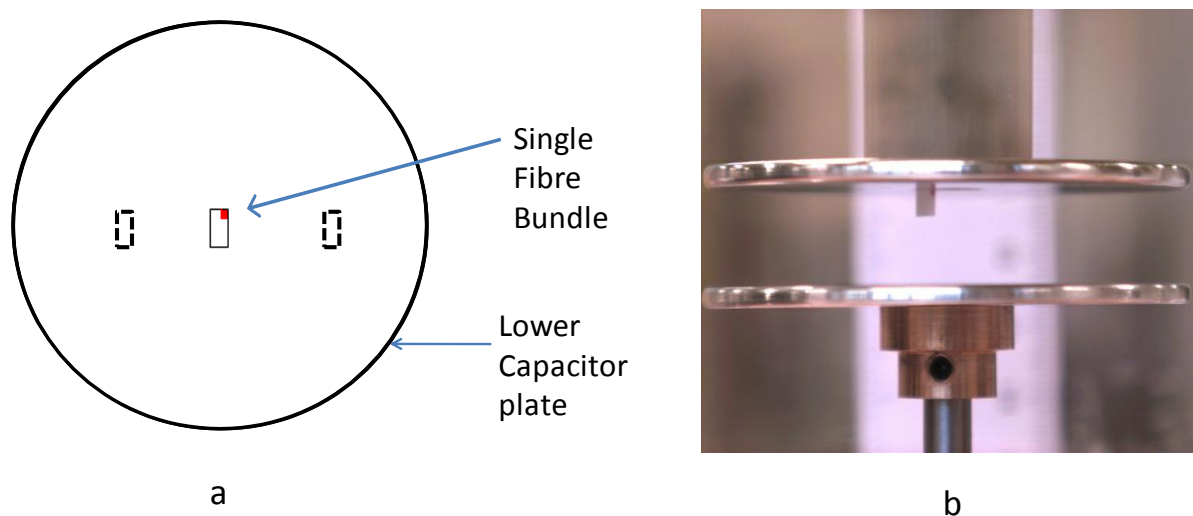
#### 4.3.2.4 Influence of electric field on dried fibre bundle

The experiment results of the dried fibre bundle are as follows:

##### (i) *Study of the dried fibre bundle motion in the electric field*


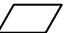







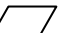
Schematic illustration Figure 4.18(a) shows that the dried fibre bundle was placed at the centre of the grounded plate. The 5 minute observation of the fibre bundle orientation was shown in Table 4.13.


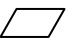

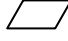
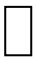
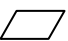


The initial motion of the fibre bundle in the electric field is shown in Figure 4.18(b).



**Figure 4.18:** (a) Schematic illustration of a fibre bundle placement on a grounded capacitor plate and (b) the initial moment of the fibre bundle after it was charged.

**Table 4.13:** Orientation of the dried fibre

<i>Number of runs</i>	<i>Voltage (kV)</i>	<i>Temperature/ Relative Humidity</i>	<i>Fibre bundle orientation between the plates (While increasing voltage from 0 kV to 15 kV)</i>	<i>Fibre bundle orientation (while reducing voltage from 15 kV to 0 kV)</i>
Run 1	12.6	23.9 °C / 25%	 (T-300 sec)	 (B-3.4 kV)
Run 2	13	23.9 °C / 25%	 (T-300 sec)	 (B-5 kV)
Run 3	13.4	24.1 °C / 25%	 (T-300sec)	 (B-0 kV)
Run 4	9.1	24.1 °C / 25%	 (B-300 sec) (B-46 sec) (B-61 sec) (T-200 sec)	 (B-7 kV)
Run 5	7	24.1 °C / 25%	 (T-2 sec) (B-2 sec) (T-2sec)(B-300 sec)	 (B-5 kV)






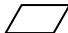

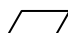

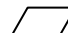
<i>Number of runs</i>	<i>Voltage (kV)</i>	<i>Temperature/ Relative Humidity</i>	<i>Fibre bundle orientation between the plates (While increasing voltage from 0 kV to 15 kV)</i>	<i>Fibre bundle orientation (while reducing voltage from 15 kV to 0 kV)</i>
Run 7	6.6	24.1 °C / 25%	 (T-15 sec) (B-7sec) (T-11 sec) (B-263 sec)	 (B-4 kV)
Run 8	9.6	24.5 °C / 25%	 (T-3 sec) (B-5 sec) (T-33 sec) (B-277 sec)	 (B-6 kV)
Run 9	11.8	24.5 °C / 25%	 (T-300 sec)	 (B-6.2 kV)
Run 10	10.1	24.5 °C / 25%	 (T- 2 sec) (B-2 sec) (T-300 sec)	 (B-6.3 kV)








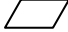

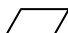
From the above table it was evident that the fibre bundle always moves vertically towards the top positive plate. The voltage required to observe the initial fibre bundle motion was between 7 kV and 13 kV.

(ii) *Study of dried fibre bundle motion in the electric field, fibre bundle marked at the corner.*

The fibre bundles used were dried for 24 hours at 80<sup>0</sup> C. The dried fibre bundle was then placed at the centre of the plate. The mass of the fibre bundle before drying and after drying was measured. The mass of the fibre bundle before drying was 0.73 mg, and after drying was 0.60 mg. The time taken for each orientation of the fibre bundles was recorded and is shown in Table 4.14.

**Table 4.14:** Orientation of the dried fibre bundle between the plates

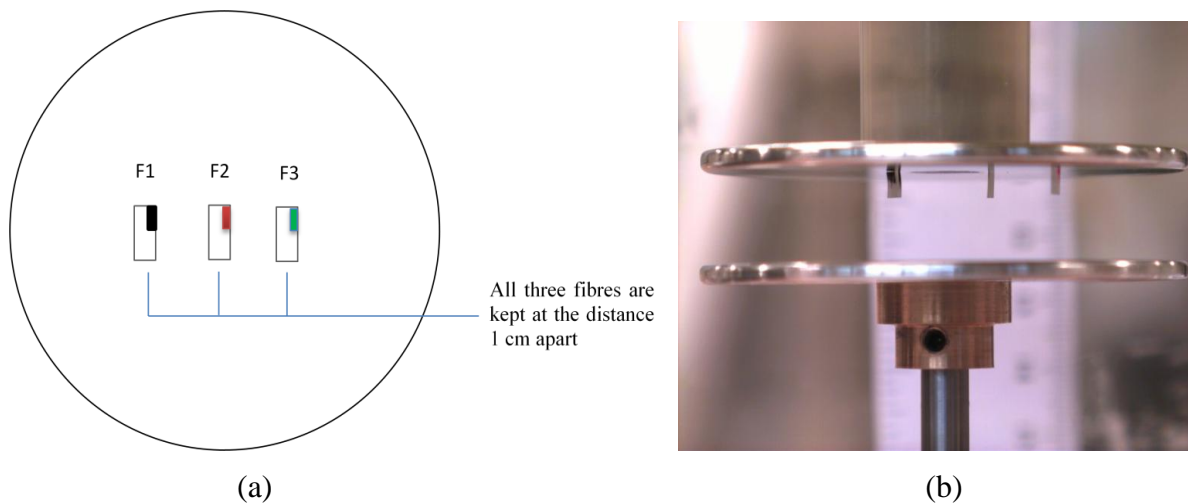
<i>Number of runs</i>	<i>Voltage (kV)</i>	<i>Temperature/ Relative Humidity</i>	<i>Fibre bundle orientation between the plates (While increasing the voltage from 0 kV to 15 kV)</i>	<i>Fibre bundle orientation (while reducing voltage from 15 kV to 0 kV)</i>
Run 1	11.4	24.5 <sup>0</sup> C / 22%	 (T-300 sec)	 (B-6 kV)
Run 2	11.8	24.5 <sup>0</sup> C / 22%	 (T-300 sec)	 (B-5.6 kV)
Run 3	10.9	24.5 <sup>0</sup> C / 21%	 (T-300sec)	 (B-0 kV)
Run 4	10.2	24.5 <sup>0</sup> C / 22%	 (T-7 sec) (B-300 sec)	 (B-7 kV)
Run 5	5.3	24.5 <sup>0</sup> C / 21%	 (T-26 sec) (B-280 sec)	 (B-5 kV)

<i>Number of runs</i>	<i>Voltage (kV)</i>	<i>Temperature/Relative Humidity</i>	<i>Fibre bundle orientation between the plates (While increasing the voltage from 0 kV to 15 kV)</i>	<i>Fibre bundle orientation (while reducing voltage from 15 kV to 0 kV)</i>
Run 6	10	24.6 °C /21%	 (T-4 sec) (B-300 sec)	 (B-5.5 kV)
Run 7	9.3	24.6 °C /21%	 (T-8 sec) (B-20 sec) (T-3 sec) (B-280 sec)	 (B-4 kV)
Run 8	8.4	24.6 °C /21%	 (T-7 sec) (B-26 sec) (T-270 sec)	 (B-6 kV)
Run 9	8.2	24.8 °C /21%	 (T-13 sec) (B-10 sec) (T-25 sec) Later continuously moving up and down difficult to record time, only few initial movements were recorded.	 (B-6.2 kV)
Run 10	9.6	24.4 °C /21%	 (T- 10 sec) (B-300 sec)	 (B-6.3 kV)

In both Tables 4.13 and 4.14, similar results were observed: The dried fibre bundles, after charging, tended to move towards the top positive plate and always stood vertically. The two reasons were: (i) the charge on the surface of the dried fibre bundles travel quickly along the longitudinal section and accumulate at the sharp cut edges. Because of the higher charge density at the cut edge of the fibre bundle, it was observed that the width of the fibre bundle will come in contact with oppositely charged upper capacitor plate. (ii) The fibre bundles were dried at a certain temperature, which thus resulted in melting the embedded resin. In run 3, at the voltage of 5.3 kV, the fibre bundles charged and took an initial lift very quickly. From these experiments, it can be said that, the maximum voltage required to charge the fibre bundles was 11 kV.

**(iii) Study of the three dried fibre bundle motion in the electric field**

The three fibre bundles were dried for 24 hours at 80<sup>0</sup> C.








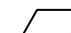

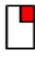

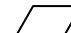









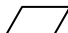
**Figure 4.19:** (a) Schematic illustration of the fibre bundle arrangement on the lower plate. All three fibre bundles are kept at the distance of 10 mm apart and the photograph (b) shows the motion of the dried fibre bundles in the electric field.

In the case of the dried fibre bundles, the voltage required for the initial movement fibre bundle is less when compared with the 'as received' fibre bundles. The minimum and maximum potential range used to charge the dried fibre bundle was (see Table 4.14) 5.3 kV and 11.8 kV respectively.



**Table 4.15:** Orientation of the dried fibre bundle between the plates

<i>Number of runs</i>	<i>Voltage (kV)</i>	<i>Temperature/ Relative Humidity</i>	<i>Fibre bundle orientation between the plates (While increasing voltage from 0 kV to 15 kV)</i>			<i>While reducing voltage from 15 kV to 0 kV</i>
			<i>F1</i>	<i>F2</i>	<i>F3</i>	
Run 1	13.6	24.5 <sup>0</sup> C/23%	 (B-30 sec) Later observed random movement between the plates	 (B-48 sec)	 (T- 15 sec)	 (B-0 kV)
Run 2	9	24.4 <sup>0</sup> C/22%	 (T-300 sec)	 (T-40 sec) Later observed random movement between the plates	 (T-80sec) Later observed random movement between the plates	 (B-0 kV)
Run 3	10	24.6 <sup>0</sup> C /22%	 (T-300 sec)	 (T-300 sec)	 (B-300 sec)	 (B-0 kV)

<i>Number of runs</i>	<i>Voltage (kV)</i>	<i>Temperature/ Relative Humidity</i>	<i>Fibre bundle orientation between the plates (While increasing voltage from 0 kV to 15 kV)</i>			<i>Fibre bundle orientation (while reducing voltage from 15 kV to 0 kV)</i>
			<i>F1</i>	<i>F2</i>	<i>F3</i>	
Run 4	9.8	24.6 <sup>0</sup> C/ 22%	 (T-300sec)	 (T-80 sec)  Later observed random movement between the plates	 (T-300 sec)	 (B-0 kV)
Run 5	10.5	24.4 <sup>0</sup> C / 22%	 (T-50 sec) Later random up and down movement was observed	 (T-300 sec)	 (T-300 sec)	 (B-7.8 kV)

From this set of dried fibre bundle experiments, it was apparent that a significant number of charged dried fibre bundles were attracted towards the upper capacitor plate. The voltage required for aligning these dried fibre bundles were also less. Similarly, the synthetic fabric materials created more static electricity, and these materials were utilised by the Kim *et al.*[38, 44] and Mirnov and Park [39] and others for designing the web formation where they obtained a high degree of fibre alignment and also less voltage range to charge fabric materials.

It can be concluded from the set of dried fibre bundle experiments that, 95% of the fibre bundles moved towards the top plate and 90% of the fibre bundles stood vertically at the top plate. Further analysis was also carried out by hydrating the fibre bundles for a certain amount of time and its effect in the electric field was studied.

#### **4.3.2.5 The study of hydrated fibre bundle motion**

The mass of the hydrated fibre bundle 1 was 0.79 mg and the mass of the hydrated fibre bundle 2 was 0.73 mg and was placed on the lower capacitor plates. By using hydrated bundle 1 and 2, the set of experimental results obtained are schematically illustrated in Tables 4.19 and 4.20. (See appendix). The graphical representation of the initial moment of the hydrated fibre bundle is shown in the Section 4.3.2.6.

In the case of hydrated fibre, the fibre bundle had no movement even at 15 kV since, the fibre bundles may not have enough charge on its surface to lift towards the upper plate, or it might require the applied potential  $> 15$  kV. Therefore, no movement was observed.

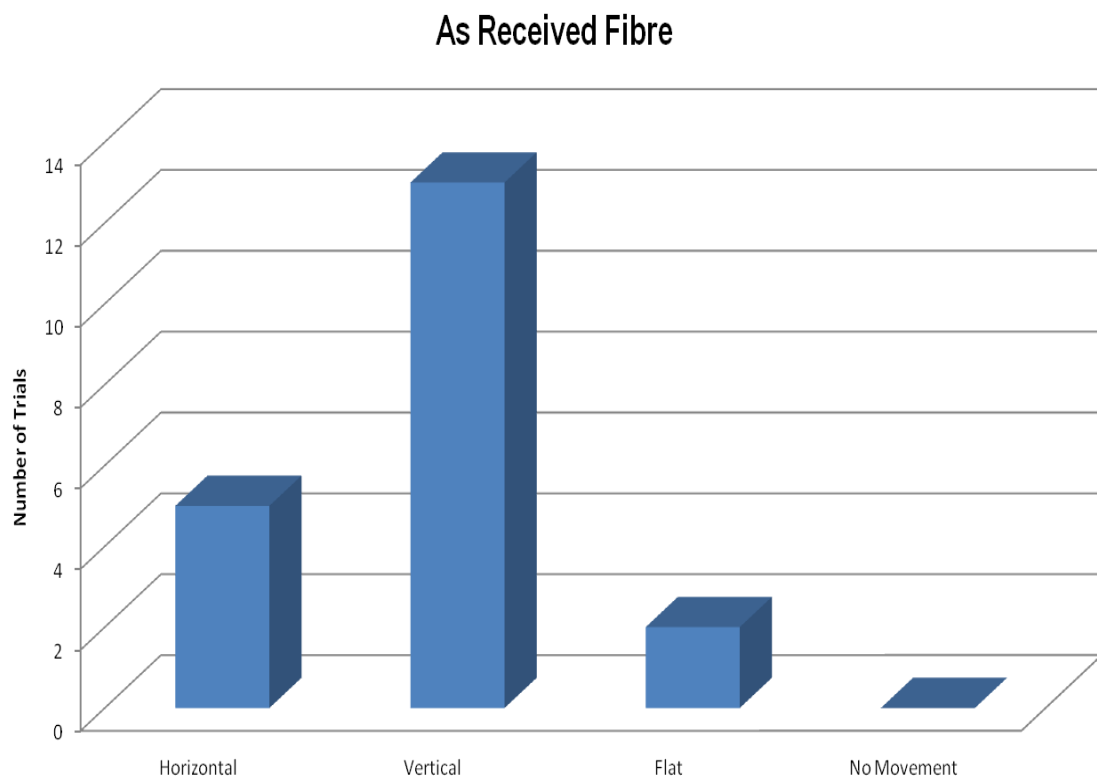
This may be due to the moisture content on the fibre bundle. From the initial 8 runs, no movement was observed at the applied voltage of 15 kV, while during the last two runs, it was observed that the fibre bundles started elevating at 13 kV, by this time. The fibre bundle might have heated up due to the electric field. When the fibre bundle is humid water molecules can collect on the surface of the materials. This can prevent the buildup of electrical charges. In contrast, the buildup of electrical charges is found where the material is dry and less humid. This was observed experimentally when the fibre bundles were dried. When the dried fibre bundle was charged, it built up electric charges on its surface, as the electrical force field came from the surface. This field will attract objects that have no charge or neutral objects. Additionally, this field will strongly attract an upper plate that has an opposite charge on its surface. Therefore, the dried fibre bundle requires less amount of external potential to charge its surface when compared to humid fibre bundle. Also, in this current research, it was experimentally proven that the dried fibre bundle can be charged by using less external potential and 98% of the fibre bundle may be aligned. In the case of 'as received' fibre bundles from the industry may require higher voltage when compared to dried fibre bundle. Also, the moment of fibre bundle in an electric field was random, and experimentally it was observed that approximately 60% of them may be aligned.

The percentage of the degree of the fibre bundle alignment in all the three conditions ('as received', dried fibre bundle and humid fibre bundle) is summarised graphically in the next section.

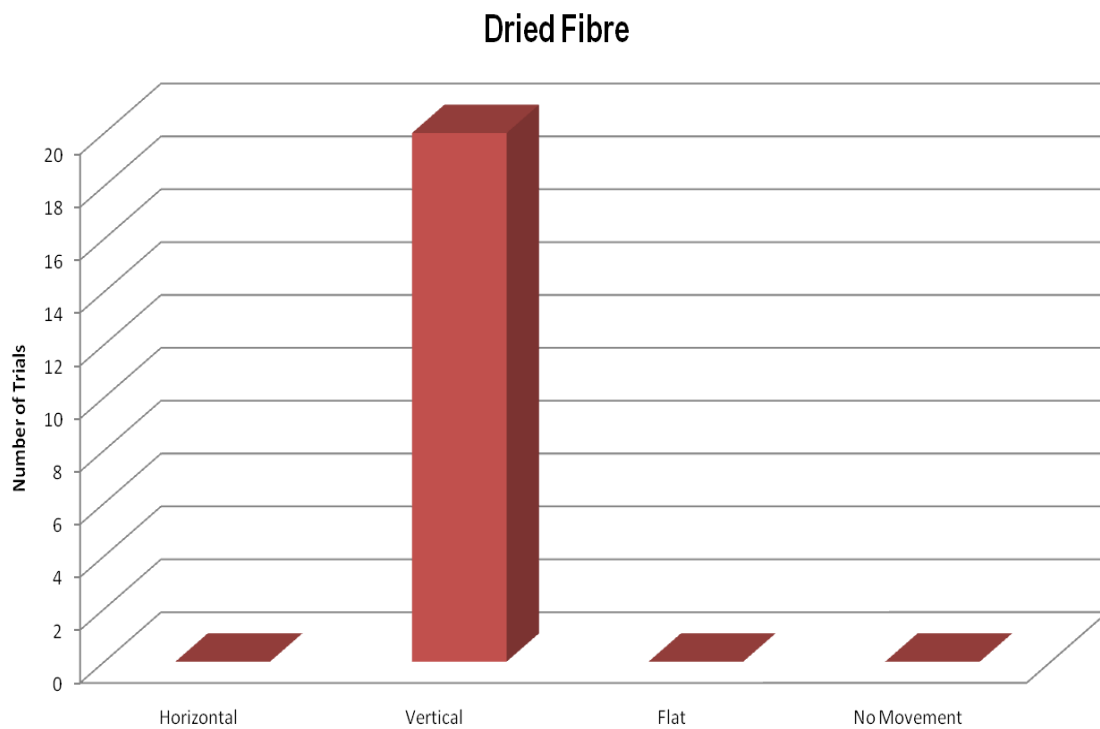
#### 4.3.2.6 Graphical representation of the fibre bundle motion in the electric field

All the above 12 tables are briefly explained in the graphical representation. Graphs were plotted for only the initial fibre bundle movement.

Figure 4.20 represents the 'as received' fibre bundle movement between the plates. The initial movement of the fibre bundle shows that only 60% of the 'as received' fibre bundles stood vertically to electrode plate.

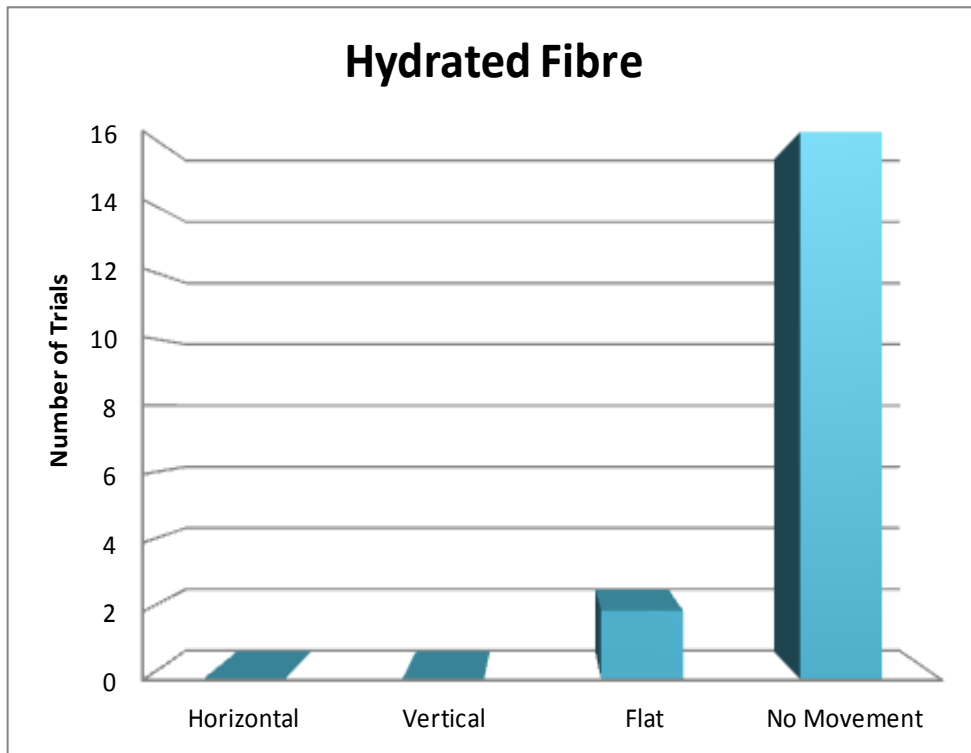


**Figure 4.20:** Graphical representation of the 'as received' fibre bundle initial movement



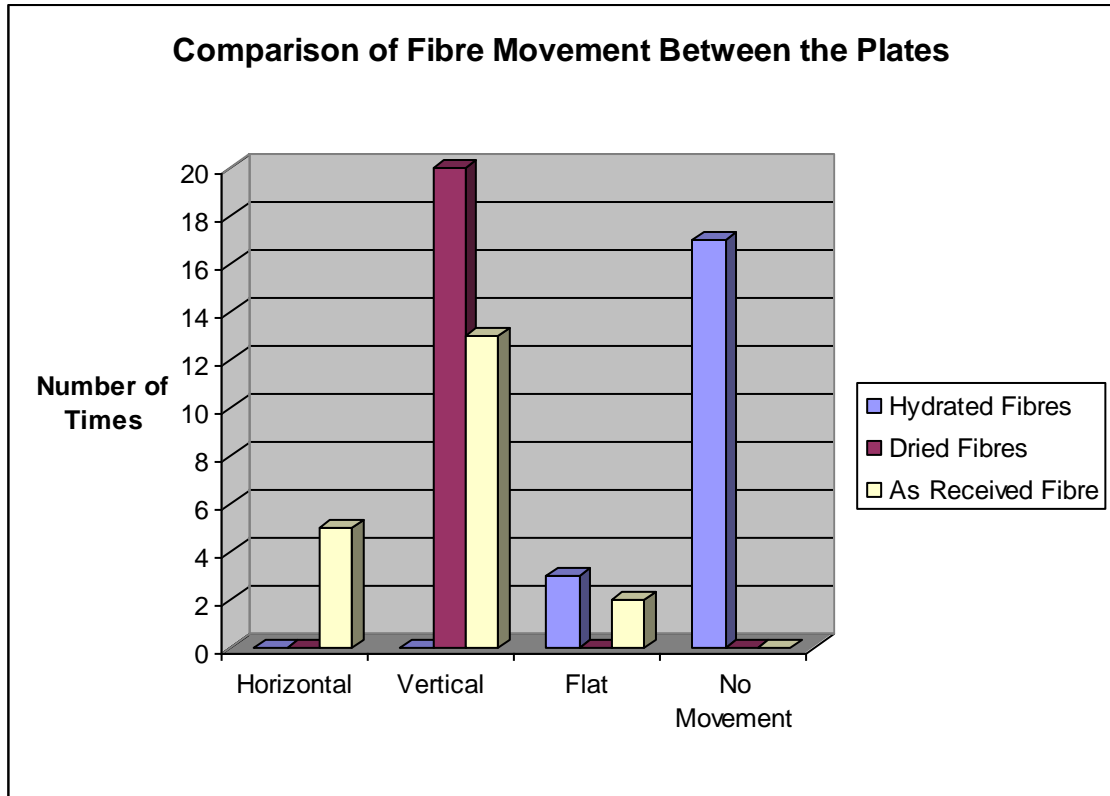
**Figure 4.21:** Graphical representation of the dried fibre bundle initial movement

From the dried fibre bundle study it was observed that the fibre bundle orientation was 99% when it was dried and exposed to electric field. While in the case of the hydrated fibre, it was very distinctly seen that no movement was observed during 16 runs. While in 4 runs, the fibre bundle stood flat at the upper electrode. The Mitalas *et al.* [51] demonstrated that as the relative humidity increased, the moisture content on the glass fibre also increased. When the moisture content on the fibre bundle increases, the weight of the fibre also increases and also that the moment of the fibre bundle was not observed in the electric field. Therefore, the humid fibre bundle resists its moment in the electric field. Figure 4.22 shows the graphical representation of the moment of the hydrated fibre bundle in the electric field between the parallel capacitor plates.



**Figure 4.22:** Graphical representation of the hydrated fibre bundle initial movement

Figure 4.23 shows the comparison between all the three types of fibre bundles, namely the ‘as received’ fibre bundle from industry, the dried fibre bundle and the hydrated fibre.



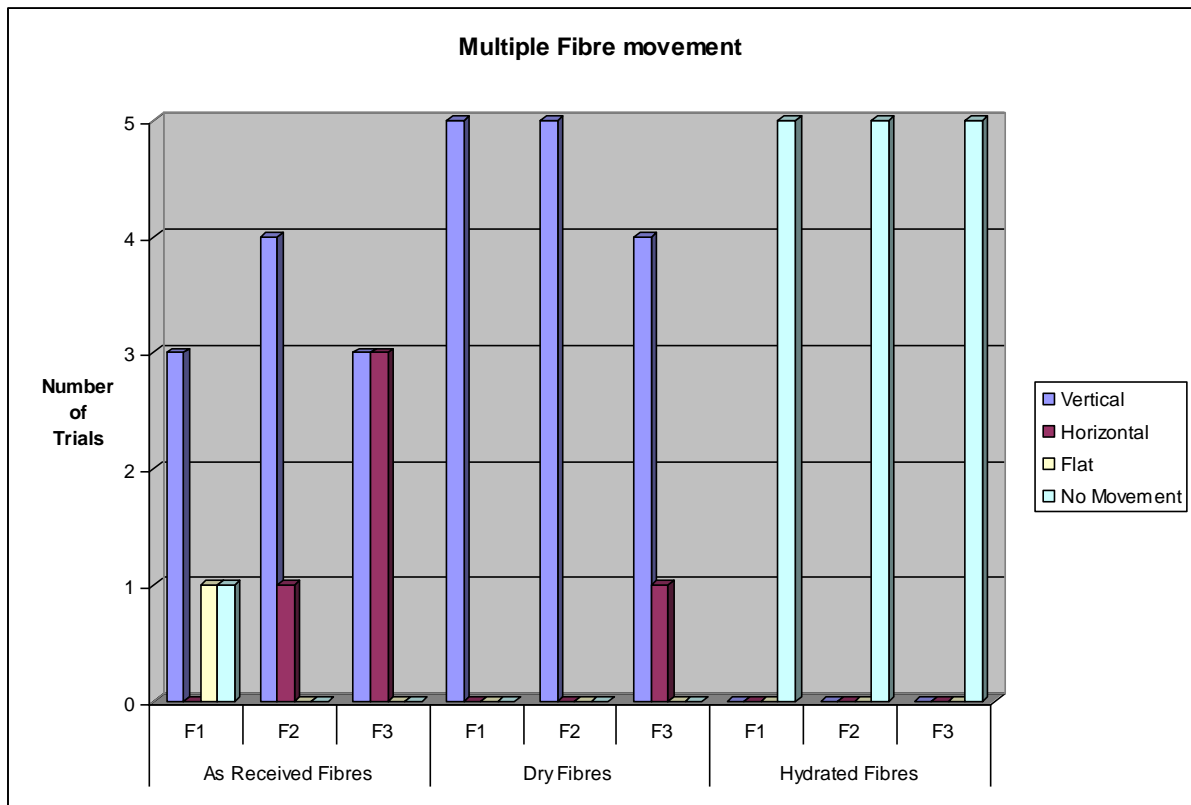
**Figure 4.23:** Graphical representation of the fibre bundle movement between the capacitor plates.

Figure 4.23 shows the graphical representation of the fibre bundle movement when the fibre bundles were dried, hydrated and ‘as received’ from industry. It can be observed from the dried fibre bundles, that a higher degree of alignment can be achieved when compared to the ‘as received’ fibre bundles from the industry. The reason for the achievement of the higher degree of alignment in case of the dried fibre bundle was the retention of the static charge.



#### **4.3.2.7 Graphical representation of the multiple fibre bundle movement**

Figure 4.24 represents the graphical representation (taken from the Section 4.3.2.3 and Tables 4.14 and 4.15) of the multiple fibre bundle movement in the electric field. The three fibre bundles (F1, F2 and F3) were used to observe its moment in the electric field. The five trials were conducted. The first set of experiments were conducted on the ‘as received’ fibre bundles from the industry and their orientation was recorded which is shown in the graph below. Meanwhile, in the second set of experiments, the fibre bundles F1, F2 and F3 were dried for 24 hours at 80 °C and their movement was observed in the electric field and recorded. Similarly, in the third set of experiments, fibre bundles F1, F2 and F3 were hydrated and their moment in the electric field was observed and recorded. As shown in the graph below, in the case of ‘as received’ fibre bundles 70 % of the fibre bundles were attracted towards the top plate. While in dried fibre bundles 99% fibre bundles were attracted towards the top plate. However, in the case of hydrated fibre bundles, no moment was observed in the electric field.



**Figure 4.24:** Graphical representation of the multiple fibre bundle movement

**Table 4.16:** Differentiating the fibre bundle behavior in the electric field.

	<i>Dried Fibre bundles</i>	<i>Hydrated Fibre bundles</i>	<i>As received Fibre bundles</i>
<b><i>Voltage (kV)</i></b>	Between - 5 to 13 kV	Minimum -15 kV	Between- 6.5 to 15 kV
<b><i>Distance between the plates</i></b>	10 mm	10 mm	10 mm
<b><i>Initial fibre bundle lift</i></b>	Always stood vertical at the initial movement.	No movement observed even at 15 kV.	Random movement between the plates.

The Table 4.16 summaries the initial fibre bundle lift and the potential range required to charge the fibre bundle.

The above table shows the difference between the dried fibre bundles, hydrated fibre bundles and 'as received' fibre bundles. The significant importance was given to the initial fibre bundle moment in all the graphical representation. For the practical perspective, the initial moment of the fibre bundle in the electric field is of paramount importance. For the manufacture of the composites, the alignment of the fibre bundle will be on the adhesive substrate. The substrate is previously coated with the resin/ adhesive material, the fibre bundles at its initial moment shifts towards adhesive coated substrate.

From the above set of experiments, it is evident that 99% alignment can be achieved from the dried fibre bundles, when compared to the 'as received' fibre bundles and hydrated fibre bundles. Therefore, in order to achieve the high degree of alignment for the composite manufacturing using the electrostatic technique the fibre bundles needs to be dried and thereby it becomes less humid. By drying the fibre bundles, static electricity charge built on its surface has an electrical force field and exposing it to the external electric field later results in the moment of the fibres with less applied voltage and higher degree of alignment. However, the charge measurement equipment also proved that the dried fibre bundles acquire three times more charge, when compared to the 'as received' fibre bundle from the industry.

## **CHAPTER 5**

### **CONCLUSIONS AND FUTURE IMPROVEMENTS**

This chapter contains conclusions and a brief summary of the recommendations for future work that could be carried out for further research.

#### **5.1 Conclusions**

The following conclusions were made from the parallel plate capacitor experiments (a) it is evident that 99% alignment can be achieved from the dried fibre bundles, when compared to the ‘as received’ fibre bundles and hydrated fibre bundles. (b) In the case of hydrated fibre, no fibre movement was observed initially, even when the voltage was increased to 15 kV, since the fibre bundle became heavier and humid, or they may require more voltage (> 15kV). (c) In case of ‘as received’ fibre bundles, some fibre bundles may be humid and some dried and therefore, random movement was observed in the fibre movement between the capacitor plates. However, by repeated experimentation, it was found that 70% of the ‘as received’ short-glass fibre bundle alignment was achieved by exposure to the external electric field, while by drying the fibre bundles the degree of alignment can be increased to 99%, which was proved by this research work.

The results obtained from the parallel plate experiments are proven by the results of the charge measuring equipment. In the case of charge measuring equipment, the dried fibre bundles acquired approximately three times the surface charge when compared to the ‘as received’ fibre bundles from the industry. This means, the surface of the dried fibre bundle acquired three times more static charge under the influence of electric field. Because the

static electric charge on the surface of the dried fibre bundle was three times more, this resulted in the higher degree of alignment of the fibres by using parallel plate capacitor set-up. Another aspect of the charge measuring device is that it does not only measure the surface charge on a bulk of short-glass fibre bundles but it can also determine the time taken for the charge decay on the surface of the short-glass fibre bundles.

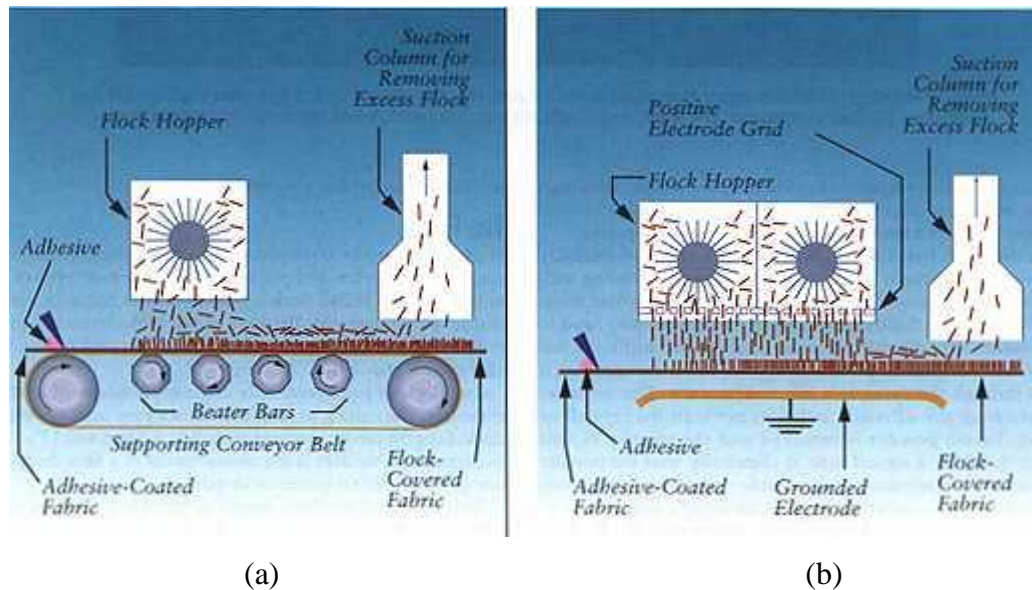
In case of fibre alignment equipment, approximately 90% of the short-glass fibre bundles were flooded on the floor as well as retained on the grid. The remaining 10% of fibres were propelled on to the grounded mandrel. Because the air stream that propelled the fibre bundles was not adjustable, it proved to be too high and the electrode arrangement required reconstruction. Therefore, the equipment needs modification.

## **5.2 *Future Improvements***

The modifications or future improvements of the fibre alignment rig are as follows: (a) Motorization of the mandrel is required. (b) It was observed that bind-free fibre bundles are charged and orientate better than the sized fibre when an electrostatic force is applied. Therefore, the short-glass fibre must be dried for a certain time and at a given temperature. This might remove the sizing on the short-glass fibre. (c) Electrode configuration must be reconsidered by replacing the grid or mesh. Instead of using the radial shaped positive electrode and circular grounded electrode, if the electrode geometry is identical, better results can be obtained. Finally (d) the air stream that propelled the fibre towards the radial electrode needs to be variable rather than constant.

### 5.2.1 Fibre alignment rig

By making use of the results from the charge measurement and parallel plate capacitor experiments, the e-deposition/ fibre alignment equipment can be prototyped and this is similar to Figure 5.1.



**Figure 5.1:** Flocking Process, used in textile industry to align the fabric [52]. (a) Flock application by vibration method and (b) flock application by electrostatic method.

In the textile industry, flocking is used extensively to align fabric materials. As shown in Figure 5.1, the grounded electrode was placed below the substrate. The hopper (short fibre delivery equipment) was embedded with the positive electrode to charge the fibre bundles. Both the electrodes were placed parallel to each other. By applying the voltage, an electrostatic field was created; this causes the flocking material to orientate perpendicular to the substrate. At the end of the substrate a suction column was introduced to remove the excess flocks. It was suggested that the flocking materials are sensitive to the atmospheric conditions, and that therefore the flocking operations should be conducted in a temperature controlled environment with humidity below 60% [6].

The above equipment can be modified for the e-deposition/ alignment of fibre bundles. The important factors/ parameters to be considered while orientating the short-fibre bundles were the density of fibres on the conveyor belt, the distance between the hopper and the substrate, the field strength and the flocking time. Also the combination of vibrating substrate and electrostatic deposition method of fibre deposition may have an advantage of spreading the fibre uniformly on the substrate. The optimal design for flocking is suggested by Liu *et.al.* [53] and Zhong *et al.* [54]. These parameters depend upon the type of fibre bundles used for flocking or pre-pegging.

In case of the parallel plate electrode set-up, the introduction of the third electrode increased the strength of the electric field, and, in turn, this increased the degree of alignment [55].

## APPENDIX

### Parallel plate capacitor experimental results

Few experimental results related to the parallel plate capacitor are given below.

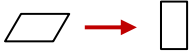


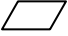

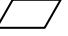

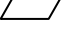

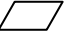
#### **I. The motion of the 0.78 mg fibre bundles in the electric field, by placing the fibre bundle at different places on the bottom plate.**

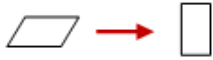
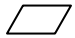
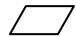
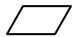

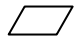
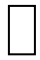
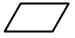
##### ***(i) The fibre bundle (0.78 mg) placed at the centre of the plate.***

A single fibre bundle of mass 0.78 mg was placed at the centre of the bottom capacitor plate. The main objective of this experiment is to find out the initial trend in the movement of the fibre bundle when placed at the centre of the capacitor plate. The 10 trials were carried out and its results are summarised in the Table 1 below.



**Table 1:** Orientation of the single short-glass fibre bundles

<i>Number of runs</i>	<i>Voltage (kV)</i>	<i>Temperature/ Relative Humidity</i>	<i>Fibre bundle orientation between the plates (While increasing the voltage from 0 kV to 15 kV)</i>	<i>Fibre bundle orientation while reducing the voltage from 15 kV to 0 kV</i>
Run 1	11.6	24.5 °C / 22%	 (T-95 sec) (T-205 sec)	 (B-2.9 kV)
Run 2	10.7	23.6 °C / 22%	 (T- 18 sec) (T- 33 sec) (B-250 sec)	 (B-0 kV)
Run 3	15	24.1 °C / 22%	 (T-300sec)	 (B-0 kV)
Run 4	13.9	24.1 °C / 22%	 (B-300 sec)	 (B-0 kV)
Run 5	12.3	24.4 °C / 22%	 (T-175 sec) (B-125 sec)	 (B-0 kV)

<i>Number of runs</i>	<i>Voltage (kV)</i>	<i>Temperature/ Relative Humidity</i>	<i>Fibre bundle orientation between the plates (While increasing the voltage from 0 kV to 15 kV)</i>	<i>Fibre bundle orientation while reducing the voltage from 15 kV to 0 kV</i>
Run 7	10.2	24.6 °C / 21%	 (T-92 sec) (B-208 sec)	 (B-7 kV)
Run 8	12.9	24.8 °C / 22%	 (B-300 sec)	 (B-5 kV)
Run 9	12.6	24.9 °C / 21%	 (T-300 sec)	 (B-0 kV)
Run 10	14.7	25.1 °C / 21%	 (B-300 sec)	 (B-0 kV)




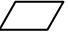


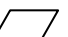

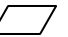
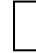

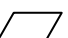
From the above Table 1, the initial lift of the fibre bundle was tended to move towards the top positive plate. It means that the fibre bundle, after charging, gets attracted to the positively charged top electrode. In this experiment, the fibre bundles moved towards the top plate in 7 trials. While out of 7 trials, in 5 trials the fibre bundles got stuck vertically. The voltage required for the movement of the fibre bundle was between 9 kV to 15 kV.





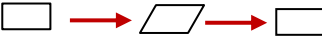




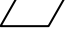
Suppose, if the fibre bundle placed towards the left of the bottom capacitor plate and to observe its orientation in the electric field.

***(ii) The fibre bundle (0.78 mg) placed at the left of the plate***

In this experiment the fibre bundle which was used in the previous experiment placed towards the left of the plate. The orientation of the fibre bundles is summarised in the Table 4. 2.

**Table 2:** Orientation of the single short-glass fibre bundles moved towards left 10 mm away from the centre of the plate.

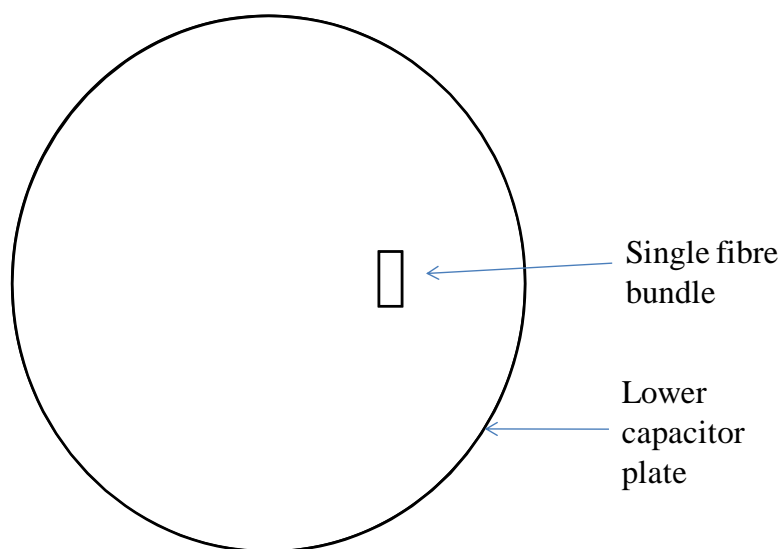
<i>Number of runs</i>	<i>Voltage (kV)</i>	<i>Temperature/ Relative Humidity</i>	<i>Fibre bundle orientation between the plates (While increasing the voltage from 0 kV to 15 kV)</i>	<i>Fibre bundle orientation while reducing the voltage from 15 kV to 0 kV</i>
Run 1	12.5	25.1 <sup>0</sup> C / 21%	 (T-300 sec)	 (B-5 kV)
Run 2	14.2	25.1 <sup>0</sup> C / 21%	 (B-300 sec)	 (B-4 kV)
Run 3	11	25.1 <sup>0</sup> C / 21%	 →  (T-11 sec) (B-290 sec)	 (B-4.8 kV)
Run 4	10.4	25.4 <sup>0</sup> C / 21%	 (B-300 sec)	 (B-5 kV)
Run 5	6.8	25 <sup>0</sup> C / 21%	 →  (T-16 sec) (B-300sec)	 (B-3 kV)

<i>Number of runs</i>	<i>Voltage (kV)</i>	<i>Temperature/ Relative Humidity</i>	<i>Fibre bundle orientation between the plates (While increasing the voltage from 0 kV to 15 kV)</i>	<i>Fibre bundle orientation while reducing the voltage from 15 kV to 0 kV</i>
Run 6	11	25 °C / 21%	 (T-15 sec) (B-300sec)	 (B-2.7 kV)
Run 7	8.4	25.1 °C / 21%	 (T-300 sec)	 (B-0 kV)
Run 8	15	25.1 °C / 21%	 (T-146 sec) (B-72 sec) (T-103 sec)	 (B-5 kV)
Run 9	10.2	25.1 °C / 21%	 (B-300 sec)	 (B-8.3 kV)
Run 10	8.4	25.1 °C / 21%	 (T-300 sec)	 (B-0 kV)

From this experiment, it was found that the fibre bundle tends to move vertically by 80% towards the top plate. Since the fibre bundle was placed at the left side of the plate, its motion was observed either at the middle or at the left side of the plate

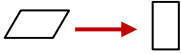
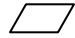

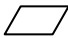


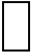
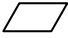

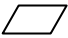
**(iii) The fibre bundle (0.78 mg) placed at the right side of the plate**

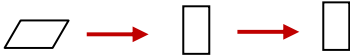


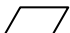
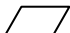
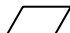


The fibre bundle was placed towards the right side of the plate, 10 mm away from the centre of the capacitor plate. The objective is to find out the movement of the fibre, if it moved towards the right side of the plate. The Table 4.3 shows the schematic illustration of the motion of the fibre bundle in the electric field.



**Figure 4.18:** Schematic illustration of the fibre bundle placement on the grounded plate, 10 mm away from the centre.

**Table 3:** Orientation of the single short-glass fibre bundles moved towards the right 10 mm away from the centre of the plate.

<i>Number of runs</i>	<i>Voltage (kV)</i>	<i>Temperature/ Relative Humidity</i>	<i>Fibre bundle orientation between the plates (While increasing the voltage from 0 kV to 15 kV)</i>	<i>Fibre bundle orientation while reducing the voltage from 15 kV to 0 kV</i>
Run 1	12.9	21.9 <sup>0</sup> C / 27%	 (T-95 sec) (T-205 sec)	 (B-2.9 kV)
Run 2	14.8	22.3 <sup>0</sup> C / 27%	 (B-300 sec)	 (B-0 kV)
Run 3	8.7	22.6 <sup>0</sup> C / 25%	 (T-36 sec) (B-219 sec) (T-45 sec)	 (B-0 kV)
Run 4	14.7	22.9 <sup>0</sup> C / 25%	 (B-300 sec)	 (B-7 kV)
Run 5	9.7	22.9 <sup>0</sup> C / 26%	 (T-219 sec) (B-97 sec)	 (B-0 kV)

<i>Number of runs</i>	<i>Voltage (kV)</i>	<i>Temperature/ Relative Humidity</i>	<i>Fibre bundle orientation between the plates (While increasing the voltage from 0 kV to 15 kV)</i>	<i>Fibre bundle orientation while reducing the voltage from 15 kV to 0 kV</i>
Run 7	7.5	22.9 <sup>0</sup> C / 25%	 (T-203 sec) (T-26 sec) (B-114 sec)	 (B-0 kV)
Run 8	7	23.1 <sup>0</sup> C / 25%	 (T-259 sec) (B-50 sec)	 (B-0 kV)
Run 9	14.4	23.1 <sup>0</sup> C / 25%	 (T-300 sec)	 (B-0 kV)
Run 10	6	23.5 <sup>0</sup> C / 24%	 (T- 300 sec)	 (B-0 kV)




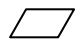
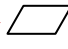



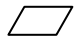
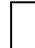
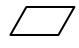

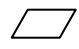
By placing the fibre bundle towards the right, in all the ten runs it was observed that the fibre bundle tends to move towards the right side of the upper electrode when charged. From this experiment it was also found that the fibre bundle tends to move towards the top plate by 80%. At this stage, comparisons are made with other experiments, it can be said that the fibre bundle has a greater tendency to move towards the top plate. A further study was carried out by placing the three fibre bundles to the left, to the right and in the centre.




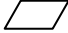



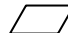




## **II. Orientation of the hydrated fibre bundle under the influence of electric field**

Below table gives the orientation of the hydrated fibre bundles. 20 runs were carried out using hydrated fibre bundles. No moment of the fibre bundle was observed when fibre bundles were under the influence of electric field. The results were represented in the tables below.









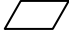


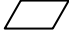
\*NM – No movement observed







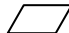


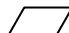




**Table 4:** Orientation of the hydrated fibre bundle 1 between the plates

<i>Number of runs</i>	<i>Voltage (kV)</i>	<i>Temperature/ Relative Humidity</i>	<i>Fibre bundle orientation between the plates (While increasing the voltage from 0 kV to 15 kV)</i>	<i>Fibre bundle orientation while reducing the voltage from 15 kV to 0 kV</i>
Run 1	15	22.9 <sup>0</sup> C / 22%	NM* →  (137 sec) (T-162 sec)	 (B-3.4 kV)
Run 2	15	22.9 <sup>0</sup> C / 22%	NM →  (220 sec) (T-80 sec)	 →  (B-7 sec) (B-0 kV)
Run 3	15	23 <sup>0</sup> C / 21%	NM →  (40 sec) (T-276 sec)	 (B-0 kV)
Run 4	15	23.4 <sup>0</sup> C / 21%	NM →  (41 sec) (B-260 sec)	 (B-7 kV)
Run 5	15	23.6 <sup>0</sup> C / 21%	NM →  (89 sec) (T-220 sec)	 (B-0 kV)

<i>Number of runs</i>	<i>Voltage (kV)</i>	<i>Temperature/Relative Humidity</i>	<i>Fibre bundle orientation between the plates (While increasing the voltage from 0 kV to 15 kV)</i>	<i>Fibre bundle orientation while reducing the voltage from 15 kV to 0 kV</i>
Run 6	15	23.4 <sup>0</sup> C / 21%	NM →  →  →  (18sec) (T-3sec) (B-131sec) (T-33 sec)	 (B-0 kV)
Run 7	15	23.6 <sup>0</sup> C / 21%	NM →  (90 sec) (B-220 sec)	 (B-4 kV)
Run 8	15	23.3 <sup>0</sup> C / 21%	NM →  (87 sec) (B-239 sec)	 (B-0 kV)
Run 9	15	23.3 <sup>0</sup> C / 21%	NM (300 sec)	 (B-0 kV)
Run 10	15	23.3 <sup>0</sup> C / 21%	NM →  →  (56 sec) (T-21 sec) (B-250 sec)	 (B-0 kV)

**Table 5:** Orientation of the hydrated fibre bundle 2 between the plates

<i>Number of runs</i>	<i>Voltage (kV)</i>	<i>Temperature/ Relative Humidity</i>	<i>Fibre bundle orientation between the plates (While increasing the voltage from 0 kV to 15 kV)</i>	<i>Fibre bundle orientation while reducing the voltage from 15 kV to 0 kV</i>
Run 1	15	23.9 <sup>0</sup> C / 21%	NM →  (200 sec) (T-110 sec)	 (B-0 kV)
Run 2	15	23.9 <sup>0</sup> C / 21%	NM →  (218 sec) (T-100 sec)	 (B-0 kV)
Run 3	15	23.9 <sup>0</sup> C / 21%	NM →  →  (105 sec) (B-80 sec) (T-120 sec)	 (B-0 kV)
Run 4	14.9	23.9 <sup>0</sup> C / 21%	 (T-300 sec)	 (B-0 kV)
Run 5	15	23.6 <sup>0</sup> C / 21%	NM →  →  (116 sec) (T-15 sec) (T-198 sec)	 (B-0 kV)

<i>Number of runs</i>	<i>Voltage (kV)</i>	<i>Temperature/ Relative Humidity</i>	<i>Fibre bundle orientation between the plates (While increasing the voltage from 0 kV to 15 kV)</i>	<i>Fibre bundle orientation while reducing the voltage from 15 kV to 0 kV</i>
Run 6	15	23.9 <sup>0</sup> C / 22%	NM →  →  (30 sec) (B-62 sec) (T-208 sec)	 (B-0 kV)
Run 7	15	23.9 <sup>0</sup> C / 21%	NM →  (187 sec) (T-120 sec)	 (B-0 kV)
Run 8	15	23.9 <sup>0</sup> C / 21%	NM →  (157 sec) (B-152 sec)	 (B-0 kV)
Run 9	13.5	23.9 <sup>0</sup> C / 21%	 →  →  (T- 188 sec) (B-66 sec) (T- 50 sec)	 (B-0 kV)
Run 10	13	23.9 <sup>0</sup> C / 21%	 →  (T-200 sec) (B-100 sec)	 (B-0 kV)

## REFERENCES

1. Berschew, E.N. *Electrostatic Charge on the Fiber in Electrostatic Flocking*. Melliand Textilberichte International Textile Reports, 1982. **63**(7): p. 535-536.
2. Farnoosh, N., K. Adamiak, and G.S.P. Castle, *Three-dimensional analysis of electrohydrodynamic flow in a spiked electrode-plate electrostatic precipitator*. Journal of Electrostatics, 2011. **69**(5): p. 419-428.
3. Wang, C.S., *Electrostatic forces in fibrous filters - a review*. Powder Technology, 2001. **118**(1-2): p. 166-170.
4. Balachandran, W. and W. Machowski, *Electrohydrodynamic atomization of insulating liquids*. 1998 Annual Report Conference on Electrical Insulation and Dielectric Phenomena, Vols 1 and 2, 1998: p. 203-206.
5. Jayasinghe, S.N. and A.C. Sullivan, *Electrohydrodynamic atomization: An approach to growing continuous self-supporting polymeric fibers*. Journal of Physical Chemistry B, 2006. **110**(6): p. 2522-2528.
6. Galicki, D., A.A. Berezin, and J.S. Chang, *Electrohydrodynamic atomization of dielectric fluids*. Ieee 1996 Annual Report - Conference on Electrical Insulation and Dielectric Phenomena, Vols I & II, 1996: p. 365-368.
7. Giles, D.K. and S.E. Law, *Dielectric Boundary Effects on Electrostatic Crop Spraying*. Transactions of the Asae, 1990. **33**(1): p. 2-7.
8. Shue, B., A. Moreira, and G. Flowers, *Review of Recent Developments in Composite Material for Aerospace Applications*. Proceedings of the Asme International Design Engineering Technical Conferences and Computers and Information in Engineering Conference, Vol 1, Pt B, 2010: p. 811-819.
9. Dragan, K. and W. Swiderski, *Studying Efficiency of NDE Techniques Applied to Composite Materials in Aerospace Applications*. Acta Physica Polonica A, 2010. **117**(5): p. 878-883.
10. Wierzicki, T.M. and U.A. Gienger, *Exploiting Advanced Composite Materials for Lightweight Shipboard Shf Satellite Communication Antennas*. 1994 Ieee Milcom Conference Record, Vols 1-3, 1994: p. 17-21.
11. Roessler, L., H. Barager, and J. Francis, *The benefits of using nylon composite materials for automotive applications*. Conference Proceedings at Antec '98: Plastics on My Mind, Vols I-3, 1998. **44**: p. 2611-2617.
12. Feynman R. P., R.B.L., M. Sands *The Feynman Lectures on Physics' Volume I*. Addison-Wesley Publishing Co, USA. 1964.
13. Feynman R. P., R.B.L., M. Sands, *The Feynman Lectures on Physics' Volume II*. Addison-Wesley Publishing Co, USA 1964.
14. Moore, A.D., *Electrostatics: exploring, controlling, and using static electricity*1968: Doubleday.
15. Harper, W.R., *Contact and frictional electrification*1967: Clarendon P.
16. Tang, C.L., *Fundamentals of quantum mechanics: for solid state electronics and optics*2005: Cambridge University Press.
17. Allen, R.C., *Triboelectric Generation: Getting Charged*. 2000.
18. (U.S.), N.R.C., *Digest of literature on dielectrics, Volume 33, P414-415*. 1973.
19. Taylor D M, S.P.E., *"Industrial electrostatics: Fundamentals and measurements"*. Research Studies Press, John Wiley. 1994.
20. <http://www.swicofil.com/flock.html>.
21. Giacometti, J.A., S. Fedosov, and M.M. Costa, *Corona charging of polymers: Recent advances on constant current charging*. Brazilian Journal of Physics, 1999. **29**(2): p. 269-279.
22. Intra, P. and Tippayawong, N. *Effect of needle cone angle and air flow rate on electrostatic discharge characteristics of a corona-needle ionizer*. Journal of Electrostatics, 2010. **68**(3): p. 254-260.
23. Giacometti, J.A. and O.N. Oliveira. *Corona Charging of Polymers*. Ieee Transactions on Electrical Insulation, 1992. **27**(5): p. 924-943.

24. Jahannama M.R. *et al.*, *Examination of Electrostatically Charged Sprays for Agricultural Spraying Applications*. ILASS-Europe'99, July 1999.
25. Krasnitskii, V.I., Apasov, A.M., and S.M. Kontush, *Induction Charging of Water Drops under Partial Blending*. Pisma V Zhurnal Tekhnicheskoi Fiziki, 1990. **16**(18): p. 77-80.
26. Zhao, S.X., Castle, G.S.P., and K. Adamiak, *Comparison of conduction and induction charging in liquid spraying*. Journal of Electrostatics, 2005. **63**(6-10): p. 871-876.
27. Moulson, A. J and Herbert, J. M, *Electroceramics, Materials-Properties Applications*. (London: Chapman and Hall, 1st Edition) P182-183. 1990.
28. Sadiku, M.N.O., *Elements of Electromagnetics, 3rd Edition*
29. Bergman, D.J., *The dielectric constant of a composite material—A problem in classical physics*. Physics Reports, 1978. **43**(9): p. 377-407.
30. Sundar, V. and R.E. Newnham, *Electrostriction and polarization*. Ferroelectrics, 1992. **135**(1): p. 431-446.
31. Rochester, S.M. and D. Budker, *Atomic polarization visualized*. American Journal of Physics, 2001. **69**(4): p. 450-454.
32. O'Konski, C.T., *Electric Properties Of Macromolecules. V. Theory Of Ionic Polarization In Polyelectrolytes*. The Journal Of Physical Chemistry, 1960. **64**(5): p. 605-619.
33. Meakins, R.J., *Mechanisms of Dielectric Absorption in Solids. Progress in Dielectrics, 3, 2.271-2.271*. 1961.
34. McCarty, L.S. and G.M. Whitesides, *Electrostatic charging due to separation of ions at interfaces: Contact electrification of ionic electrets*. Angewandte Chemie-International Edition, 2008. **47**(12): p. 2188-2207.
35. Diaz A. F. and Felix-Navarro, R. M. *A semi-quantitative tribo-electric series for polymeric materials: the influence of chemical structure and properties*. Journal of Electrostatics, 2004. **vol. 62**(No. 4): p. pg. 277-290.
36. Breithaupt, J., *Physics, second edition, Palgrave Macmillian publishing* . 2003.
37. *Electric Fields & Electric Field Lines*, © studyphysics.ca. 2005.
38. Kim, Y. K., Langley, K. D., Lewis, A. F., and Seyam, A. *Electro-static web formation. NTC Project: F03-MD01 National Textile Center Annual Report*, . 2005.
39. Mironov, V.S. and M. Park, *Electroflocking technique in the fabrication and performance enhancement of fiber-reinforced polymer composites*. Composites Science and Technology, 2000. **60**(6): p. 927-933.
40. Verse, N., *Advances in the Electrostatic Flocking of Plastics Moldings, Profiles and Sheets*. Kunststoffe-German Plastics, 1988. **78**(10): p. 1011-1014.
41. Kim, Y. K., Langley, K. D., Lewis, A. F., and Seyam, A. *Scientific Study of Flock Materials and the Flocking Process*. 1999.
42. Kim, Y. K., Langley, K. D., Lewis, A. F., and Seyam, A. *Electro-static web formation. NTC Project: F03-MD01 National Textile Center Annual Report*. 2004.
43. Kim, Y. K., Langley, K. D., Lewis, A. F., and Seyam, A. *Electro-static web formation. NTC Project: F03-MD01 National Textile Center Annual Report*, . 2009.
44. Kim, Y. K., Langley, K. D., Lewis, A. F., and Seyam, A. *Electro-static web formation. NTC Project: F03-MD01 National Textile Center Annual Report*, . 2006.
45. Chirdon, W.M., W.J. O'Brien, and R.E. Robertson, *Diffuse reflectance of short-fiber-reinforced composites aligned by an electric field*. Dental Materials, 2006. **22**(1): p. 57-62.
46. E.M. van Veldhuizen, W.R.R., *Corona discharges: fundamentals and diagnostics*.
47. Lowke, J.J., R. Morrow, and J. Haidar, *A simplified unified theory of arcs and their electrodes*. Journal of Physics D-Applied Physics, 1997. **30**(14): p. 2033-2042.
48. Chubb, J., *New approaches for electrostatic testing of materials*. Journal of Electrostatics, 2002. **54**(3-4): p. 233-244.
49. Zhao, L. and K. Adamiak, *EHD flow in air produced by electric corona discharge in pin-plate configuration*. Journal of Electrostatics, 2005. **63**(3-4): p. 337-350.
50. Feng, J.Q., *Electrohydrodynamic flow associated with unipolar charge current due to corona discharge from a wire enclosed in a rectangular shield*. Journal of Applied Physics, 1999. **86**(5): p. 2412-2418.

51. Kumaran, G.P.M.a.M.K., *Simultaneous heat and moisture transport through glass fibre insulation: An investigation of the effect of hygroscopicity* 1987.
52. <http://www.swicofil.com/flock.html>.
53. Liu, L.F., et al., *Optimal design of superfine polyamide fabric by electrostatic flocking technology*. Textile Research Journal, 2011. **81**(1): p. 3-9.
54. Zhong, J., et al., *Electrostatic Flocking of Superfine Fiber*. Proceedings of the Fiber Society 2009 Spring Conference, Vols I and II, 2009: p. 276-278.
55. Semenov, V.A., S.P. Hersh, and B.S. Gupta, *Increasing Pile Density in Electrostatic Flocking by Introducing a Guiding Electrode*. IEEE Transactions on Industry Applications, 1983. **19**(1): p. 127-132.